SPACE DIVISION

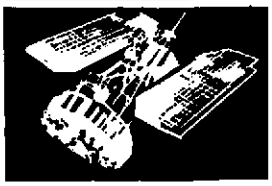
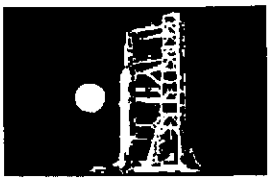
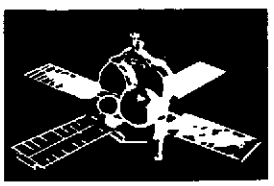
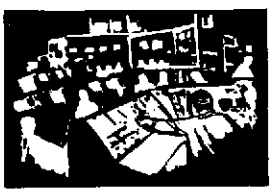
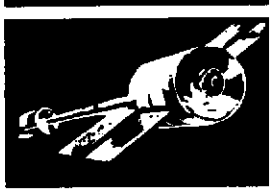
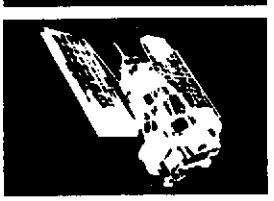

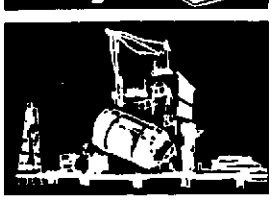

NASA CR - 134525

BASIC FAILURE MECHANISMS IN ADVANCED COMPOSITES

by

V. F. Mazzio, R. L. Mehan and J. V. Mullin

GENERAL ELECTRIC COMPANY
SPACE SCIENCES LABORATORY

Prepared for

NATIONAL AERONAUTICS AND SPACE ADMINISTRATION
NASA-Lewis Research Center
Contract NAS 3-15835

Tito T. Serafini, Project Manager

GENERAL ELECTRIC

NASA CR - 134525

BASIC FAILURE MECHANISMS IN ADVANCED COMPOSITES

by

V. F. Mazzio, R. L. Mehan and J. V. Mullin

GENERAL ELECTRIC COMPANY
SPACE SCIENCES LABORATORY

Prepared for

NATIONAL AERONAUTICS AND SPACE ADMINISTRATION
NASA-Lewis Research Center
Contract NAS 3-15835

Tito T. Serafini, Project Manager

FOREWORD

This is the final report for NASA Contract NAS-3-15835, "Basic Failure Mechanisms in Advanced Composites." The program was accomplished during the time period April 3, 1972 to June 3, 1973 for NASA Lewis Research Center, Cleveland, Ohio, with Dr. Tito T. Serafini as NASA Program Manager.

The individuals who contributed to this program are:

Mr. Ernest Muziani and Mr. Robert Grosso
in the preparation and testing of specimens

Mr. M. Birenbaum in composite characterization.

The authors also wish to thank Dr. T. T. Serafini and Dr. C. C. Chamis for their helpful technical suggestions.

This report has been prepared in accordance with the requirements of NASA Policy Directive NPD 2220.4 (September 14, 1970) regarding the use of SI units.

BASIC FAILURE MECHANISMS IN ADVANCED COMPOSITES

by

V. F. Mazzio, R. L. Mehan and J. V. Mullin

Summary

This final report covers the period April 3, 1973 to June 3, 1973 performed under Contract NAS 3-15835 with Dr. Tito T. Sarafini as NASA Program Manager.

The purpose of this research effort is to establish the fundamental failure mechanisms which result from the interaction of thermal cycling and mechanical loading of carbon-epoxy composites. This work is confined to epoxy resin unidirectionally reinforced with HTS carbon fibers. The approach consists of first identifying local fiber, matrix and interface failure mechanisms using the model composite specimen containing a small number of fibers so that optical techniques can be used for characterization. After the local fracture process has been established for both mechanical loading and thermal cycling, engineering composite properties and gross fracture modes are then examined to determine how the local events contribute to real composite performance. In this way, the critical events in the fracture process can be identified and a rational basis for optimizing the properties of these materials established.

Much of the effort in model specimen studies has been directed toward the tensile and compressive behavior under fast and slow thermal cycling between 220°K and 422°K (-65°F and +300°F). Parameters such as resin modification (to alter the load carrying capabilities of the resin under mechanical and thermal cycling conditions), oxidative surface treatment of the fiber, variations in fiber spacing, and the effects of thermal cycling rates on polymer molecular structure and behavior have been considered.

The use of acoustic emission analysis in studying the failure process and mechanical behavior in both model specimens and engineering specimens of carbon-epoxy composites, as well as equipment and techniques has also been given a good deal of consideration.

Considerable emphasis, in this year's program as in the prior work reported in NASA CR 121000, has been placed on the correlation of single fiber and tow observations with gross fracture modes. The relation between fiber content and bulk fracture modes is particularly interesting with lower fiber contents resulting in more localized fracture zones for the most part. Further,

there is strong evidence that weaker composites, regardless of fiber content, tend to cleave on a single plane while the stronger specimens exhibit extensive fracture zones as a result of cumulative damage. Of particular importance and interest is the fact that this type of behavior is the same before and after thermal cycling of composite specimens up to 500 thermal cycles. Assessment of the mechanical and thermal cycling behavior of engineering composites of carbon-epoxy has been extended to include transverse tensile strength and modulus, compression strength and modulus, flexural strength and modulus, as well as the longitudinal tensile properties and short beam shear strength studied in last years work.

It has been observed in model composite specimens that compression type failures have occurred under thermal cycling conditions up to 250 thermal cycles. This is probably due to residual stresses induced by the fabrication process such that the fibers are placed in compression and the matrix in tension. This same effect is present in the more heavily reinforced engineering composites but because there are many more fibers to resist resin shrinkage after cure, the result is a more complex residual stress condition which varies considerably from point to point.

In a unidirectionally reinforced composite after thermal cycling and having a fiber content of 55 fiber volume percent, the tensile modulus in the direction of the fiber increases slightly (11%) probably due to overcoming the initial residual compression in the fibers which tends to misalign them and thus prevents all fibers from contributing their inherent stiffness. As thermal cycling relieves the resin induced stresses greater fiber efficiency can result and thus the slight increase in modulus. Transverse modulus is primarily that of the resin because the fibers are discontinuous in the load path. This results in loss of modulus (5%) as thermal cycling causes scission of bonds in the polymer making it less stiff. In longitudinal tensile strength tests it appears that thermal cycling relieves the residual compression in the fibers and the strength diminishes. This behavior could represent some interfacial debonding, which suppresses the brittle cleavage failure mode. Transverse tensile strength tends to level off at about 60 MN/m^2 after 200 cycles.

In 25 fiber volume percent composites the longitudinal modulus cycling begins to degrade the interfacial bond, thus the modulus decreases. The transverse modulus depends upon the resin and as molecular scission occurs a decrease in transverse modulus results. However, the effect is less because of the greater bulk of resin present. The longitudinal strength appears to increase due to post-curing effects of thermal cycling. The transverse tensile strength again is representative of the resin itself. Local stress concentrations around fibers are of lesser importance at lower fiber content so relaxation of them has no significant effect.

The most prominent effect of thermal cycling on compressive stress is that on compressive strength of 25 v/o and 55 v/o engineering specimens. A significant decrease in compressive strength results for the higher fiber content, while the lower fiber content retains about the same strength after thermal cycling. This is an indication of degradation of either fibers or interfacial bond between fiber and resin as a result of thermal cycling the higher fiber content specimens.

Flexural strength in high fiber content specimens shows an increase in strength with increased thermal cycling. Similar behavior is noted for 25 v/o material up to 200 cycles; however, there is a drastic reduction after 200 cycles indicating a major loss of integrity probably through the accumulation of local cleavage cracks in the tensile region. The loss of interfacial bond in the compressive region would have a similar effect.

There was little change in interlaminar shear strength with the number of cycles, using the latest improved lot of prepreg material. There is a slight decrease in strength at 100 cycles and then an increase of about 15 percent. This follows the behavior referred to earlier where residual stresses are relieved with some slight loss of resin integrity. After this, the composite shear strength is enhanced by a combination of post-curing resin strengthening and improved interfacial action.

The mean values and standard deviation are presented for engineering property values because of the vast amount of individual test results before and after thermal cycling. This greatly facilitates correlation and analysis of data and enables the significant material and property variables to be identified.

TABLE OF CONTENTS

TABLE OF CONTENTS (Continued)

LIST OF TABLES

LIST OF FIGURES

LIST OF FIGURES (Continued)

LIST OF FIGURES (Continued)

LIST OF FIGURES (Continued)

1.0 INTRODUCTION

Advanced composite materials are now being used in a number of aerospace applications where structural efficiency is the primary consideration. The ability to tailor their mechanical and thermal response characteristics carries with it the inherent difficulty of predicting rather complex failure modes. Several research efforts have been directed toward identifying failure modes under mechanical loading but thermal cycling effects have received considerably less attention.

The objective of the research described here is to establish the fundamental failure mechanisms which result from the interaction of thermal cycling and mechanical loading of carbon fiber/epoxy composites. This effort is a continuation of earlier work on mechanical response of similar materials and is confined to epoxy resin unidirectionally reinforced with HTS fibers. The approach consists of first identifying local fiber, matrix and interface failure mechanisms using the model composite specimen containing a small number of fibers so that optical techniques can be used for characterization. After the local fracture process has been established for both mechanical loading and thermal cycling, engineering composite properties and gross fracture modes are then examined to determine how the local events contribute to real composite performance. In this way the critical events in the fracture process can be identified and a rational basis for optimizing these materials established. In support of the optical techniques, acoustic emission analysis has been used in this study to identify specific failure events. It is hoped that this effort will provide both designer and materials engineer with a more reliable prediction of the response of this class of materials.

2.0 MATERIALS CONSIDERATIONS

2.1 Thermally Induced Failure Mechanisms

Most advanced reinforcing fibers have thermal expansion coefficients which differ from that of the epoxy matrix with the magnitude of the difference varying with the type of fiber. Carbon fibers with a zero to slightly negative thermal coefficient of expansion along the fiber axis represent the most extreme case and will be treated in this discussion. Cure temperatures for most epoxy resin systems are on the order of 450°K (350°F) with typical operating temperatures going as low as 220°K (-65°F). This represents an extreme thermal excursion in which the matrix tends to compress the fibers along their axes and the fibers in turn tend to stretch the resin matrix causing shear stresses to develop at the interface. Depending on the fiber volume fraction and the transverse thermal expansion coefficient of the fibers, radial and circumferential stresses can be generated in both fibers and matrix in addition to the longitudinal stresses. Hoffman (1) has computed thermally induced stresses in laminates and uniaxially reinforced composites for a range of volume

fractions assuming each constituent to be homogeneous and isotropic and has applied his analysis to metal composites where Poisson's ratio of reinforcement and matrix are about equal. Although these assumptions do not apply to the carbon/epoxy system there are similarities in the approach and the stress inducing mechanisms are essentially the same.

Here we will confine the discussion to a qualitative description of the forces at work on fiber and matrix during thermal excursions and the probable failure mechanisms they can be expected to produce. Figure 1A shows a typical composite element with a fiber of radius r_f inside a sheath of matrix having radius R. Since the differences in thermal expansion coefficient between fiber and matrix are greater along the fiber axis than in the direction normal to the fiber we will confine our discussion to axial effects for the time being. As the composite is cooled down from the cure temperature, the matrix, having a higher thermal expansion coefficient, tends to compress the fiber axially, thus generating the first possible failure mode, local fiber buckling (Figure 1b). The fiber is loaded by shear stresses generated at the interface by the thermal mismatch. When the bond strength is low, interface failure may result and unbonding should be evident in the high shear stress regions such as at fiber ends (Figure 1c). When the resin is extremely crack sensitive and the bond is strong the high shear stresses near fiber ends can generate resolved tensile cracks on the plane of maximum principal stress as shown in Figure 1d. These cracks are similar to those predicted and identified under tensile load but inverted in direction. It is interesting to note that a broken fiber in compression can generate two such cracks which intersect and interfere with one another's growth as shown in Figure 1e, thus, resulting in a self-limiting fracture mechanism. The degree to which any one of these modes is present in a composite subjected to thermal cycling depends on the individual properties of the constituents, their volume fractions, and the nature of the interface. Fiber buckling has been observed a number of times in specimens prepared earlier under NASw-2093 and NASw-1543 under cool down or resin shrinkage, as well as under mechanical loading. Debonding at the interface has also been observed under mechanical loading. Debonding at the interface and fiber matrix damages have been observed in model specimens after 250 thermal cycles.

2.2 Material Properties

2.2.1 Fiber Properties:

In past NASA studies (NASA CR-121000) initial experiments involved the evaluation of untreated High Tensile Strength Fibers (HTU) in both modified and unmodified epoxy-novolac. Subsequently, the effects of fiber surface treatment were evaluated and compared to the untreated behavior. However, since the greater volume of fibers used in prepreg systems for structural applications have a surface treatment, this study has focused on the treated HTS carbon fibers in one of the most commonly used resin systems. Results of previous experiments

(a)

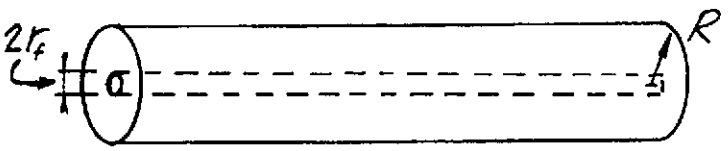

Cured at 450°K
Cooled to 220°K

Composite Element

(b)

Local Fiber Buckling

(c)

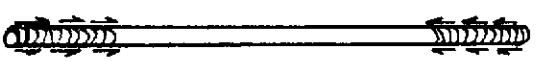

Local Interfacial
Debonding at Fiber Ends

(d)

Resolved Tensile Cracks
Due to Shear at Ends

(e)

Self Arresting Tensile Cracks at
Fiber Break

Figure 1 Possible Failure Mechanisms Under Thermal Cycling

involving HTS fibers in unmodified epoxy-novolac indicated a very strong bond with no evidence of fiber pull-out and fracture primarily by cleavage. Although the behavior of HTS fibers in modified resin is different, there is also evidence of good bonding and little fiber pull-out is observed at the fracture sites.

Hercules' HTS fibers were used exclusively in this program. Previous data and observations of fractures in model composite and in engineering composite systems, both produced from these fibers, were found to be valuable in comparing failure mechanisms resulting from the interactions between thermal cycling and mechanical loading as discussed in Section 2.1.

The HTS fibers used in all of the work on failure mechanisms to date have been of meter length. As discussed earlier, meter length tows produced by Courtauld's and later by Hercules have been well characterized. The same HTS fibers in continuous form produced by Hercules have not been as extensively evaluated. Early in this year's program when fibers were purchased for model specimen evaluation from Hercules and commercial prepreg was ordered from Fiberite it was our understanding that the meter length HTS fibers received from Hercules were still those produced originally by Courtauld's and later by Hercules licensed to use Courtauld's process; whereas, the currently available continuous fibers are those produced by a modified Hercules process. Typical fiber properties for both fiber types are shown in Table 1.

Table 1

Fiber Form	Tensile Strength		Tensile Modulus		Density	
	GN/m^2	$x10^3$ psi	GN/m^2	$x\ 10^6$ psi	Kg/m^3	# in^3
HTS (Meter) Courtauld's Lot # PT 117/201 Z	2.51	364	248.2	36.0	1800	0.065
HTS (Continuous) Hercules Lot # 5-1/86B-2	2.50	363	265.4	38.5	1750	0.0632

Note in Table 1 that modulus is the only parameter that differs between the two types of fibers. The only other significant difference between fibers which must be considered is "surface treatment" and its effect on composite properties. There is still much to be learned concerning the effect of surface treatment on fracture modes under mechanical loading as well as under thermal cycling conditions: these effects are the subject of a separate investigation.

2.2.2 Matrix Characteristics

1. Resin Selection

The epoxy resin selected for evaluation in model specimens and engineering composites under thermal cycling conditions represented a moderate change in formulation and modification from the epoxy-novolac resin used in previous NASA studies under contract NASw-1543 and NASw-2093. The resin system selected for use during this period of study was based on a diglycidyl ether of bisphenol A. The main criteria established for final selection were: First, it is capable of being easily modified without degrading its load transfer function to prevent rapid and catastrophic crack propagation. Secondly, it is a system that is widely and successfully used in major structural programs. There are several suppliers of the basic resin; however, for purposes of consistency and reproducibility in this program Shell's Epon 828 was used.

2. Resin Formulation and Modification

Several amine and anhydride curing agents were considered for use with Epon 828. While it was known that the amines had many advantages over the anhydrides such as higher heat distortion temperature (HDT), lower viscosity, lower hygroscopy and optimum physical properties of cured castings, they lacked the heat resistant characteristics required in this work. Anhydrides, on the other hand, possessed this characteristic, together with a moderate HDT which was considered an advantage in thermal cycling. Hexahydrophthalic anhydride (HHPA) was chosen as the curing agent because of its stability when combined with epoxies, ease of handling, and compatibility with modifiers. Because of the hygroscopic nature of anhydrides in the unreacted state, storage was maintained in a closed container at ambient temperatures and extremely low humidity. Benzyldimethylamine (BDMA) was used as the accelerator for the unmodified system, and DMP-30 was used in the modified system.

Two flexibilizers were evaluated for modifying the basic formulation to obtain 12 to 15 and 15 to 20 percent elongation, and matrix toughness as required. One was EM-207, a typical hydroxy functional modifier, and the other was EPI-Rez 502, an aliphatic diglycidyl ether. Both function as co-reactants and become an integral part of the resin structure, so that, upon

continued exposure to moisture and heat, leaching from the system is not possible. Several plate castings 30.5 x 30.5 x 0.63 cm were prepared for formulation screening tests. These castings represented formulations with various stoichiometric amounts of HHPA curing agent and modifiers. The ratios of HHPA evaluated were 64, 68, 78 and 83 parts per hundred parts of resin. The two modifiers were used in the following amounts: EM-207 - 20, 50 and 65 Phr* and Epi-Rez 502-30 parts/Epoxy Resin 50 parts, 40/60 and 50/50. Each of the castings prepared for evaluation was cured according to the cure schedule for unfilled resin castings described in Section 2.3.3.3. The use of EM-207 resulted in non-uniform properties and non-reproducible fabrication processes; the spread of property values increased with larger amounts of modifier used. Epi-Rez 502 provided a more uniform set of strength properties at each level of modification. On the basis of the strength data, the formulations shown in Table II were selected. Figure 2 shows the influence of modification on toughness and strength of Epon 828 resin. The toughness of each formulation has been arbitrarily categorized as hard-strong, hard-tough and soft-tough. The tensile strength of formulation C is reduced considerably below the unmodified formulation A. Further modification of C to increase elongation would result in corresponding decrease in strength even though these formulations represent modification with Epi-Rez 502, which provided less effect on strength than EM-207.

2.3 Specimen Preparation and Testing

2.3.1 Resin Castings for Screening

Resin plate castings, 30.5 x 30.5 x 0.63 cm, were prepared in aluminum molds. The mold assembly consisted of two 1.27 cm thick aluminum plates clamped together with 0.63 x 0.63 cm spacers positioned between the plates around three of the four edges. One side was open for filling the mold and for volatile release during cure. The inside surfaces of the plates were cleaned and sprayed with mold release. The three spacers were held to both plates with double backed masking tape. The three closed edges of the assembly were then sealed permanently with RTV-108 to prevent resin from flowing out during cure.

The resin was poured into the mold and the assembly was then placed in an oven where cure was accomplished according to the cure schedule given in Section 2.3.3.3. After cure, the castings were cooled down to room temperature at the rate of 8.3° K/hr. (15°F/hr), removed from the molds and cleaned of flashings and mold release agent. Barcol hardness readings (934-1 scale) were recorded on both sides of the casting. Results are shown in Figure 2. Five specimens each for tensile strength, density and heat deflection temperature (HDT) were machined from each casting. Tensile tests were performed in an Instron testing machine at a strain rate of 2 percent per minute. Heat deflection tests were conducted to determine the effect of thermal cycling on

* Parts per hundred parts of epoxy resin used.

TABLE II

CAST EPOXY RESIN PROPERTIES

Resin Properties Formulation	Density Kg/m^3	Elongation %	Thermal Expansion $x10^{-5}m/m/^{o}C$	Tensile Strength		Tensile Modulus		Compressive Yield Strength	
				MN/m^2	KSI	GN/m^2	KSI	MN/m^2	KSI
A Epon 828/HHPA/ BDMA 100/78/1	1200	2.7	4.8*	70.7	10.25	2.89	4.2	124	18
B Epon 828/HHPA Dmp-30/ Epi-Rez 502 60/68/1.5/40	1190	12.1	5.6*	56.3	8.2	2.63	3.81	96.5	14
C Epon 828/HHPA Dmp-30/ Epi-Rez 502 50/64/1.5/50	1190	17.2	–	32.4	4.7	2.34	3.4	-	-

* Data from Manufacturer's Literature

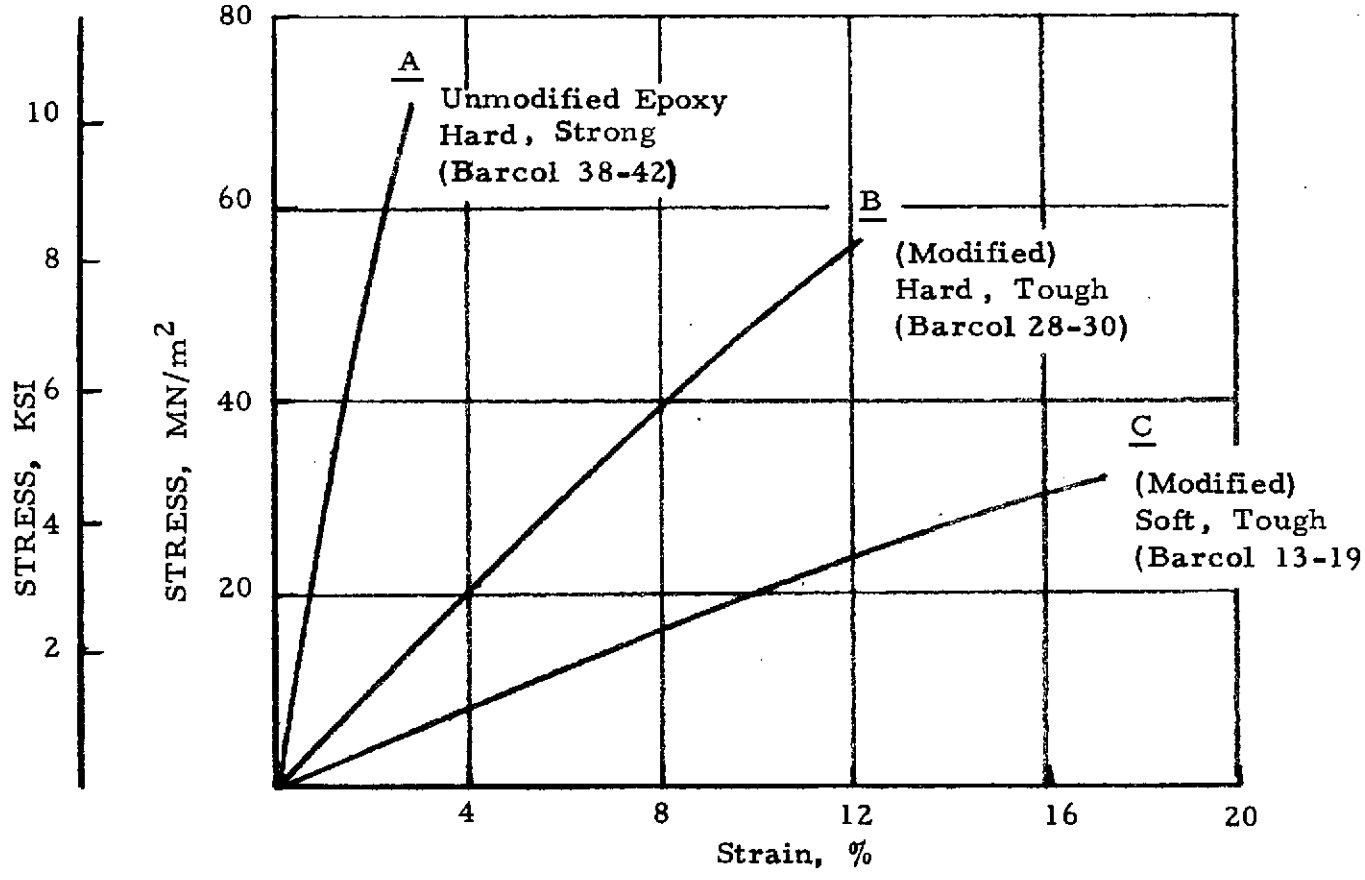

Figure 2 Stress-Strain Curves for Unmodified and Modified Cast Epon 828 Epoxy Resin

resin structure. These tests were performed in an American Instrument Company (AMINCO) deflection testing machine in accordance with ASTM specification D648-56. A constant load of 1.82 MN/m^2 (264 psi) was used and the bath temperature was increased at the rate of 2°C per minute. The test was carried beyond the arbitrary 2.54×10^{-4} m (10 mil) deflection point to determine the slope of the curve as a function of time with increasing temperature. Results of the tests are discussed in detail in Section 3.1.1.

2.3.2 Model Specimens

Model composite specimens containing isolated HTS fibers in both unmodified and modified resin were prepared and tested in both tension and compression. Rods, 0.63 x 0.47 x 10.2 cm, containing single and multiple fibers in epoxy were prepared in shallow 10 cm square molds. The molds were formed between 0.63 cm brass inserts spaced 0.63 cm apart. In both the unmodified and modified epoxy resin specimens a thin layer (about 0.16 cm) of epoxy resin was poured into the mold and partially gelled for one hour at 355°K (180°F). After gelling, the fibers were laid down parallel and centered as much as possible. Additional epoxy resin was then poured over the fibers to allow for an equal thickness of resin on both sides of the fibers. The composite, regardless of matrix form, was then cured for two hours at 355°K (180°F), followed by a stepwise increase in temperature to 450°K (350°F), for a two hour cure at this temperature. The specimens were removed from the mold, sanded and polished to desired thickness. All simple tensile specimen tests were conducted at the same strain rate (2 percent/min). The tests were interrupted at regular intervals for microscopic examination. All tests were carried out on an Instron testing machine with complete recording of load and deformation.

Microscopic examination was performed on a Bausch and Lomb microscope, and a Reichert polarizing microscope for high magnification examination. Magnifications were between 60 X and 620 X. The details of the failure process for the various test parameters are presented in Section 3.2.

2.3.3 Engineering Composites

Composites containing 25, 40 and 55 fiber volume fraction were prepared and tested. Only unmodified epoxy resin (Formulation A) was used during the engineering phase of the program. The number of test specimens required for evaluation were sufficient to warrant the use of an outside vendor to provide the amount of prepreg material necessary for uniform property data. Several suppliers were contacted and Fiberite Corp. was selected. An assessment of the prepreg materials obtained from Fiberite is presented in the following section.

of the prepreg materials obtained from Fiberite is presented in the following section.

2.3.3.1 Prepreg Material

Six separate lots, totaling twelve pounds of material, were purchased from Fiberite Corporation. This material was classified as a custom tailored prepreg system because not only was the HTS/828-HHPA combination another of a long line of proprietary materials in advanced composites, but also, the prepreg had to be supplied in a specified form to produce the 25, 40 and 55 fiber volume composites. The characteristics of the six lots received are shown in Table III. The first lots received were the 2C series for each volume fraction level. The resin content and ply thickness were the two properties which were to be controlled during processing to achieve the desired fiber volume levels in the final composite. Material flow was determined in order to establish a cure schedule for each. As shown in Table III, the flow for the lower fiber volumes was high; however, the cured ply thickness was good, and the material was uniform in appearance. In the case of the 55 percent material, the resin content appeared to be a little low as there were areas along the edge which showed insufficient fiber wetting. There were very few defect areas in all of the material received. These defects, located near the edge of the material, were in the form of slightly wavy and slightly twisted tows.

The next lot of material received was two pounds (lot #3A19) to replace some of the previously mentioned materials which presented processing problems. Visual and microscopic examination of both sides of the material indicated good resin distribution and fiber wetting. However, the bottom side possessed more uniform resin distribution along the fibers than the top side where the resin was present as globules. There was evidence of slip planes in the resin along the top surface, probably caused by repetitive rolling over the surface during the "B" stage or advancement period. The resin appeared more advanced on the top surface than it did on the bottom surface. Viewing the opened prepreg tows under 60 and 80 X magnification indicated that the inner fibers were uniformly wet-out. Over most of the prepreg the resin was tacky to the touch. Fiber uniformity and orientation between tows and along the length of the fibers was good. Counts of gaps between tows in a 20.48 x 30.48 cm ply numbered approximately 26; the widest gap measured $\sim$ 0.051 cm, and the longest $\sim$3.81 cm. In another ply gaps numbered $\sim$33; with the widest gap measuring 0.081 cm and the longest 4.45 cm. The most detrimental feature of this lot of prepreg was the non-uniform thickness of resin across the width of each ply. Micrometer measurements across a 30.43 cm width ranged from 0.048 cm at one edge to 0.061 cm in the center to 0.053 at the opposite edge. This was not considered to be too detrimental because the resin would

TABLE III

CHARACTERISTICS OF GRAPHITE/EPOXY PREPREG MATERIAL*

1. Material - HTS Graphite Fibers / EPON 828 Resin

2. Reinforcement Properties

Tensile Str. (min.)	363 Ksi	384	371
Modulus (min.)	38.6×10^3 ksi	35.4	365
Specific Gravity	1.74	1.74	1.75
Filament Diameter	8.9	8.3	8.4
Filaments/Tow	~10,000		

3. Prepreg Data (Fiberite Test Results)

Fiber Volume % (1)	25	25	40	40	55	55
Lot Number (2)	2C-18	3A-53	2C-17	3A-19	2C-16	3A-52
Date Received	9-7-72	3-9-73	9-7-72	1-31-73	9-7-72	3-9-73
Resin Solids, %	64.5	65.0	46.5	48.5	29.8	49.9
Volatile Content, %	1.3	3.1	3.2	3.4	3.3	3.3
Gel time @ 170°C min.	3.5	15	5	4	-	14
Prepreg Ply thickness, mils	18	19	15	14-31	8	14.5
Flow, % 100 psi, 5 min. @ 300°F	53.2	-	36.3	38.9	-	-
Cured ply thickness, mils	7.3	10.9	6.7	8.1	8.0	7.2
Lot Material Designation	Old	New	Old	New	Old	New

(1) Lots shown to be used for fiber volume levels indicated.
(2) All prepreg materials were estimated to have a 45 day shelf life from date of shipment.

* Vendor data

flow uniformly during cure. However, other plys ranged from 0.053 to 0.076 cm, primarily in the middle. This variation in thickness manifested itself in variation in individual ply weights for each ply in a composite panel. This meant that in order to achieve some semblance of uniformity in the composite, ply stacking had to be accomplished by matching thicknesses.

The final two lots of prepreg material (3A52 and 3A53) were received, and upon careful characterization it was determined that they were the most uniform and most carefully prepared prepreg materials obtained. This was the result of working more closely with the vendor in the area of Quality Control. For instance, the resin content for 55 v/o material was increased, as was the gel time to allow the resin more time to flow and distribute more easily before further conversion of the resin structure. In the preparation of composite panels from this material it was evident that the resin flow characteristics were greatly improved over past materials. Because of the overall improvement, there was less air entrapment in the resin during cure, and the tackiness indicated potential for better strength characteristics. In Section 3.3.3 mechanical data for engineering composites are presented for "old" material and "new" material. The "old" material refers to the first lots of material received in 1972 and the "new" refers to three lots received in 1973 which was of much better quality. These desig nations appear in Table III.

2.3.3.2 Specimen Preparation

Initially seven composite panels 30.48 cm x 30.48 cm x 8.0 cm thick were prepared from the first three lots of prepreg, to perform all the 25, 40 and 55 fiber volume tests required before and after thermal cycling. These composites were prepared by stacking the desired number of unidirectionally oriented plies between aluminum plates, placing the assembly into a preheated press 355°K (180°F) and curing according to the cure cycle described in section 2.3.3.3. During the cure process of some of these panels the resin appeared to remain tacky for long periods of time ($\sim$ 3 hours) without indications of hardening and developing strength. Additional time was used at the maximum cure temperature 450°K (350°F) to develop the necessary polymer conversion strength. After the additional time the resin became rigid but was weak and brittle. The panels were given an additional post-cure of 8 hours in the press to further develop strength. Visually the panels appeared sound. It was not until the preparation of the first room temperature tensile specimens, in which glass/epoxy end tabs were bonded to the specimen and exposed for three hours at 355°K (180°F) to cure the adhesive that it was discovered that the graphite/epoxy composite specimen softened, deformed and delaminated. At first it appeared that the deformation was due to stress relieving. To confirm this smaller specimens from other panels were placed in an oven at 355°K (180°F) without constraint. These specimens behaved

in the same manner as the tensile specimens, and once they cooled down to room temperature they became rigid. They appeared to lack integrity; particularly in the direction normal to the fibers.

Other tests were performed to determine the cause of this behavior. First, resin extracts were prepared from remnant pieces of the prepregs used in the panels to determine whether or not the BDMA catalyst was present. These extracts were compared in Infra-Red analysis to a freshly prepared quantity of the resin. The results of the I.R. Analysis showed that -amine was present in sufficient amounts in both samples. In the preparation of the extracts there was one instance (40 V_f prepreg) in which the extract was turbid. IR Analysis was performed to determine whether the white substance was a highly branched carboxylic acid used sometimes on fibers as a protection during fiber processing. The analysis showed the white substance to be small amounts of reacted epoxy resin.

The vendor (Fiberite) was contacted concerning the problem. Their records showed that all constituents were incorporated in stoichiometric amounts. Fiberite did point out that the flow and gel time values were unusually high. The seven fabricated panels were then given a 16 hour post-cure at 450°K (350°F). The results of panel characterization are discussed in Section 2.4. Subsequent to this phase of specimen preparation, two additional 30.48 cm x 30.48 cm (12" x 12") composite panels were prepared for 40 v/o tests. This provided ample material for precycle and post-thermal cycle testing. The preparation of the remaining 25 and 55 fiber volume spec imens was changed, in the interest of conserving material and achieving higher strength properties, to smaller panels 16.5 cm x 16.5 cm (6.5" x 6.5") for short beam shear, flexure, transverse tension and compression specimens. Tensile specimens were prepared as individual bars 1.27 cm wide x 22.9 cm long x $\sim$ 0.20 cm thick. In addition to the reasons just mentioned, it was more economical in both time and materials to prepare specimens by the latter approach. In preparing the smaller sized panels and individual tensile specimens, the prepreg-mold assemblies were placed in a cold press and the material was precompacted to remove entrapped air prior to cure. The press was then heated up to 250°F, using only contact pressure during heat-up. Final cure followed according to cure procedures discussed in the next Section. These procedures were used for preparing the remaining 25, 40 and 55 v/o specimens. A total of 5 panels 16.5 cm x 16.5 cm (6.5 inches x 6.5 inches) and 48 bar specimens 1.27 cm wide x 22.9 cm long x 0.20 cm, were prepared, which allowed for additional specimens to repeat some of the early tests. The test results are discussed in Section 3.4.

2.3.3.3 Cure Cycles

Cure cycles are discussed separately here because of the variations in make-up and form of the following materials : 1) unreinforced

epoxy castings, 2) model specimens containing few HTS fibers and 3) engineering composites at three fiber volume levels.

An attempt was made to maintain the cure of the three forms as uniform as possible, with the realization that shrinkage and behavior characteristics of the resin would be different in each case. It was desirable to have the graphite fiber filled resin of the latter forms behave in the same way under thermal cycling and mechanical loading conditions. Although cure conditions were not a major task in this program, it is felt that much work still needs to be done to determine the effects of cure and post-cure on the behavior of advanced composites. Recently, Johnson and Owston (2) studied the effects of cure cycle on the properties of carbon/epoxy composites, and found that there is a correlation between mechanical and physiochemical properties. For example, for a cycloaliphatic resin the deflection temperature shows a correlation to mechanical properties similar to that given by Tg.

Standard cure cycles recommended by suppliers to produce optimum properties are not always relevant to practical applications. Equipment used by the supplier for producing optimum strength materials, may be different from that available to end users. Therefore, new cycles must be adapted to suit the material, tooling and equipment available. Many variables must be considered in arriving at an optimum cure, since a slight deviation of one variable will change properties significantly. An example of this was experienced in this program with the variability in prepreg characteristics from the first lot to the final lot of material. The cure cycle utilized for the original lot was not the same to be used for the later lots received.

Resin Castings

The first material form to be cured and evaluated was the unfilled resin casting. Figure 3 shows the cure cycle used in curing that form. The early part of the cure was designed to provide a uniform transfer of heat through the mold walls, initiating the cure of the resin, and allowing for uniform structure formation throughout the panel. This procedure obviates premature resin advancement at the mold-resin interface, thus reducing the chances for non-uniform shrinkage. Slow cooldown to room temperature provides for additional reduction in shrinkage.

Model Specimens

Model specimens filled with only few fibers, much thinner cross-section and less volume, were cured differently because of the process used to prepare the specimens. Figure 4 shows typically the cure used for model specimens of unmodified and modified resin. In this program only unmodified resin was used and is represented by the solid line.

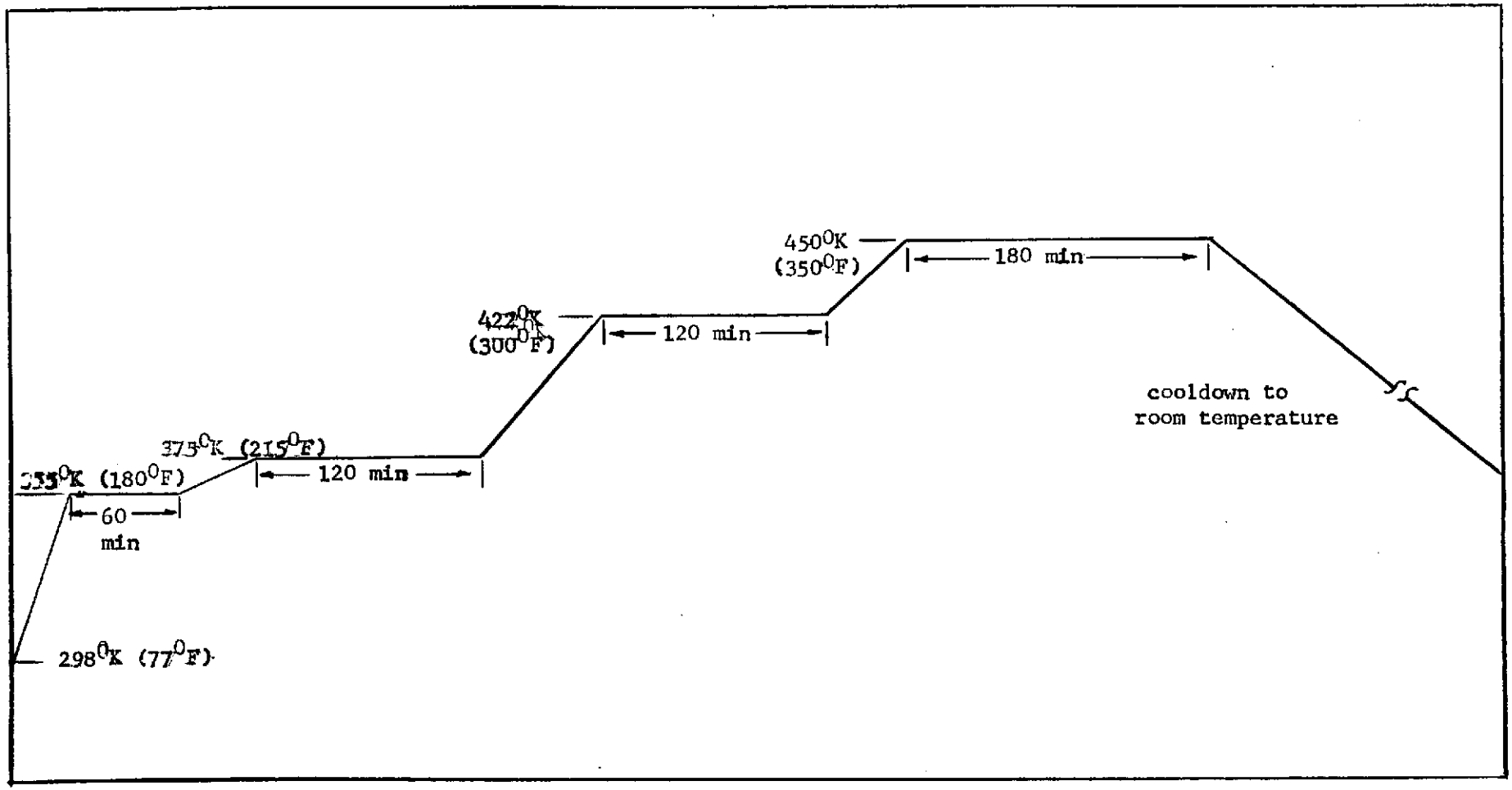

Figure 3. CURE CYCLE - EPON 828 RESIN CASTINGS

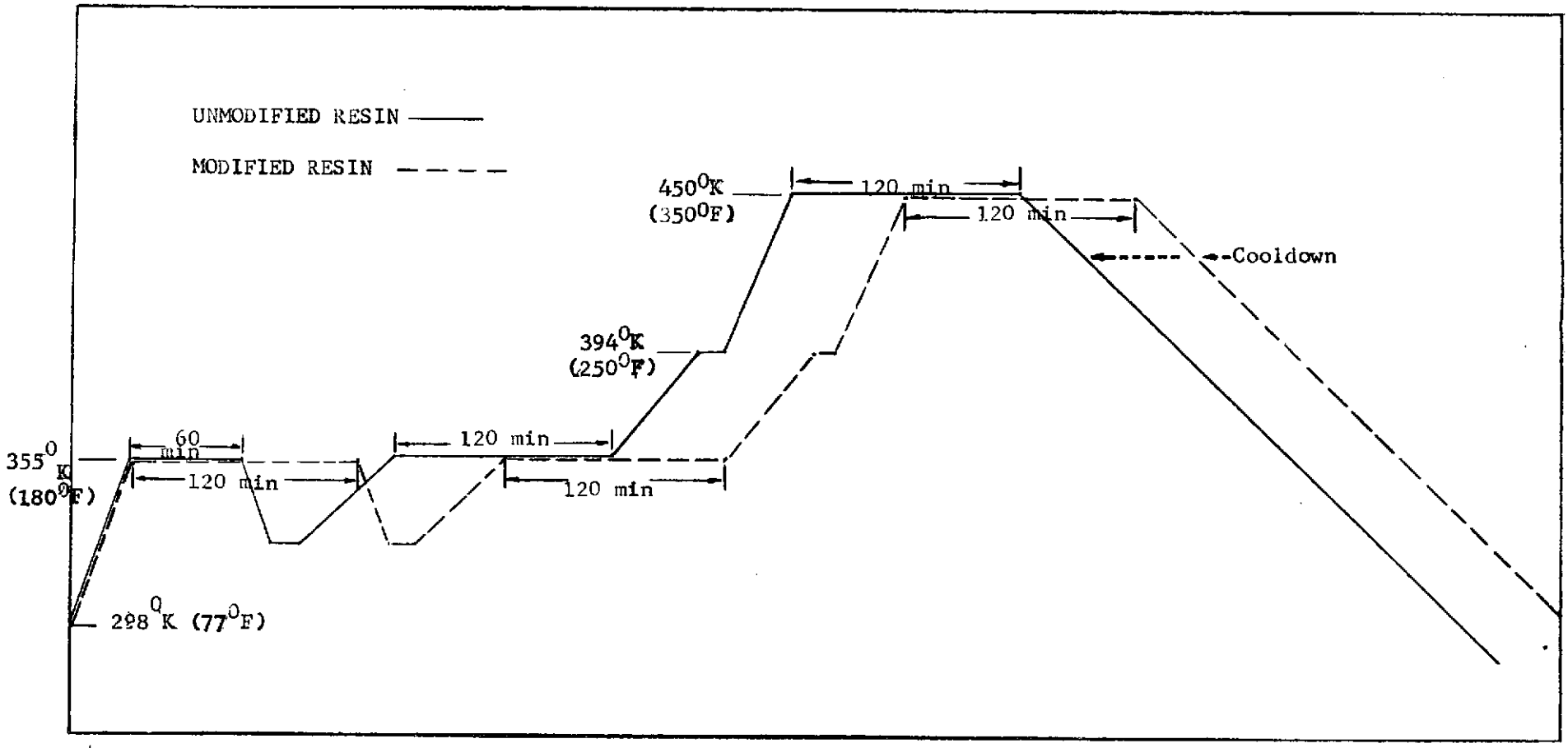

Figure 4. CURE CYCLE- MODEL SPECIMENS - EPON 828/HTS FIBERS

After 1 hour at 355°K (180°F) the first layer of resin was removed from the oven for fiber incorporation. The resin temperature dropped to about (316-322°K) during the 15 minutes out of the oven. The resin for the second layer was maintained at 316-322°K (110-120°F), so the shrinkage differential could be minimized; however, the first layer experienced higher initial temperatures 355°K (180°F). Prepared specimens in which the fibers were held intact and resin poured around them and cured as a single structure developed greater shrinkage stresses in the finished part. The long, slow cooldown to room temperature was found desirable for low shrinkage.

Engineering Composites

Figure 5 shows the cure cycle used for the original lots of prepreg received from Fiberite for larger composite panels. Because of the tacky nature of the resin flash during the regular cure, an 8 hour post-cure was added. Since this did not help to optimize properties, a 16 hour post-cure in an oven under weight was added. This offered some improvement in properties but little toward increased behavior after thermal cycling. A new cure cycle was developed for smaller sized specimens as shown in Figure 6. The new lot of prepreg material possessed higher gel and flow properties, so a precompaction stage was used to purge entrapped air considered present in the resin, and to provide the opportunity for higher density. After pre-compaction, the high pressure (150 ps was reduced to contact pressure; the heat was applied and after 0.5 hours at 394°K (250°F), curing pressure of 100-125 psim was applied. The cure continue for 1 hour at 394°K, and 16 hours at 450°K (350°F). It was found that this cur was highly satisfactory for smaller sized composites.

2.4 Engineering Composite Characteristics

Sufficient composite panels were fabricated to provide the number of specimens for test and evaluation at room temperature before and after therma cycling, in compliance with the Test Plan shown in Table IV. Other properties measured as part of quality control of the fabrication process were density, fibe volume, resin content and void content. After cure, all panels and bar specimer were measured for thickness uniformity; and all were visually and microscopicall examined. A summary of results of all composites fabricated for evaluation in the program is contained in Table V. The summary indicates problem areas and disposition of each of the materials. The void content for seven of the first twelve panels was high, which accounted for the lower density and lower properties values for panels 1242-10 and 12. As a result, tests were repeated from higher quality composites. The results of mechanical test data are discuss in Section 3.4. The fiber volume fraction range for each level was as follows -

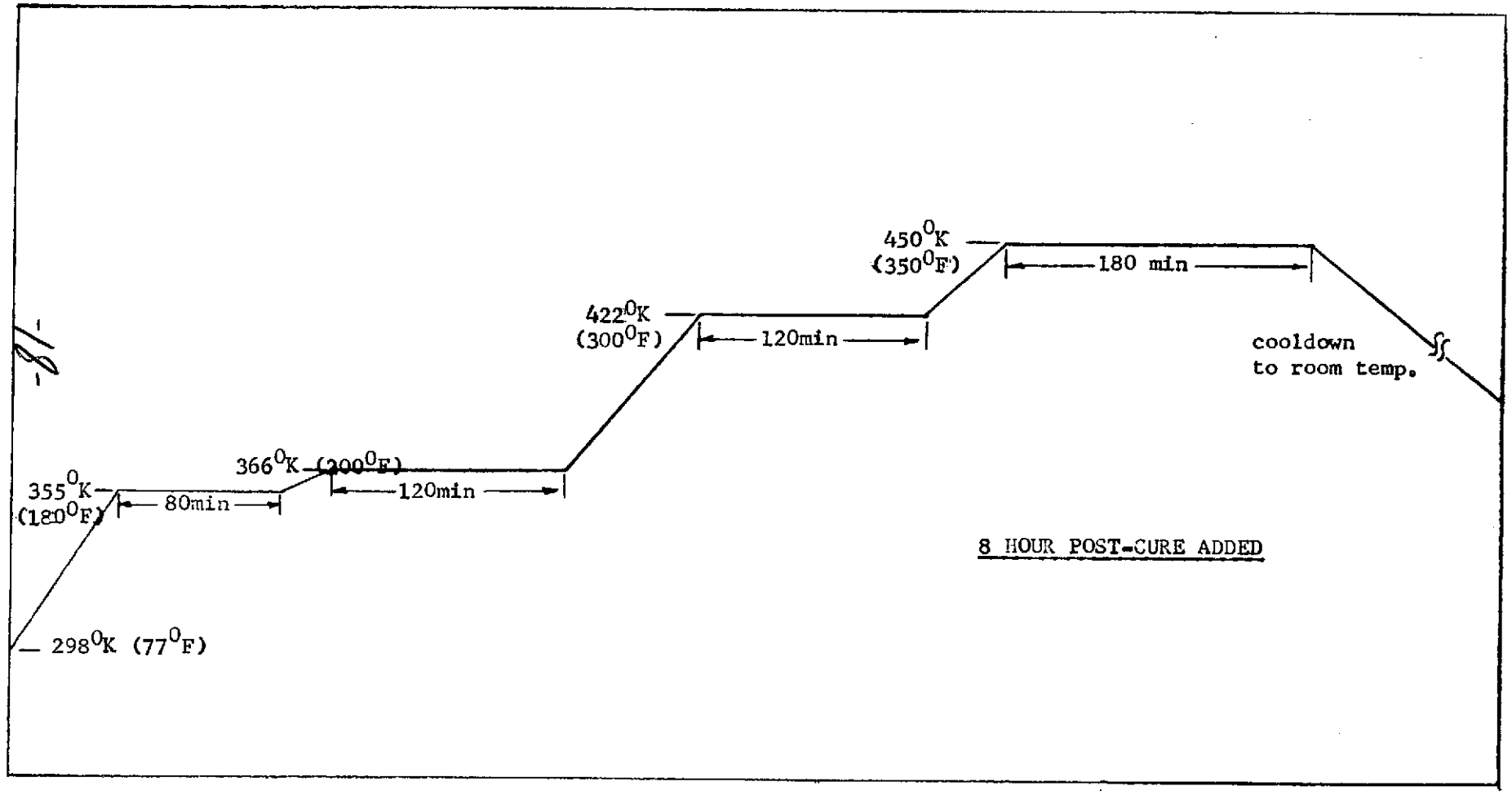

Figure 5. CU RE CYCLE- ENGINEERING SPECIMENS - EPON 828/HTS FIBERS (OLD MATERIAL)
(30.48cm^2 x 8.0cm size)

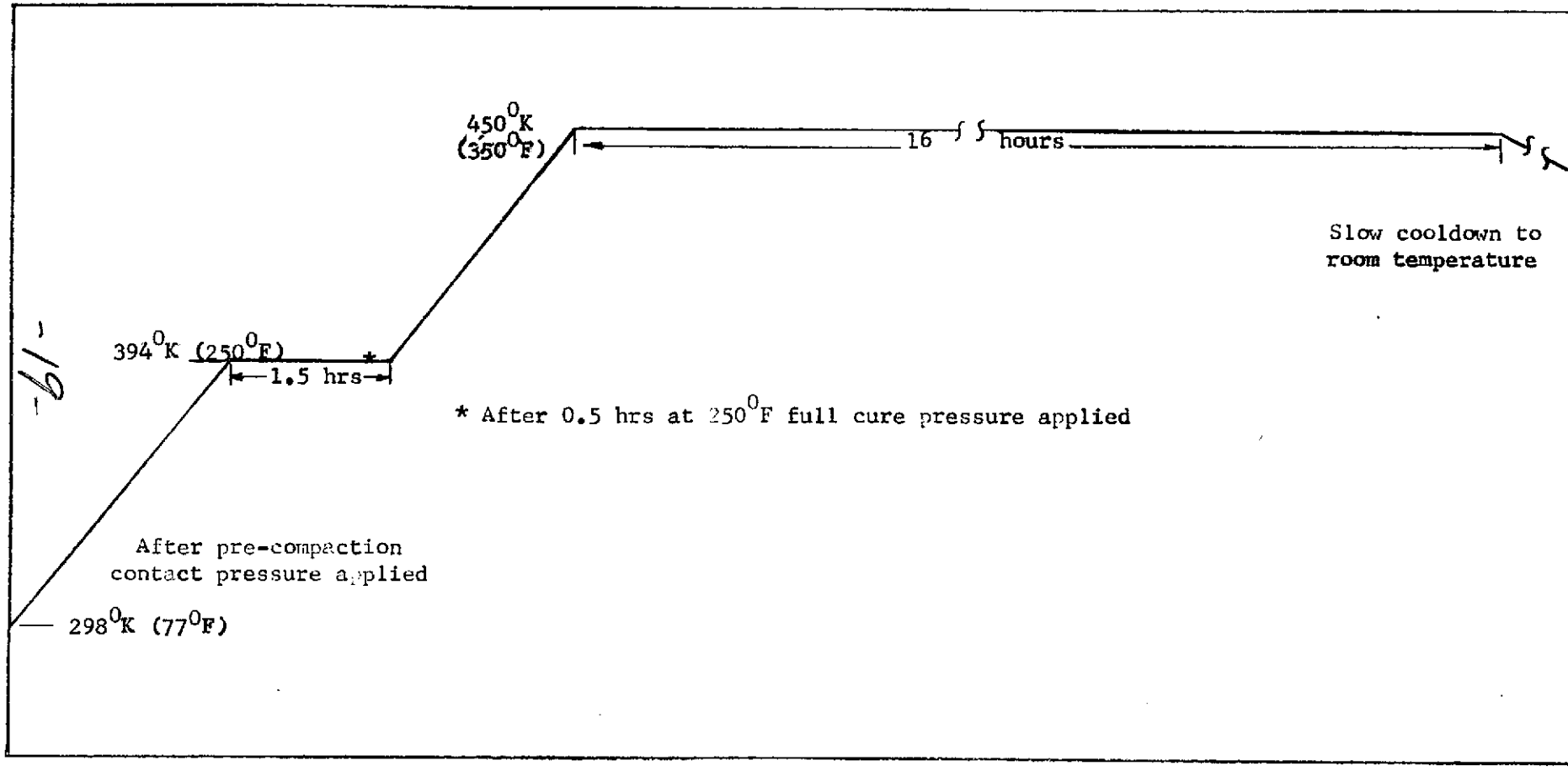

Figure 6. CURE CYCLE- FOR SMALLER ENGINEERING SPECIMENS- EPON 828/HTS (NEW MATERIAL)
(16.5 cm^2 x 8.0cm and 22.9cm x 1.27cm)

TABLE IV. TEST PLAN FOR EVALUATION OF ENGINEERING C/E COMPOSITE SPECIMENS BEFORE AND AFTER THERMAL CYCLING

TYPE TEST	TYPE OF CYCLING											
	SLOW									FAST		
	NO. OF CYCLES									NO. OF CYCLES		
	0			250			500			500		
	Vol. Fraction			Vol. Fraction			Vol. Fraction			Vol. Fraction		
	25	40	55	25	40	55	25	40	55	25	40	55
Longitudinal Tension	5	5	5	5	5	5	5	5	5	5		5
Transverse Tension	5		5			5	5		5			
Flexure	5		5	5		5	5		5	5		5
Compression	5		5				5		5			
Short-Beam Shear	5	5	5	5	5	5	5	5	5	5		5

Note: Slow = 1 cycle/hr.
Fast = 3 cycles/hr.

TABLE V

CHARACTERIZATION OF HTS CARBON FIBER/EPOXY COMPOSITES

Panel No.	Pre-Preg Lot No. Used	Density Avg. lb/in^3	Density Avg. Kg/m^3	Fiber Volume, % Avg. (5)	Resin Content wt. % Avg. (5)	Void Content, Vol. % Avg. (5)	Observations and Disposition
1242-1	2C-16	0.0531	0.147	51.3	39.3	2.2	Visually there appears to be good interply integrity. Microscopically there were no signs of delaminations. Usable on 50-55 V_f testing, pre and post T/C.
1242-2	2C-16	0.052	0.145	46.3	44.4	4.2	Visually the panel surface appears uniform, but looking at the panel (fiber ends) there are obvious voids between tows. Hold panel for possible use on 42-48 V_f testing.
1242-4	2C-17	0.045	0.124	52.0	25.4	N.A.	Very poor quality due to extreme dryness. Values obtained are only approximations. Rejected.
1242-5	2C-16	0.152	0.145	45.5	45.4	5.5	Visually the panel surface is good. Transverse properties are weak. Some tensile properties obtained. Preliminary data are below optimum. May still be usable on 42-48 V_f work.
1242-6	2C-18	0.048	0.133	37.9	50.1	2.1	Void content taken in best part of composite to determine quality of that part. Density ranges from 0.133 to .155 kg/m^3 Rejected because of excessive delaminations due to poor interlaminar bonding.
1242-7	2C-17	0.049	0.137	52	32.8	6.9	Poor transverse properties. Composite appears drier than others. Voids are more numerous. Rejected.
1242-8	2C-17	0.052	0.1453	46.6	43.9	4.3	Void content taken in areas not delaminated. There were many blisters after post-cure resulting in severe delaminations. Rejected.
1242-9	2C-17	0.055	0.1514	62.9	22.2	9.3	High voids; however, the low resin and high fiber volume lend to higher density. Microscopically there were only certain areas of higher void. Good part of composite usable.
1242-10	2C-18	0.054	0.150	58.2	33.4	9.4	Visually the panel looks good. Knitting seemingly better than most panels with high voids. Most of the panel is usable as interlaminar bond is good.
1242-11	2C-16	0.055	0.151	56.24	34.8	8.8	Microscopically and visually this panel is equivalent to previous panels 9 and 10. Usable for high volume tests.
2273-12	3A19	0.051	0.142	38.73	52.1	9.5	Resin content is high in center of panel. Void content and fiber volume low in center. Opposite is true on outer edges. This condition is due to non-uniformity of prepreg; compounded by 0° stacking sequence. Usable for 40 V_f tests.
2673-13	3A-19	0.054	0.149	51.54	33.8	9.3	Same observations as panel 12 above. Use for 50-55 V_f tests.

TABLE V (Continued)

Panel No.	Pre-Preg Lot No. Used	Density Avg. lb/in^3	Density Avg. Kg/m^3	Fiber Volume, % Avg. (5)	Resin Content wt. % Avg. (5)	Void Content, Vol. % Avg. (5)	Observations and Disposition
31273	3A52	0.052	0.145	---	---	---	There is good integrity and good density. Used for 40 V/O tensile and short beam shear tests.
31373	3A52	0.0515	0.144	39.91	60.54	---	Good visually & microscopically. Used for 40 V/O tensile, modulus & short beam shear testing.
31473	3A53	0.051	0.142	33.97	57.33	0.54	Good density, but a little high for 25 V/O composite testing. Used for tensile testing. Good strength.
31673	3A53	0.049	0.138	28.69	62.34	2.96	Good visually for lower fiber volume composites. 25 V/O tensile strength seems comparable to other materials.
32173	3A53	0.049	0.138	33.30	66.74	0.39	Good visually with evidence of good fiber orientation & distribution. Used for flexural strength tests.
32273	3A53	0.049	0.138	33.37	66.06	0.58	Good visually. Used for 25 V/O transverse tensile tests.
32673	3A53	0.049	0.138	32.05	67.56	0.46	Very good visually with good ply integrity and fiber distribution. Used for 25 V/O compression and short beam shear tests.
32773	3A53	0.049	0.139	34.57	63.79	2.78	Excellent fiber distribution. Used for 25 V/O tensile strength.
32873	3A52	0.055	0.151	54.38	36.69	0.26	Excellent fiber distribution and orientation. Used for 55 V/O transverse tensile strength tests.
32972	3A53	0.049	0.136	25.92	65.86	1.06	Excellent fiber distribution for lower fiber volume composites. Used for tensile tests.
4273	3A53	0.049	0.138	28.91	62.20	0.83	Excellent integrity. Used for 25 V/O tensile strength & modulus.
4473	3A52	0.055	0.1525	55.83	27.62	2.69	Excellent integrity producing high tensile strength & modulus.
4573	3A52	0.055	0.152	57.70	29.88	0.65	Excellent integrity. Used for 55 V/O tensile strength.
4673	3A52	0.056	0.154	57.86	29.00	0.81	Excellent integrity. Used for 55 V/O tensile tests.
5473	3A53	0.048	0.133	---	---	---	Excellent visually for 25 V/O specimens with good fiber distribution. Used for tensile tests.
12473	3A53	0.049	0.138	31.86	58.79	1.16	Good visually. Used for 25 V/O tensile tests.
12573	3A52	0.055	0.153	64.60	30.85	0.72	Excellent integrity with good fiber distribution. Used for 55 V/O flexural and short beam shear tests.
12673	3A52	0.056	0.154	---	---	---	Excellent integrity with good fiber orientation & distribution. Used for 55 V/O tensile tests.

nominal 25 $^{v}/_{o}$ - actual 30 $\pm$ 4 $^{v}/_{o}$; nominal 40 $^{v}/_{o}$ - actual 42.1 $\pm$ 4.2 $^{v}/_{o}$ and nominal 55 - actual 59.5 $\pm$ 5.1 $^{v}/_{o}$. The reason for the greater variation in the material with higher fiber content is that greater resin flow occurred during cure. The resin in the lower fiber volume material had to be contained during the early stages of cure. Void content values were considered acceptable for the lower than optimum fiber volume fraction composites.

Composites of each fiber volume fraction level were microscopically examined in cross-section to obtain some indication of fiber distribution. Typical fiber distribution in specimen cross-sections for the three levels is shown in Figure 7. The 25 and 55 $^{v}/_{o}$ photomicrographs show fairly good distribution; whereas, the 40 $^{v}/_{o}$ shows a combination of concentrated resin rich and high fiber volume areas. This is typical of most of the 40 $^{v}/_{o}$ composites and may account for some of the variation in mechanical properties.

3.0 EXPERIMENTAL PROCEDURES AND OBSERVATIONS

3.1 Chemical Considerations

Throughout the course of this program emphasis was placed on the behavior of the fiber-resin composite system under mechanical loading and thermal cycling conditions. The objective was to determine the variation in composite mechanical properties with temperature. Reference was made to modifed and unmodified epoxy resin; modification resulting from the incorporation of a reactive polymeric modifier into the basic polymer backbone to increase toughness. Chemical modification succeeded in increasing toughness and, at the same time, decreased cross-linking density.

Less consideration has been given to date to changes in polymer structure regularity and behavior, due to disruption by the graphite fibers; both chemically and mechanically. The question of the chemical nature of the polymer at the interface as opposed to some distance from the interface is of concern and should be further investigated. Efforts in this program were directed mainly at the mechanical aspects of the failure process. Therefore, little has been done regarding the chemical aspects that could possibly be affected. An attempt was made, on a limited basis, to determine the effects of temperature on structure of the unmodified and modified resin systems. This work is discussed in the following sections.

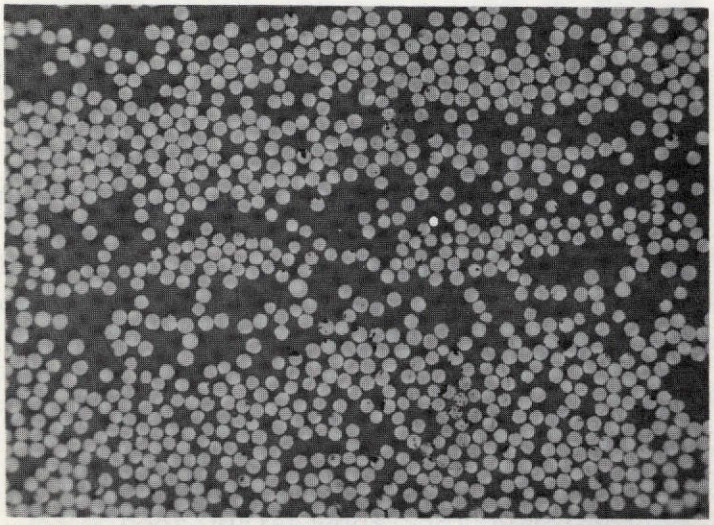

(a) Nominal 25 V/O Composites

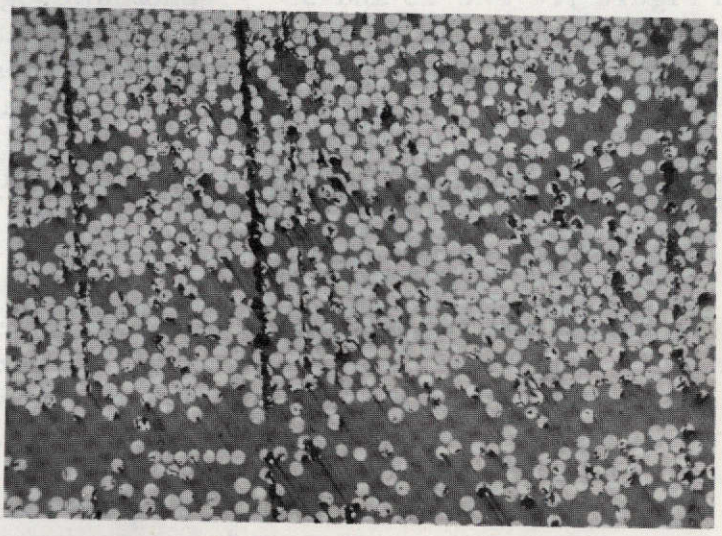

(b) Nominal 40 V/O Composites

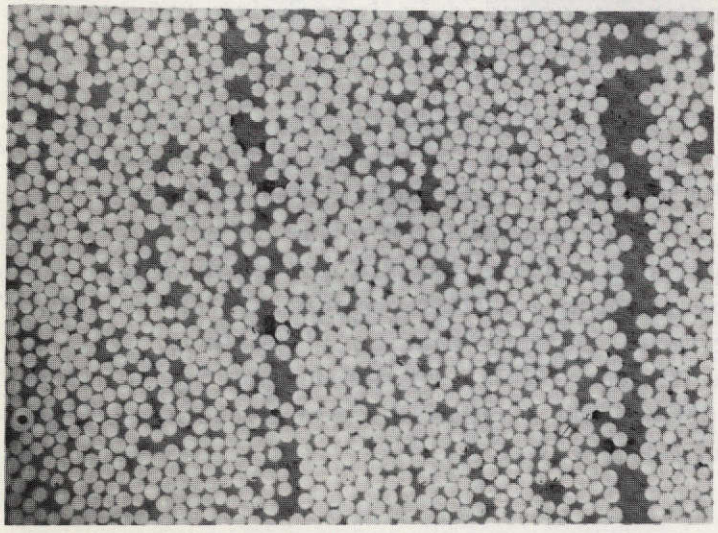

(c) Nominal 55 V/O composites

FIGURE 7. Typical Fiber Distribution in HTS Carbon Fiber/Epoxy Composites. Mag 240 X

3.1.1 Heat Deflection Temperature of Cured and Thermal Cycled Resin Specimens

Heat deflection temperature tests were performed on oven cured and thermally cycled unmodified and chemically modified resin specimens to obtain some indication of resin performance or behavior under temperature change. The three epoxy formulations discussed in Section 2.2.2 have been tested both before thermal cycling and after exposure to 250 slow thermal cycles. The data are shown in Table VI. Formulation A is the unmodified version used in the prepreg material for the engineering composites. HDT values for this formulation are about 13 percent lower than theoretical because the specimens were tested in the 0.635 cm thickness direction instead of the 1.27 cm direction. All the specimens shown in Table VI were tested in the same manner so a good comparison was possible as far as temperature performance was concerned. Although the data presented are lower than actual for the resin system, it should be noted that the specimens were 0.635 cm thick and were tested in the thickness direction, causing the lower HDT. The data show that there is more of a temperature effect on the unmodified structure than there is on the modified resin. A possible explanation may be that the intermolecular forces in the unmodified version are affected by temperature over an extended time period; whereas, in the modified versions the chain segments have already been extended to the point where the added temperature and time have little or no effect on structure.

The test results are best illustrated in the following figures for each of the formulations tested. Figure 8 shows that the pre-cycle and post-cycle forms of the unmodified resin follow the same general behavior, in that segmental extensions or scissions occur essentially in the same region, except in the region of greatest temperature difference where the pre-cycle resin offers slightly greater resistance to deformation. It would be expected that this kind of behavior would have some kind of effect on transverse modulus.

Figure 9 shows the effect of slight modification on HDT. Once again, there is more resistance to deformation on the pre-cycle resin, but at the deflection temperature the slope of both curves are linear.

Figure 10 shows that additional modification of the polymer, to 17 percent, HDT is reduced to approximately one-third the value of the unmodified version. More important is the fact that after 250 thermal cycles the HDT reveals a soft, highly ductile system.

Unfortunately, time did not permit evaluation of the composite system under the same conditions, for both uniaxial and transverse directions.

TABLE VI

HEAT DEFLECTION TEMPERATURE OF EPOXY RESIN CASTINGS

FORMULATION	ELONGATION, %	PRE-CYCLE			250 SLOW THERMAL CYCLES		
		Spec. No.	δ, m x 10^{-4}	Temp., °K	Spec. No.	δ, m x 10^{-4}	Temp., °
(A)	~2.7	4E	2.54	383	4B	2.54	371
		4F	2.67	387	4C	2.79	373
		4G	2.67	381	4D	2.54	367
				AVG. 384			AVG. 370
(B)	~12.1	8D	2.54	330	8A	2.54	325
		8E	2.54	327	8B	2.29	327
		8F	2.79	328	8C	2.79	327
				AVG. 328			AVG. 327
(C)	~17.2	9D	2.79	314	9A	2.54	315
		9E	2.29	314	9B	2.79	311
		9F	2.54	313	9C	2.54	311
				AVG. 314			AVG. 312
				SI			SI

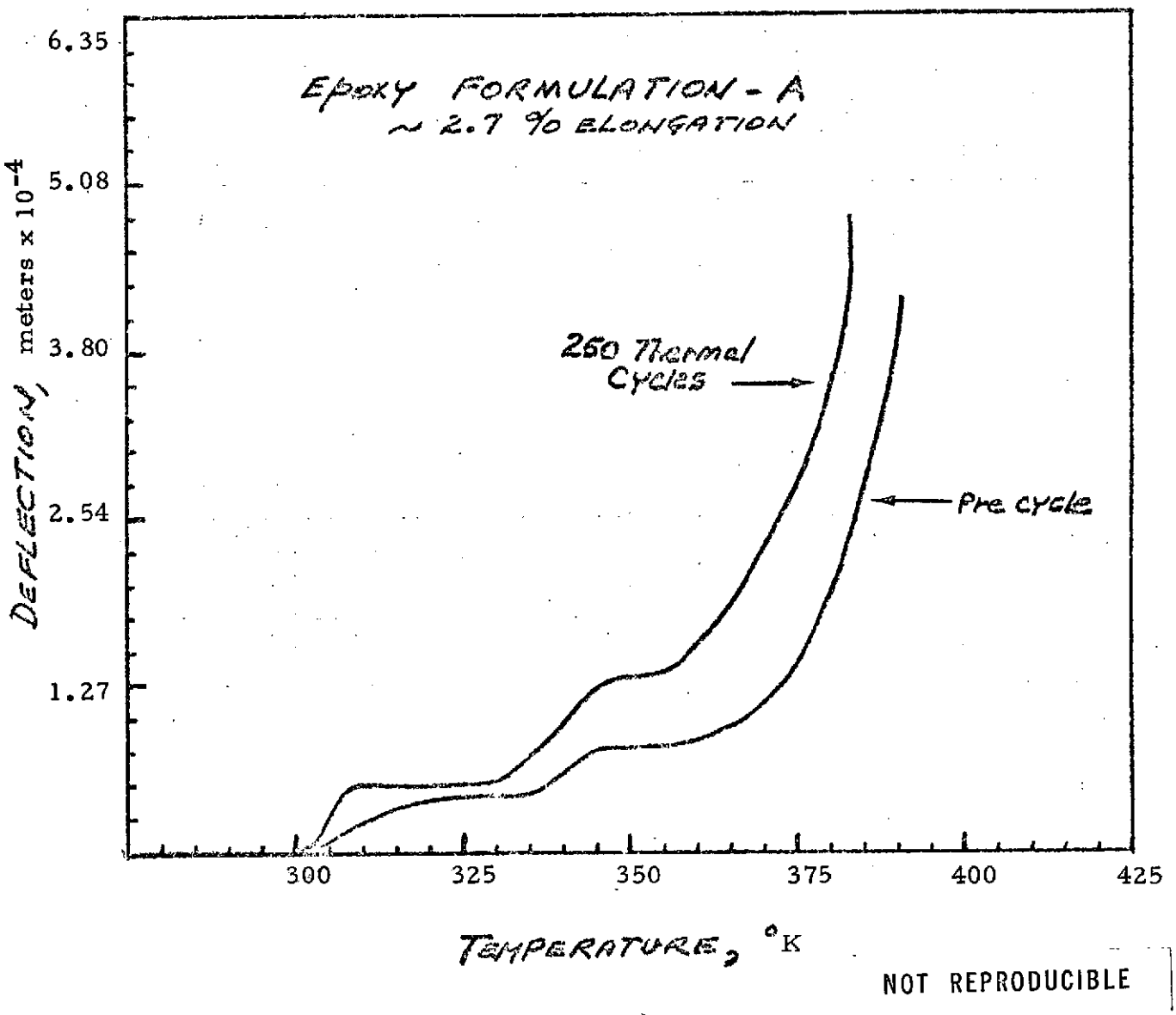

FIGURE 8. HEAT DEFLECTION TEMPERATURE OF UNMODIFIED EPOXY RESIN BEFORE AND AFTER THERMAL CYCLING.

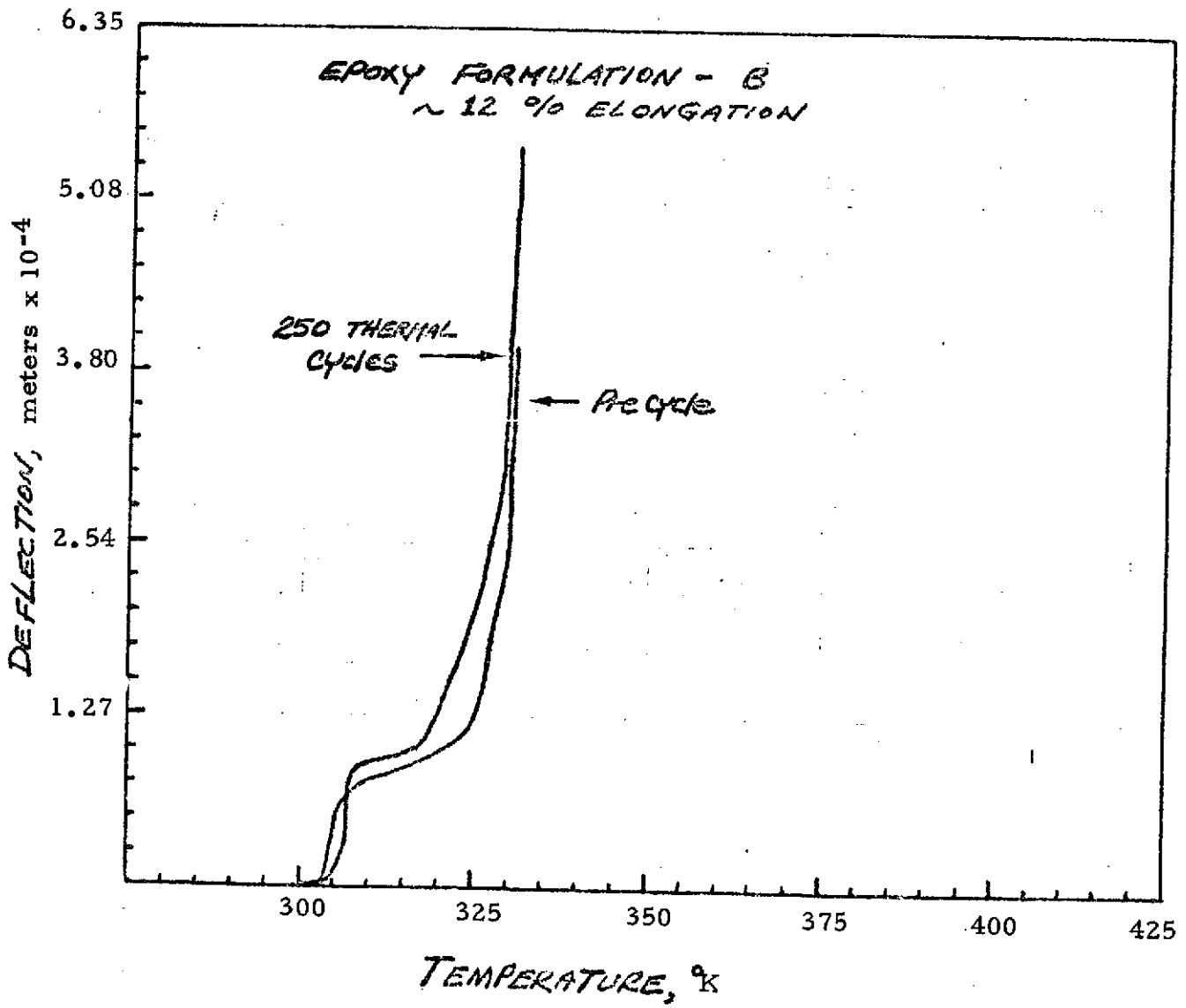

FIGURE 9. EFFECT OF 12% MODIFICATION ON H.D.T. PERFORMANCE OF EPOXY RESIN BEFORE AND AFTER THERMAL CYCLING.

NOT REPRODUCIBLE

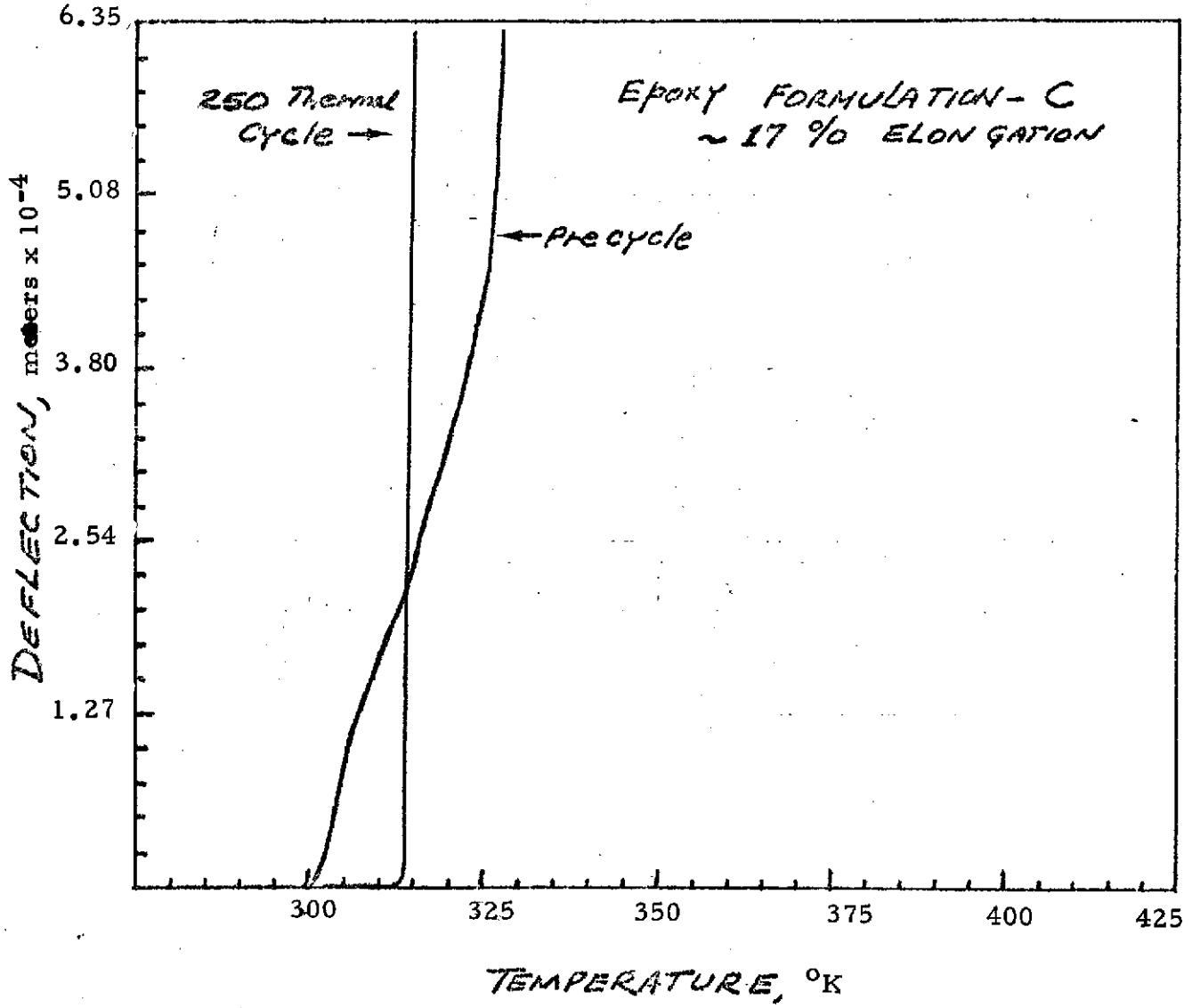

FIGURE 10. EFFECT OF 17% MODIFICATION ON H.D.T. PERFORMANCE OF EPOXY RESIN BEFORE AND AFTER THERMAL CYCLING.

3.1.2 Infrared Analysis of Cured and Thermal Cycled Resin Specimens

Infrared analysis was performed on unmodified cast resin specimens to determine whether additional conversion occurred as a result of thermal cycling. Absorption peaks for material before and after cycling were compared at frequencies of 2960 cm^{-1} and 1580 cm^{-1}. I.R. spectra of the resin before and after cycling are shown in Figure 11 . Absorption ratios were determined from peak to peak measurements between the two materials, at the two frequencies just mentioned. The results of these measurements are shown in the following Table.

Table VII

Before Cycling	2960 cm^{-1}	=	0.655	ratio = 0.16
	1580 cm^{-1}	=	0.105	
After Cycling	2960 cm^{-1}	=	0.407	ratio = 0.145
	1580 cm^{-1}	=	0.059	

The slight difference indicates that the resin was adequately cured by the regular cure cycle and that the additional temperature exposure afforded little or no further epoxide conversion.

3.2 Mechanical Loading of Model Composite Specimens

In order to identify fundamental fracture mechanisms for the HTS fibers in Epon 828 resin under thermal cycling conditions it was first necessary to establish a basis for comparison. Following the procedures established earlier for carbon fibers in epoxy-novolac, model composite fracture specimens containing small groups of fibers were subjected to mechanical loading both in tension and compression to establish their fundamental failure mechanisms. Compression tests were given somewhat more emphasis than tension tests since the nature of the thermal cycle will tend to load the fibers primarily in this way. This section describes the results of those experiments. Originally the intention was to use only the unmodified Epon 828 resin formulation having an elongation of about 2.7 percent. However, it was decided that modification of the resin to provide higher total strain to failure would be worthy of study because of the higher thermal expansion coefficients which results, as well as the reduced crack sensitivity at higher elongation. The following discussion will therefore include comparisons of unmodified resin behavior with two degrees of resin modification, one giving about 12% total strain to failure and the other 17%.

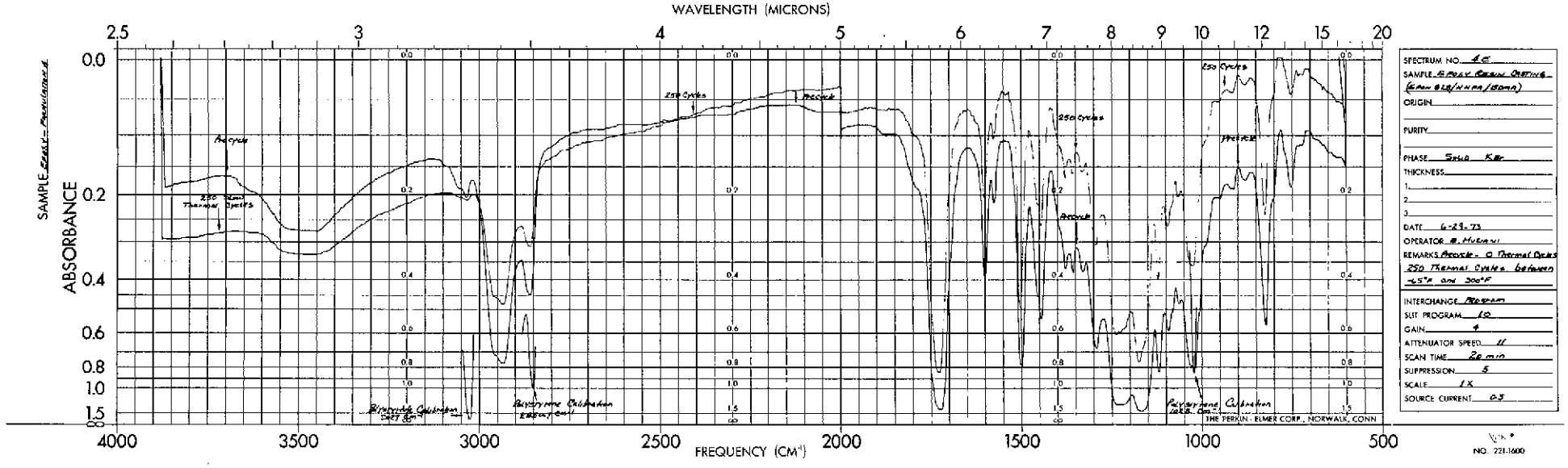

FIGURE 11. IR SPECTRA OF ANHYDRIDE CURED EPOXY RESIN BEFORE AND AFTER THERMAL CYCLING.

3.2.1 Tensile Behavior

A number of model composite specimens were prepared as described in Section 2.3 and subjected to tensile loading at 2 percent per minute strain rate. The test was interrupted at regular intervals to make a thorough microscopic examination over the gage length and compare the results to pretest photographs. Figure 12 shows the typical fracture mode which resulted for HTS fibers in ummodified Epon 828 subjected to tensile load. The upper photo (a) shows the fracture surface with the fiber ends appearing as black dots. The fiber which initiated the fracture is indicated in the upper photo and also in profile in photo (b) at lower left. An interesting difference exists between this fracture and that obtained in last year's work in DEN 438 epoxy novolac. Photo (c) shows a group of broken fibers at some distance from the specimen fracture surface. This area is indicated by arrow at 60 X but is barely discernible at that magnification. These cracks are very minute extending only a fraction of a fiber diameter into the resin. The significant point is that no such cracks were found in the DEN 438 system at the same percent elongation but rather, the first fiber fracture resulted in failure of the specimen.Epon 828, on the other hand, appears to be able to sustain at least a few local fractures in the more closely spaced fibers before a fiber fracture with sufficient energy to generate an unstable crack. This behavior suggests that, even in the unmodified state, Epon 828 resin is more effective in isolating local fiber fractures in higher volume fraction composites than DEN 438 in the unmodified state. Figure 13 shows a typical single fiber fracture at much higher magnification. Note how small the crack in the upper photo and the absence of any interfacial debonding. The lower photo shows the stress concentration around the crack under polarized light. It should also be noted that the identification of these very minute cracks is difficult optically and acoustic emission techniques were used to detect their occurrence. More detail relating to the value of combining the optical and acoustic emission techniques will be presented in Section 3.2.4.

3.2.2 Compression Behavior

Model composite photographs were also obtained under compressive load to establish the fundamental fracture mechanisms for that condition. Figure 14 shows typical compression behavior of the HTS fibers in unmodified Epon 828. Photo (a) illustrates how uniformly the fibers fail in compression with bright areas indicating resin fracture at each fiber fracture in compression. The very regular spacing of the fiber fractures is shown in photo (b) at 150 X with very little evidence of debonding. The bottom photo (c) shows an individual fracture at 375 X magnification under polarized light. Note the shape of the fracture in the resin. It appears to be diamond shaped in profile and is quite similar to the resolved tensile crack mechanism predicted in Figure 10. This is evidence of a very strong interfacial

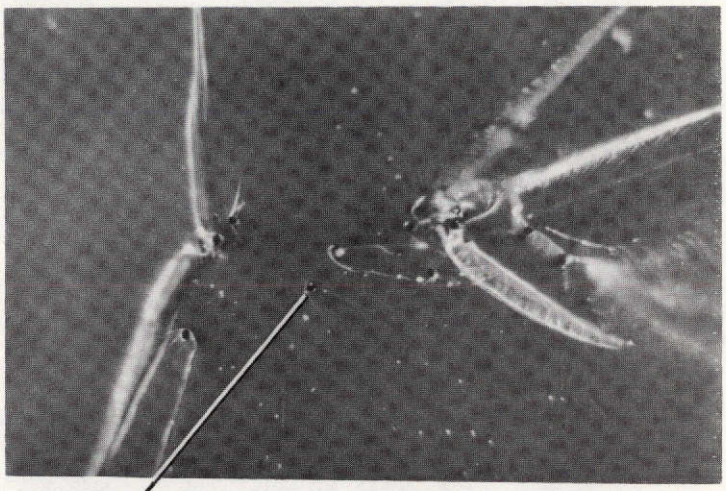

a) Fracture Surface 150 X

Fracture Source

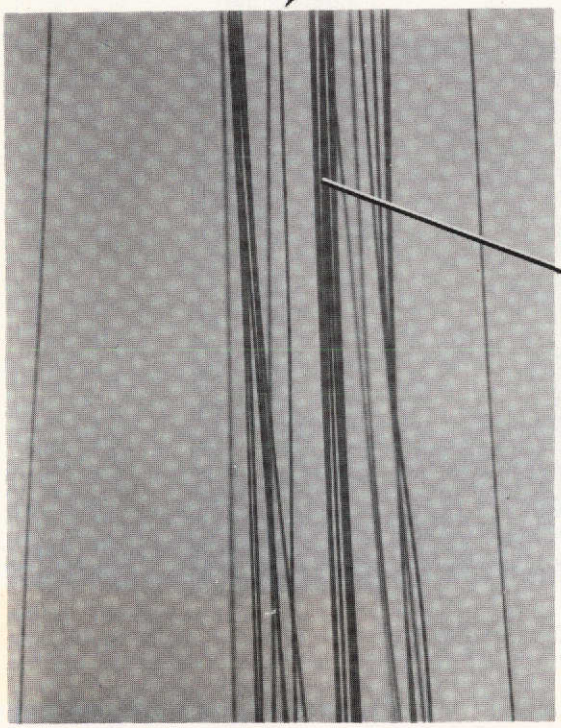

b) Profile Showing Source 60 X

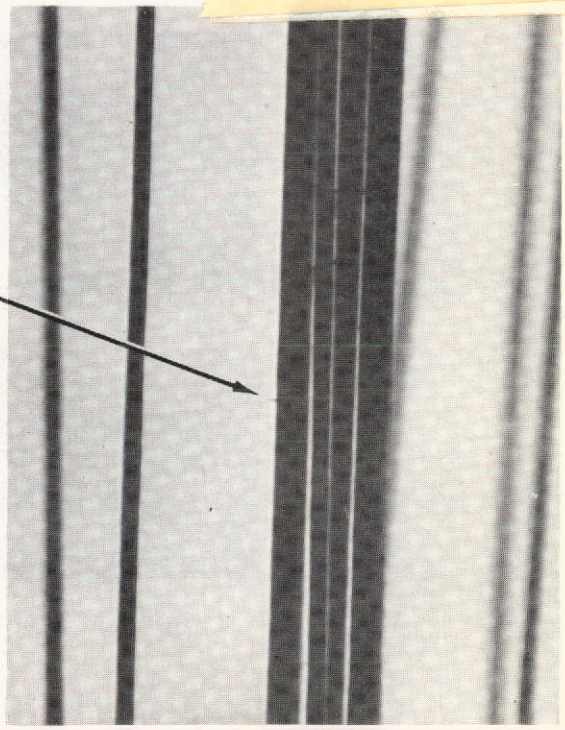

c) Small Resin Cracks in Closely Spaced Fibers 270 X

Figure 12. Tensile Fracture Mechanisms for HTS Fibers in Unmodified Epon 828 Resin

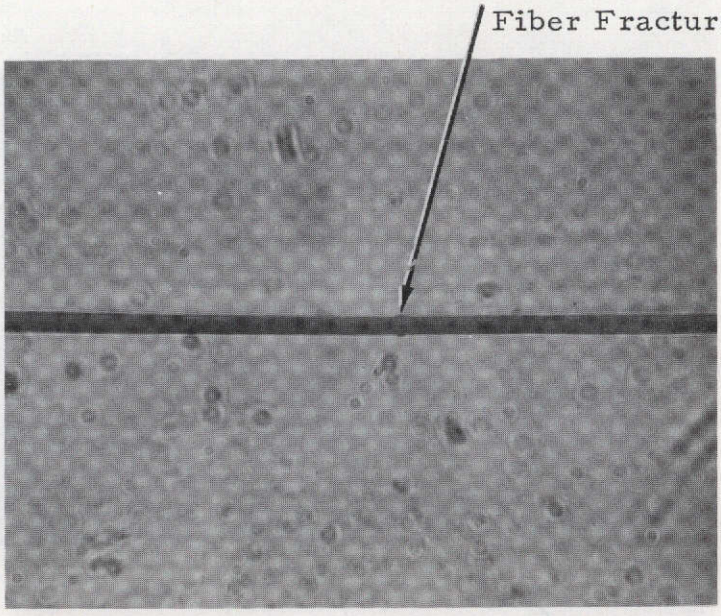

300X

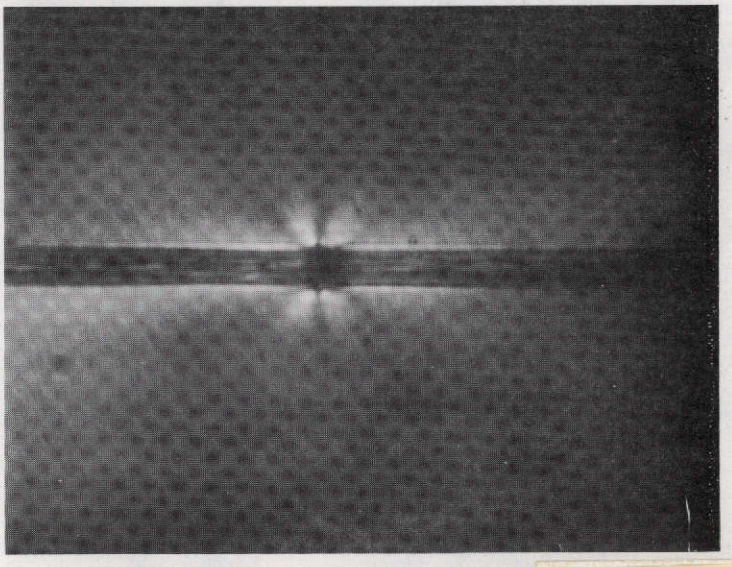

600 X Polarized Light

Figure 13 Fiber Fracture in a Microfracture Specimen Consisting of a Single HT-S Carbon Fiber in Unmodified Epon 828 Resin and Tested in Tension

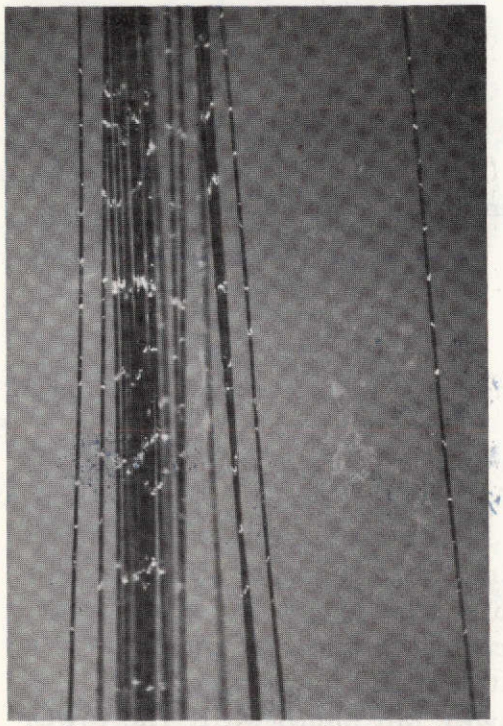

a) Compression Failure 60 X

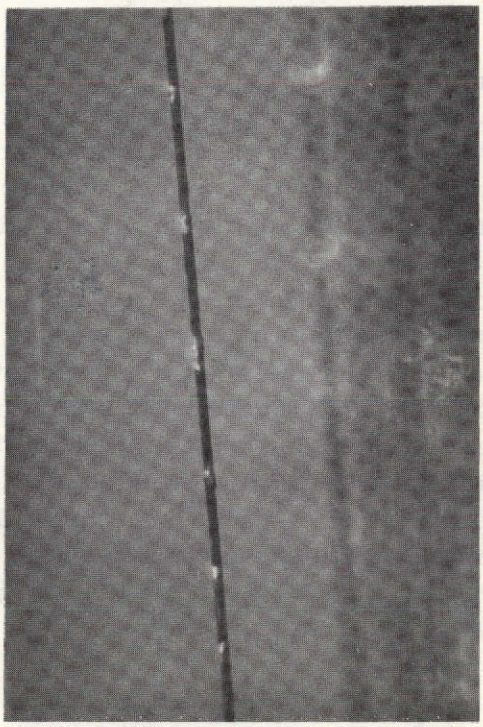

b) Local Fractures 150 X

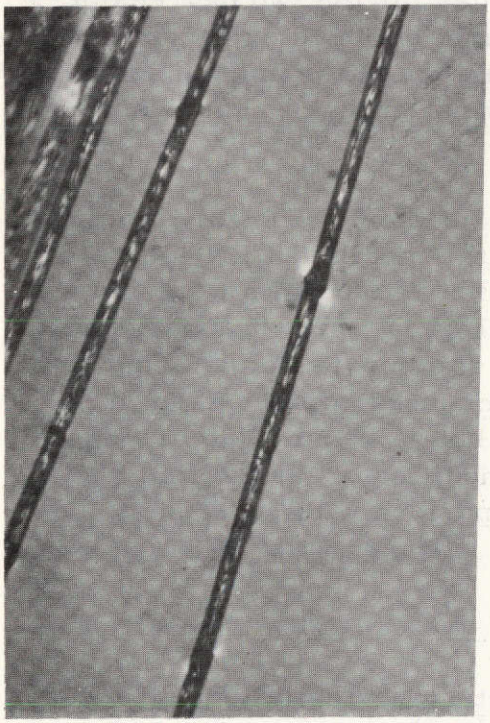

c) Viewed Under Polarized Light 375 X

Figure 14. Typical Compression Failure Mechanisms for HTS Fibers in Unmodified Epon 828 Resin

bond which causes tensile failure in the resin at about 45° to the fiber axis as the fiber ends move together at the break. However, similar fracture patterns could be due to brooming of the fiber ends and subsequent resin crazing at the interface.

3.2.3 Effect of Resin Modification

Compression tests were also conducted in the modified Epon 828 resin formulation at two levels of modification. The upper photos in Figure 15 show typical local fracture mechanisms in the resin modified to obtain a 12% elongation. Note that the uniform dispersion of fiber fractures is quite similar to that of the unmodified resin shown in Figure 14. However, there is much evidence of local debonding in the modified resin and in the upper right photo of Figure 15 it is clear that new fiber ends have sheared past one another at several locations. In the lower photos of Figure 15 we see that the local compressive failures occurred during the last 10% of the load range. Only a few very localized failures are evident in the lower left photo while the lower right photo at final fracture shows numerous fiber fractures which have their ends sheared past one another. It appears from these photos that there is no significant difference in compressive failure modes for the two degrees of resin modification. However, there does appear to be more evidence of interfacial debonding in the modified resin of Figure 15 than in the unmodified resin of Figure 14, although the difference is probably not enough to cause a major change in gross fracture modes.

Finally, a comparison was made of the more highly modified Epon 828 resin formulation (17% elongation) and the modified DEN 438 resin formulation (20% elongation) used in earlier work. The results were quite similar under compressive load and are shown in Figure 16. It appears that the local mechanical response of the HTS fibers in compression is about the same in each system. Further, a significant amount of compression in the fibers (either mechanically induced or as a result of a thermal excursion) should result in visible fiber damage in either modified or unmodified resin. This information now serves as a basis for comparison with subsequent observations on thermally cycled specimens.

3.2.4 Acoustic Analysis of Failure Modes

The use of acoustic emission in studying the failure processes in carbon epoxy composites, as well as the equipment and techniques used in the Space Sciences Laboratory, have been fully detailed in the report of the previous year's work [4]. For studying the mechanical behavior of model specimens, however, several changes and/or simplifications in procedure have been made.

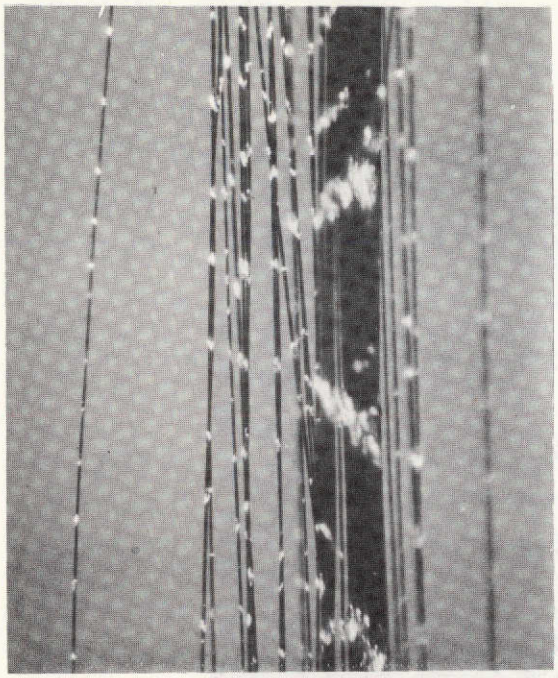

Ultimate Load 60 X

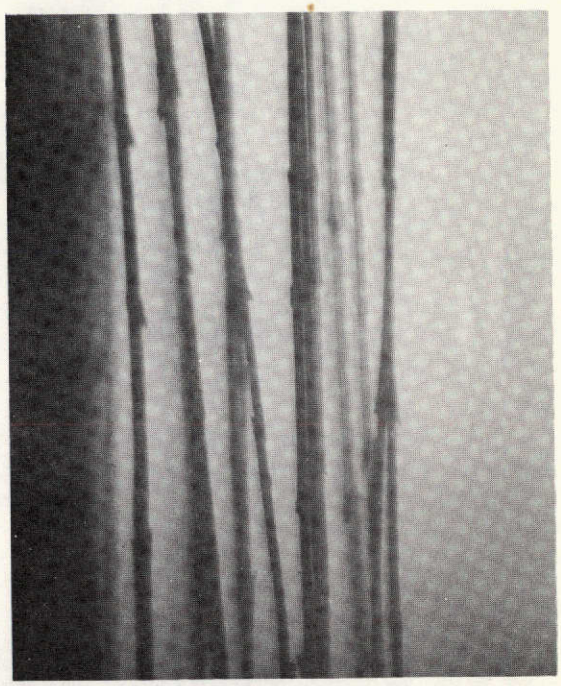

Ultimate Load 150 X

a) Compression Failures in Modified Epon 828 (12% Elongation)

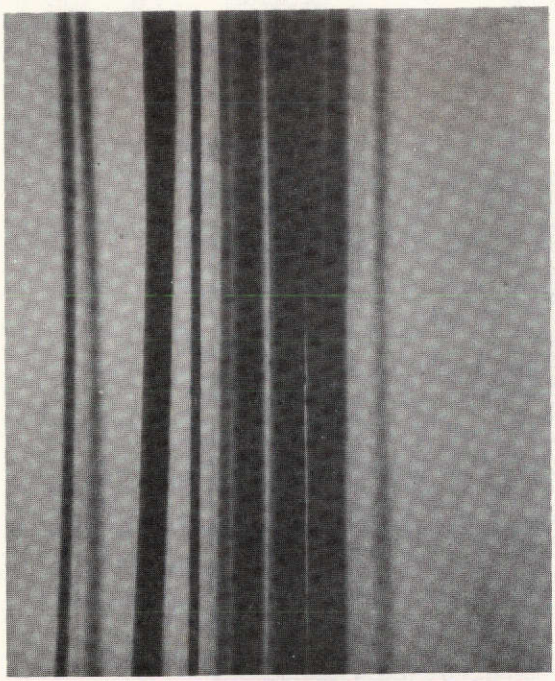

90% of Ultimate Load 150 X

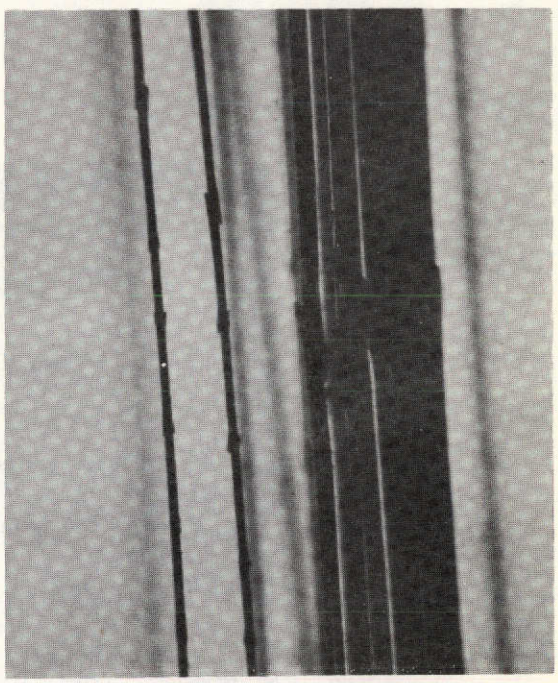

Ultimate Load 150 X

b) Compression Failure in Modified Epon 828 (17% Elongation)

Figure 15. Comparison of Compressive Failure Mechanisms for Epon 828 at Two Levels of Modification

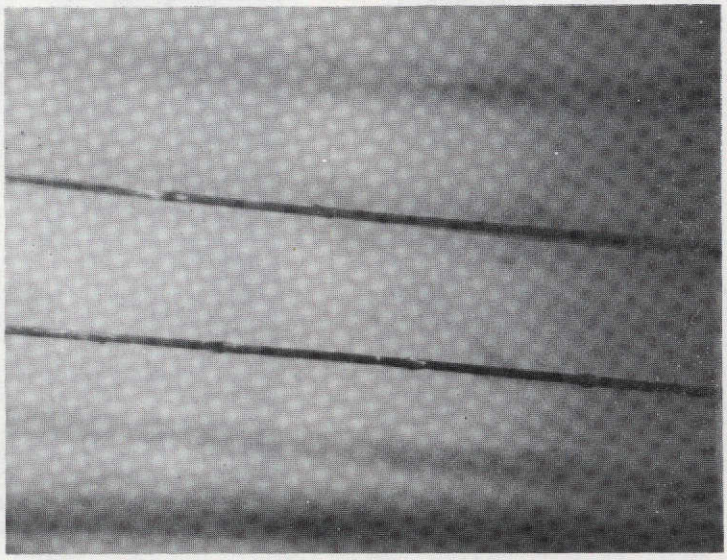

a) Local Compression Failures for HTS Fibers in Modified Epon 828 Resin (17% Elongation)

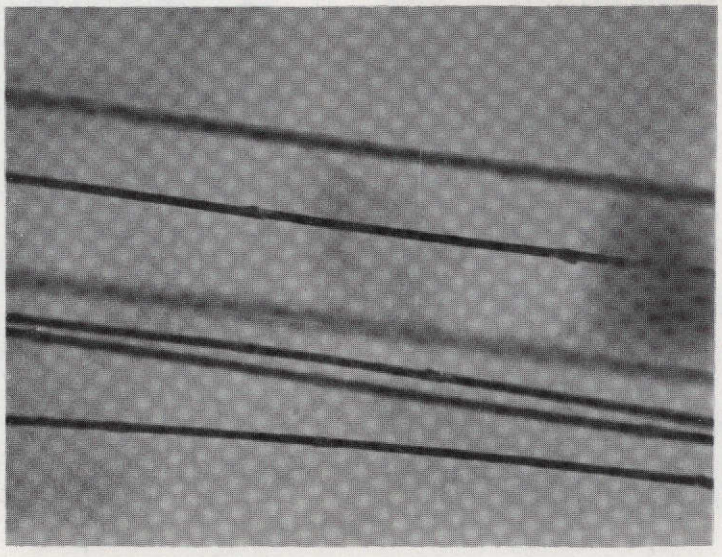

b) Local Compression Failures for HTS Fibers in Modified Epoxy Novolac (20% Elongation)

Figure 16. Comparison of Typical Compression Behavior of Epon 828 and Epoxy Novolac in Modified Form

1. Model Composite Failure Mechanisms

The first change involved a much simpler gripping system. For heavily reinforced composites, spurious acoustic signals emanating from the grips are a major problem. However, for the model specimens, when the volume fraction is less than 1.0%, grip noise was not found to be a problem at amplifier gains of 65 db. The specimens were held in smooth-faced steel lined Instron air grips, and based on tests of pure resin, no emissions in the 40-50 KHz range (the range where fiber fracture induced transducer resonance occurs) was found. Apparently, the contact of steel on Epon 828 is acoustically quiet. The same effect was found in compression. When tests were run on unreinforced resin compressed between steel platens, no significant acoustic emissions were noted. This is in marked contrast to the case of metals or ceramics.

The second change involved an improvement in the counting of individual acoustic events. As explained in the previous final report,[4] ordinary counting methods "count" each event many times, depending on the amplifiers discriminator level and the shape of the damped sinusoidal signal. For the present case of model specimens, where a relatively small number of total acoustic events precede failure, it was found possible to count each individual event approximately once. This was accomplished by using the + gate output from a Tektronix 545B oscilloscope. The controls were adjusted so that each time an incoming signal exceeded $\pm$ 75 mv, the oscilloscope was triggered. The original data were recorded on tape using a gain setting of 65 db. The sweep rate was 50 msec/cm, which was chosen so a typical event occupied about 7 cm of the available 10 cm display. The gate output was sent to an amplifier which converted it into a +5 volt spike, and this in turn was fed into the RCL analyzer for counting.

There are three circumstances under which an individual event will be either not counted or counted more than once. An individual acoustic event obviously will not be counted if the signal amplitude level is too low to trigger the oscilloscope. It is also possible that two events may occur so closely together than the second event cannot trigger the oscilloscope and hence will not be counted. Alternatively, if the signal level from an individual event is quite large and has a long delay time, it is possible that such a signal will trigger this oscilloscope more than once and the event will be counted more than once. As indicated earlier, when relatively few events are occurring, these three constraints are not too important.

To check this new counting procedure, a single carbon filament was encapsulated in an unmodified Epon 828 resin and the specimen was tensile tested to failure. Twenty-eight (28) acoustic events were recorded. The fiber was carefully examined after test and at least 22 fiber fractures were observed. Considering the difficulty in detecting some of these breaks, the agreement between acoustic events and visual fiber fracture is considered acceptable.

Another check of this counting procedure was performed. Shown in Figure 17 is a series of time delay oscilloscope photographs showing the acoustic events prior to failure of a tensile model specimen of HTS fibers in an unmodified Epon 828 resin. The individual events may be manually counted; there are about 28. The RCL analyzer counted 40 events. In all subsequent tensile model specimen work, therefore, it was assumed that each count from the analyzer represented a single fiber break.

Acoustic emission of compression model specimens proved difficult to interpret. Sharp individual events like those detected in tension were not found. Several low level events did occur, but they were barely detectable and did not always correlate with optical examination at the interrupted loading intervals used. Similarly, evidence of damage was observed optically which was not detected acoustically (the reverse was true in tension). Evidently, the energy released in fiber compression failure is much less than in tension, even if the failures occur in fairly large groups.

2. Engineering Composite Failure Mechanisms

Although there is a good deal of variation in the total counts recorded from one test to another, it appears that thermal cycling of 55 V_f composites tends to decrease the scatter. This is probably due to the stress relieving effect which thermal cycling seems to provide up to 250 cycles. Note that the total counts vary between 800 and 2650 for the 55 V_f specimens before cycling but after 250 cycles the total counts range is 1500 to 1800. With the highly stressed sites relieved by thermal cycling it appears that more consistent total counts to failure result on subsequent flexural testing to failure.

The 25 V_f composites show a similar change in comparing the uncycled behavior to that obtained after 250 cycles. However, further cycling to 500 cycles tends to result in more counts to failure and more scatter as shown by the solid circles in Figure 18. This seems to indicate damage to the fibers or interface which results in more noisy sites giving more acoustic activity even though the strength is somewhat improved. These data do support to some degree the model proposed earlier for mechanical behavior of thermally cycled composites.

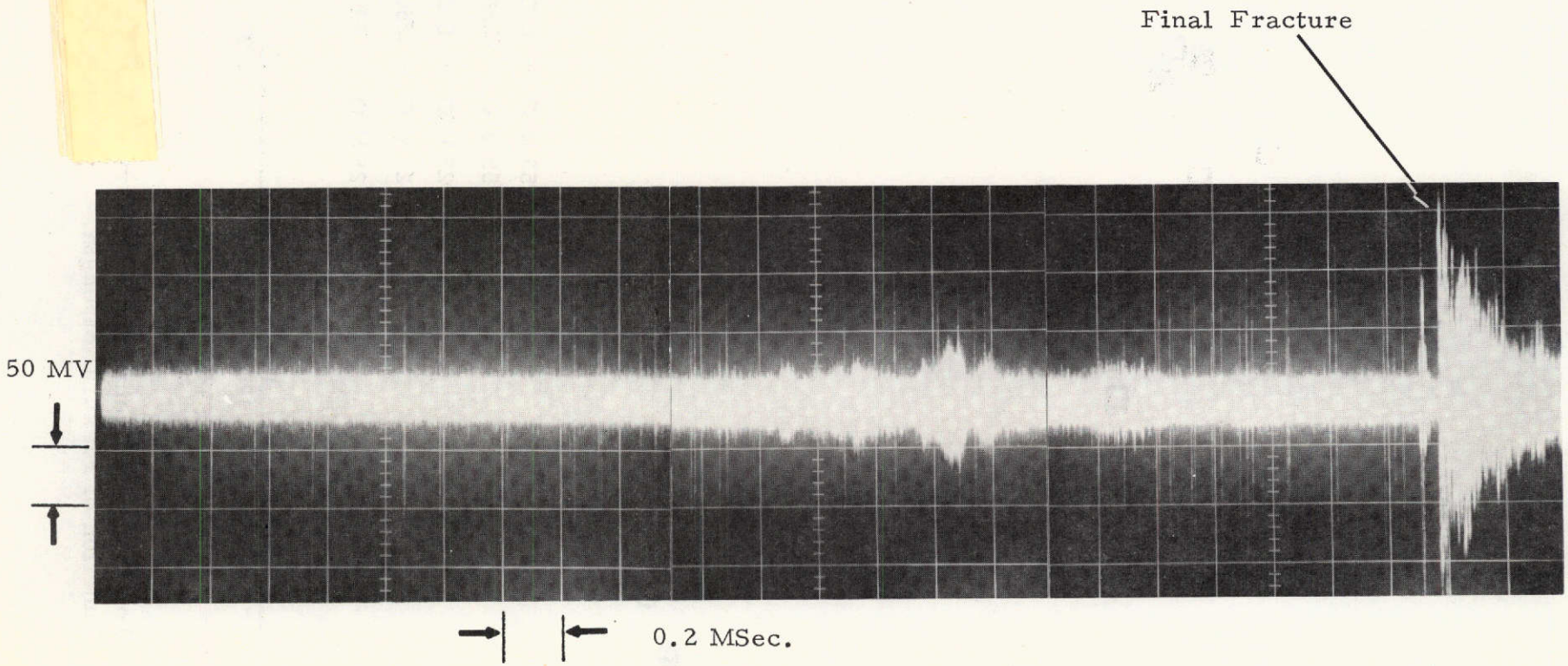

Figure 17 Photograph of Oscilloscope Record of Failure Sequence in Microfracture Specimen HTS-R3. There are about 38 Discernable Fiber Fractures Prior to Final Fracture

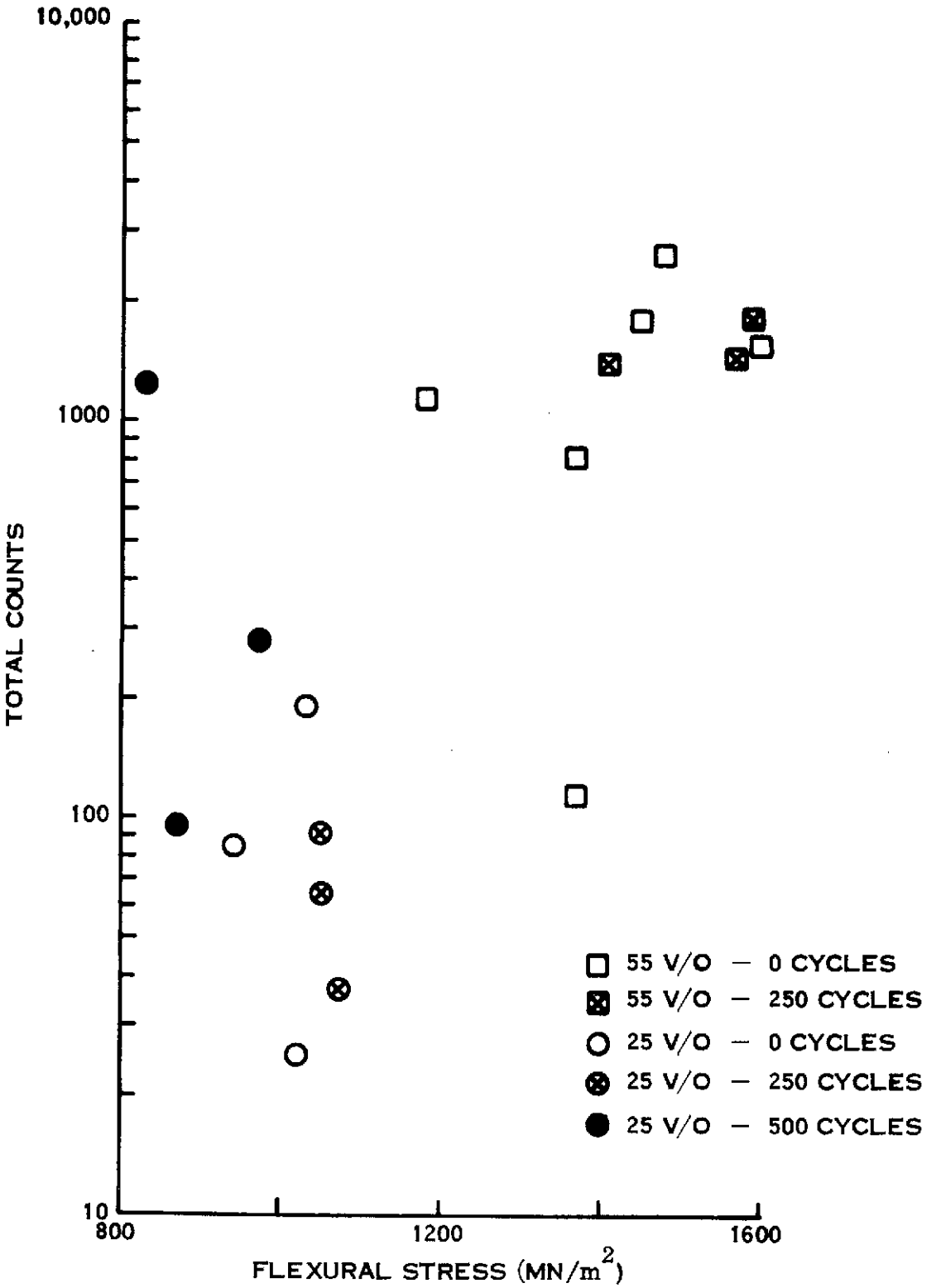

Figure 18. Total Acoustic Emissions for Carbon-Epoxy Composites as a Function of Flexural Strength.

Figure 19 shows a typical acoustic response for a 25 V/O carbon-epoxy flexure specimen after 250 thermal cycles.

Preliminary work toward acoustic monitoring of composite specimens during thermal cycling indicated that the thermal cycling chambers produced far too much noise to allow such work to be performed in it. Relay contacts making and breaking the solenoid valve opening and closing, and the nitrogen gas flow all combine to produce excessive background noise. The cold chamber of the fast thermal cycling rig proved to be acoustically quiet; however, thermally induced failures were compression failures and it was difficult to detect such damage with our standard acoustic emission techniques.

3.3 Thermal Cycling of Model Specimens

3.3.1 Experimental Procedure

During this quarter, thermal cycling tests were conducted in a hot-cold chamber manufactured by the American Instrument Company, shown in Figure 20 and in a special facility described below. The chamber has internal dimensions of 50.6 cm x 17.8 cm x 71 cm deep (20" x 7" x 28"). Heat was supplied by Calrod heating elements, and cooling by metered liquid nitrogen. A West program controller cycled the box between 220°K and 422°K (-65°F and +300°F), with a heating and cooling rate of the order of 8.1°K/min. (14.6°F/min.) and a five minute heating period at the temperature extremes. The box could be continuously cycled for about 20 hours before the liquid nitrogen had to be replaced. Specimens were placed in the bottom of the box and the control thermocouple was placed near them.

In addition to the facility described above, a second cycling facility was constructed to allow a smaller number of specimens to be cycled faster and also to subject them to a greater thermal shock. In this case, the specimens were moved from a cold chamber at 220°K (-65°F) to a hot chamber at 422°K (300°F) by a solenoid operated air actuated hydraulic cylinder. The cold chamber was maintained at temperature by dry ice and a variable speed fan. The unit is shown in Figure 21. Again, about a five minute constant temperature hold period was maintained at the end temperature. Because of the mass of the ram and specimen

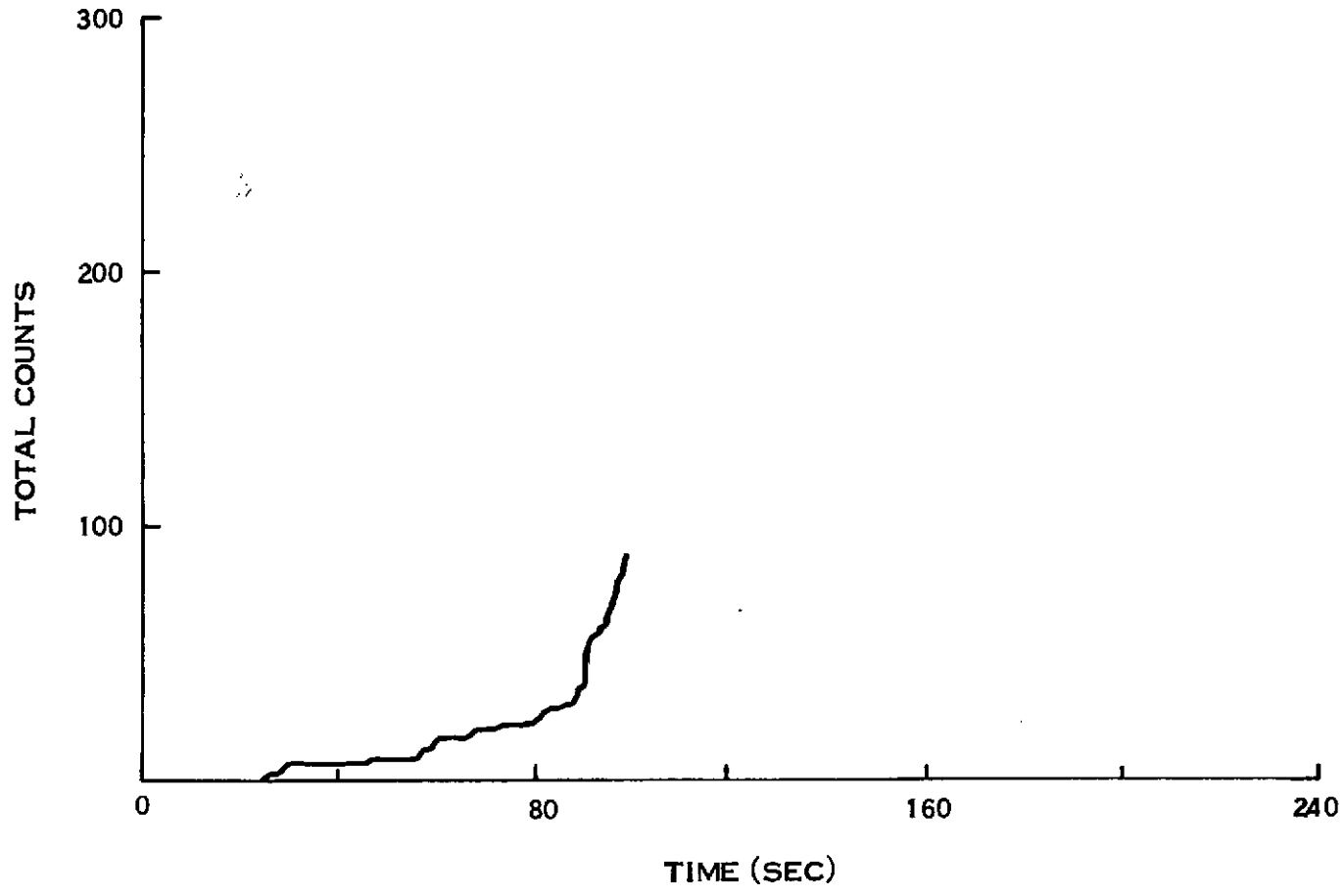

Figure 19. Typical Acoustic Emission Test Data for a 25 V/O, Carbon-Epoxy Flexure Specimen After 250 Thermal Cycles.

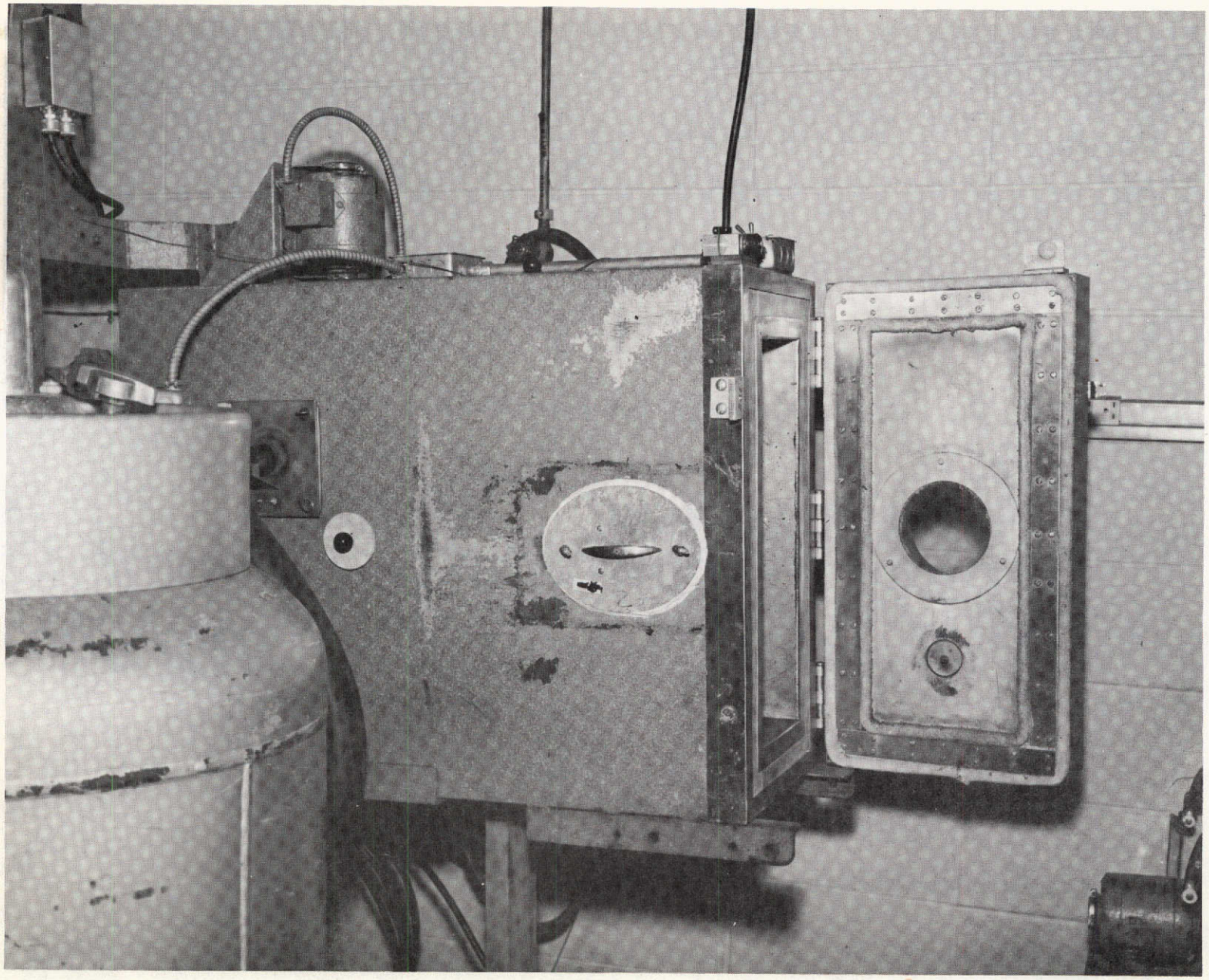

Figure 20. Photograph of Slow Thermal Cycling Facility

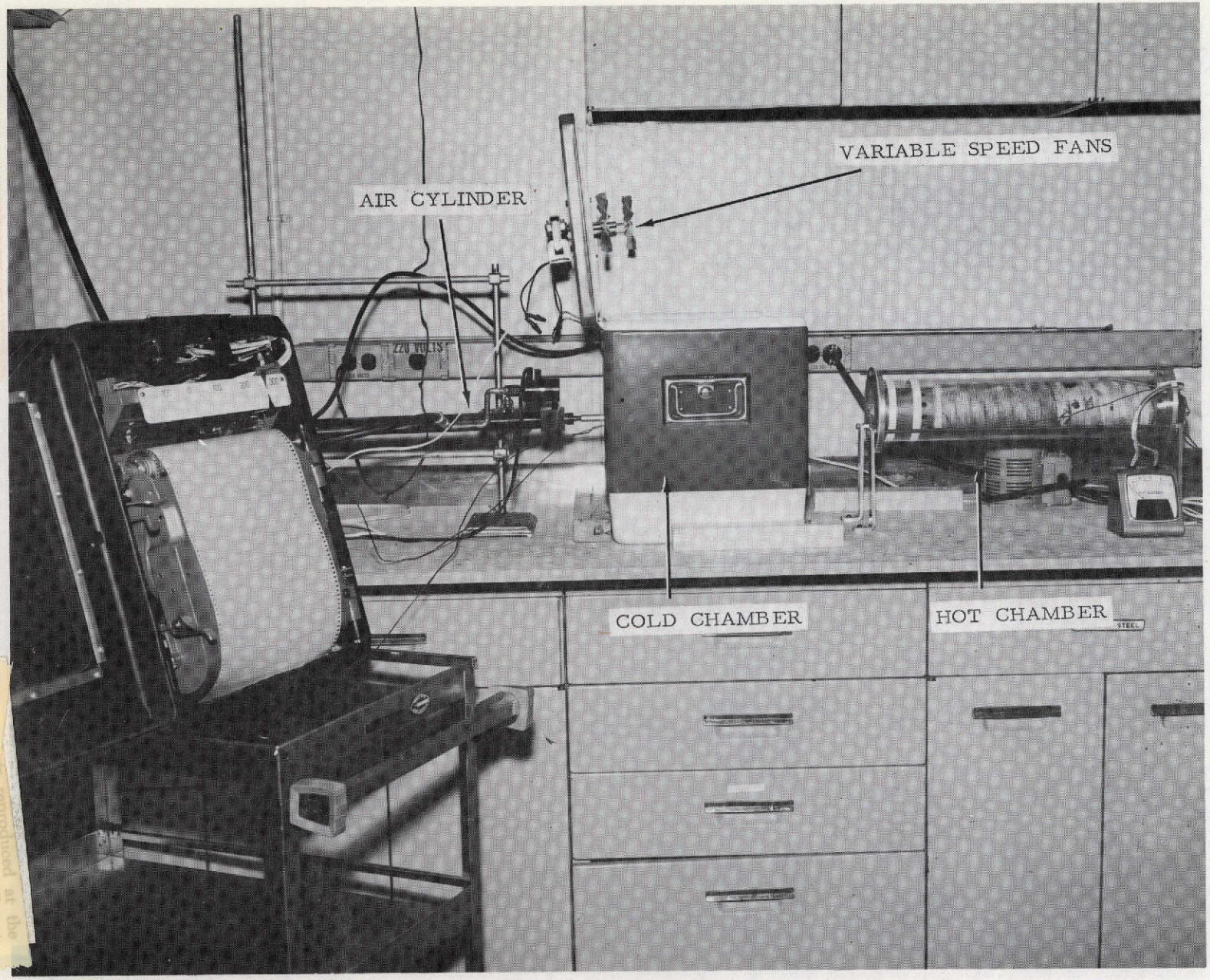

Figure 21. Photograph of Fast Thermal Cycling Facility

transport system, some time was needed for the temperature to stabilize at each extreme. Typical temperature cycles of both the hot-cold chamber and the more rapid system are shown in Figure 22. The increased severity of the thermal shock may be noted for the latter system.

3.3.2 Observations After Thermal Cycling

3.3.2.1 Model Specimens of Unmodified Resin

A number of model specimens were subjected to thermal cycling in the chamber and examined optically at regular intervals during this exposure to determine the nature and extent of local failure mechanisms. First experiments showed very little evidence of local damage, with only occasional interface debonding apparent at or near a fiber end. This first series of tests was conducted on the unmodified resin formulation which has a fracture strain of about 4% to failure.

Figure 23 shows some evidence of damage which occurred up to 50 thermal cycles in model specimens of HTS fibers in the unmodified Epon 828 resin. The upper photo shows what appears to be interfacial debonding over a very localized region on an individual fiber after 25 thermal cycles. Photo (b) shows the local stress concentrations which result at fiber ends from thermal cycling when viewed under polarized light. This birefringent response of the matrix near the fiber ends was observed after 35 cycles. Photo (c) shows a pointed end of a fiber in a model specimen which was thermally cycled 50 times. Because of the unique shape of the fiber end it was possible to locate and examine it optically at several intervals during thermal cycling. After 50 cycles the two small bright areas developed and appear to be either debonding or fracture and separation of the fiber.

It should be pointed out that these local anomalies were very difficult to find and difficult to photograph in the unmodified resin formulation. A much greater amount of local damage as a direct result of thermal cycling was anticipated at lower levels of cycling in the model specimens where relatively few fibers are subjected to considerable stressing by the bulk of resin.

Five additional model tensile specimens from the same batch tested previously were thermally cycled 250 times. At the end of this time the specimens were microscopically examined for damage. Observations made on one of the specimens showed debonding and fiber damage had occurred at regular intervals in 24 different locations within the gage section. Typical of the types of failures which occurred are shown in Figure 24. Note in photo (a) the compression type of failure in the single fiber as compared with the same type of damage within the group of fibers adjacent to it. Apparently the energy released by the single fiber

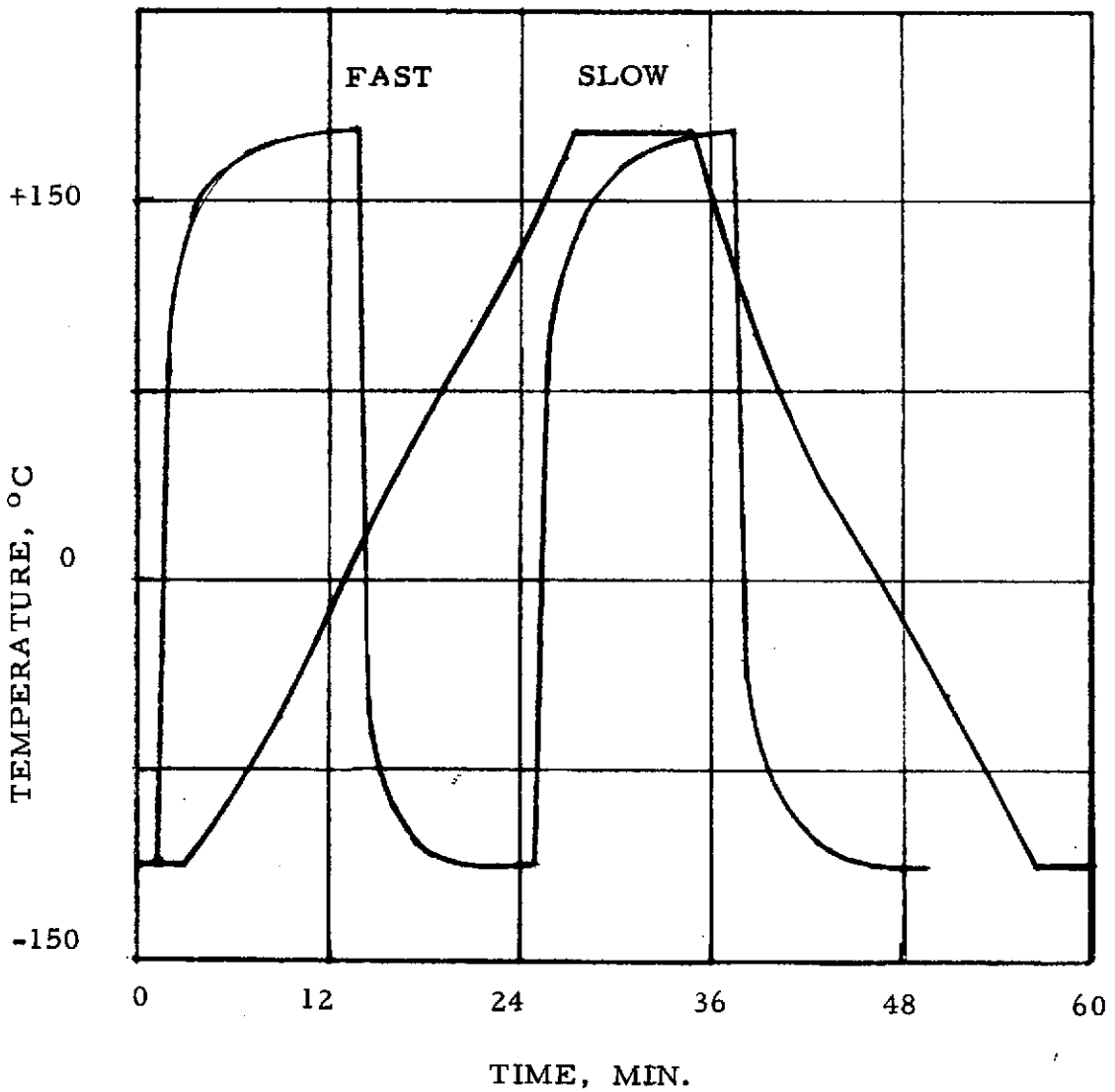

Figure 22. SCHEMATIC OF THERMAL CYCLES FOR TEMPERATURE CYCLING SYSTEMS

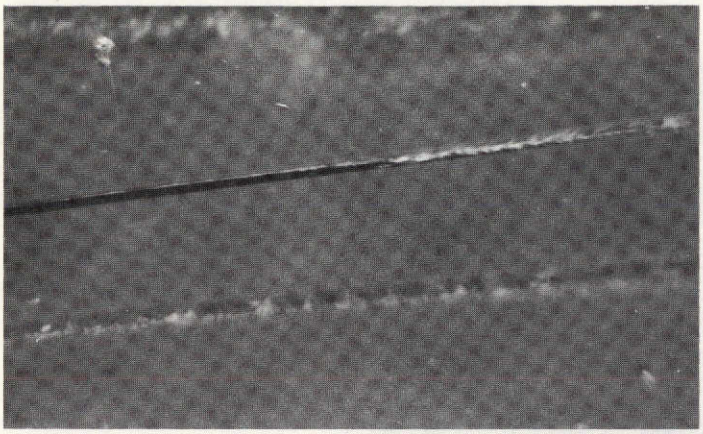

a) Apparent Local Debonding After 25 Cycles 150 X

b) Stress Patterns at Fiber Ends Under Polarized Light After 35 Cycles 390 X

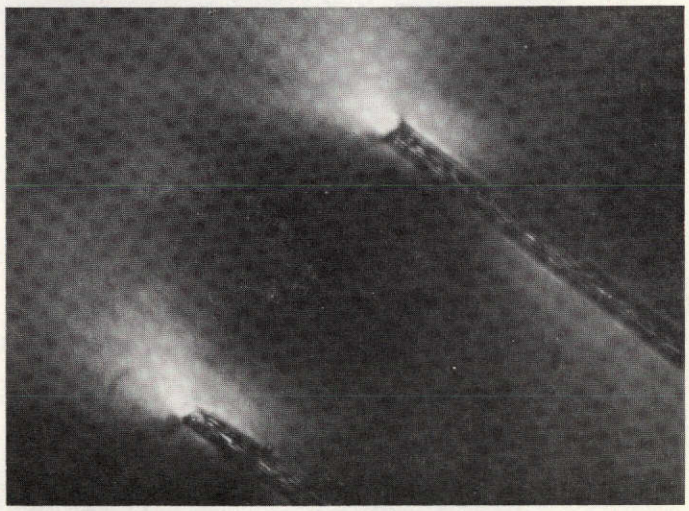

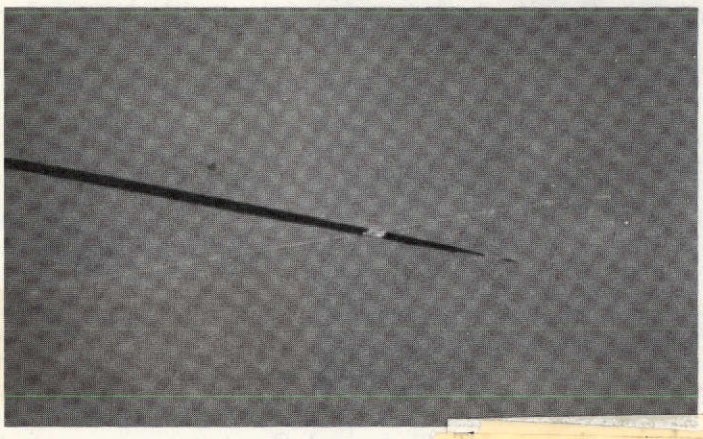

c) Apparent Local Interface and Fiber Fracture After 50 Cycles 150 X

Figure 23. Observations on Microfracture Specimens After Exposure to Thermal Cycling Conditions

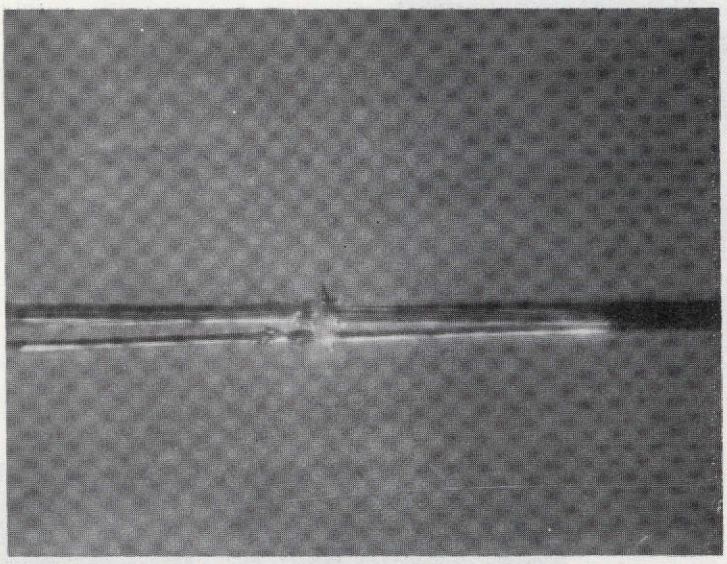

(a) Local Debonding and Fiber Fracture After 250 Thermal Cycles - 150 X

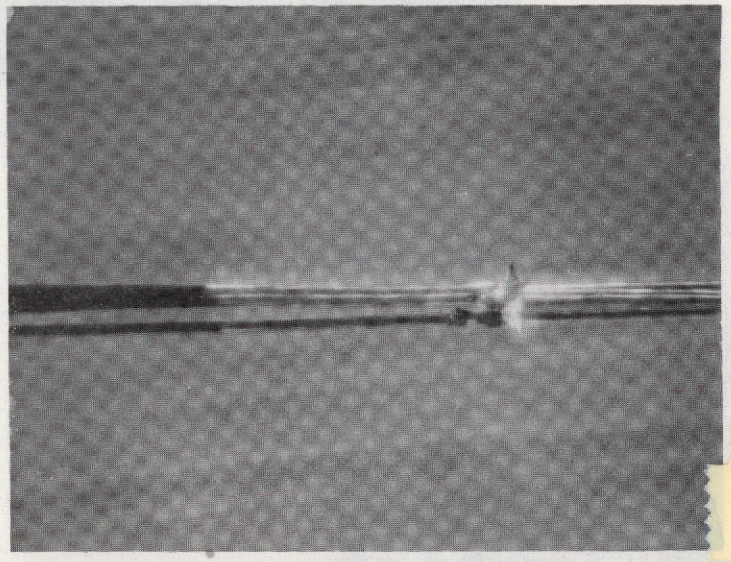

(b) Local Debonding and Fiber Fracture After 250 Thermal Cycles and Tensile Test - 150 X

FIGURE 24. Comparison of Model Specimen Behavior After Exposure to Thermal Cycling (-54°C to +149°C) and Mechanical Test.

due to compression was not sufficient to damage the matrix around it. On the other hand, the adjacent bundle of fibers which were in compression provided sufficient resistance to the tensile forces of the matrix, causing matrix failure. The behavior of the model specimen during thermal cycling may be explained by the behavior of the neat resin under load during heat deflection test. As was discussed in Section 3.1, thermal cycling of the unmodified resin to 250 cycles destroyed some of the primary valence bonds during the early stages of test, and thus weakened the polymer structure. Since in the model specimen the compression forces on the fibers and the tensile forces of the resin were behaving in a manner similar to fatigue testing, the primary valence bonds were probably being broken in a cumulative manner and the slope of the curve between 50 thermal cycles and 250 thermal cycles is linear. Despite the damage resulting from thermal cycling, the tensile strength of the model specimen was the same (8×10^3 psi) as the strength of the neat resin casting before thermal cycling. Photo (b) shows the same damaged area as shown in photo (a) after tensile testing. This area appeared unchanged after tensile testing as did many others, which indicates that stress was relieved in the areas. The specimen failed in an area immediately adjacent to those shown in Figure 24. The correlation which is believed to exist between pre-cycled and post-cycled resin castings and model specimens, with regards to HDT, provides another area which should be investigated in engineering composites, and which should include extending the number of thermal cycles to about 1000.

3.3.2.2 Model Specimens of Modified Resin

The resin formulation was modified to yield a 12% fracture strain and a 17% fracture strain. This would result in a lower strength but much more crack resistant resin with a higher thermal expansion coefficient. Immediate evidence of thermal cycling damage was observed for model specimens containing HTS fibers in the resin modified to a 12% fracture strain. This is evident in the photographs of Figure 25. The upper photo shows typical pretest condition of the fibers with no visible damage. The middle photo (b) shows fractured fibers and accompanying matrix damage after 15 fast cycles. The bottom photo (c) shows a single fiber fracture under polarized light and at higher magnification. Note the highly stressed resin area under polarized light near the fiber break. In every instance the fracture of the fibers appears to be due to compression with broken ends sheared past one another at several locations. These observations are entirely consistent with the postulated failure mechanisms discussed in Section 2.1. Similar observations were made on a model specimen containing more closely spaced fibers in the resin modified to a 12% fracture strain. Figure 26 shows typical thermally induced fractures for closely spaced fibers with the upper photo(a) clearly indicating fan-shaped resin cracks and the lower photo (b) showing clear evidence of interfacial debonding and fiber buckling. These specimens were also exposed to only 15 fast cycles when the damage was observed.

a) Typical condition of fibers prior to thermal cycling 150 X

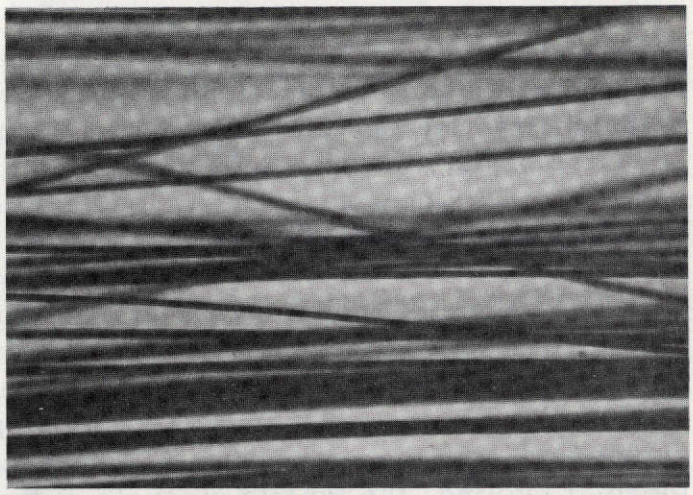

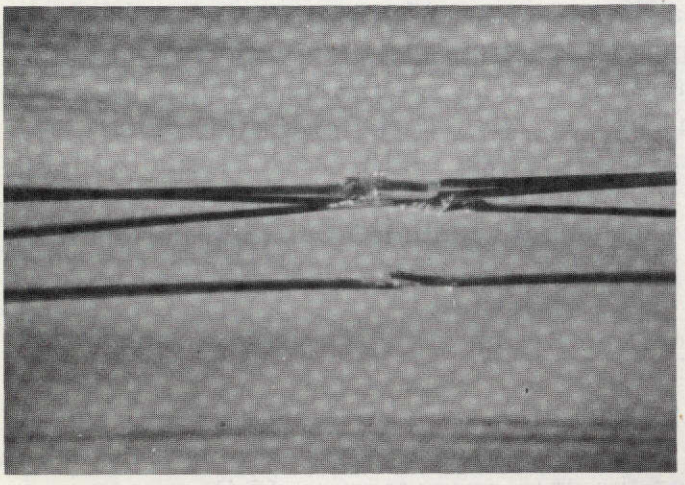

b) Typical damage after 15 fast thermal cycles 150 X

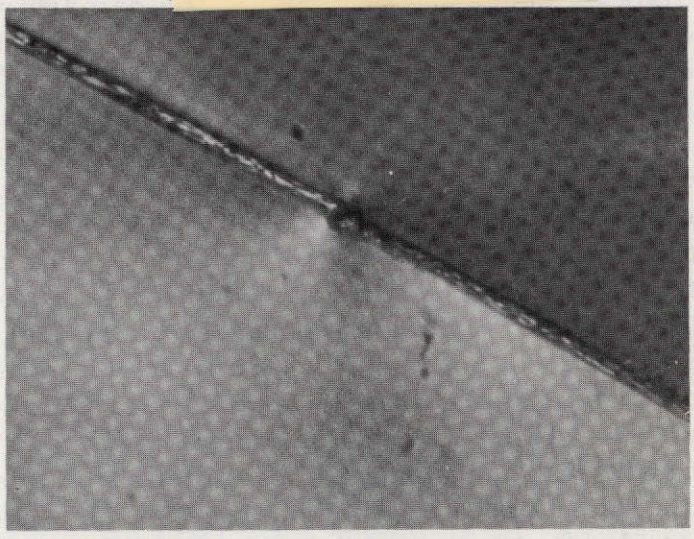

c) Single fiber fracture under polarized light after 15 fast cycles 315 X

Figure 25: Effect of Fast Thermal Cycling on Model Specimen of HTS Fibers in Modified (12% Elongation) Epon 828 Resin

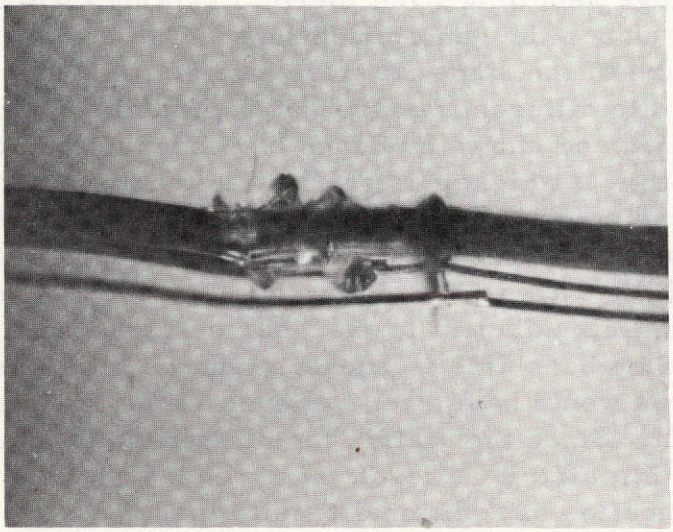

a) Local Damage After 15 Fast Thermal Cycles - 150 X

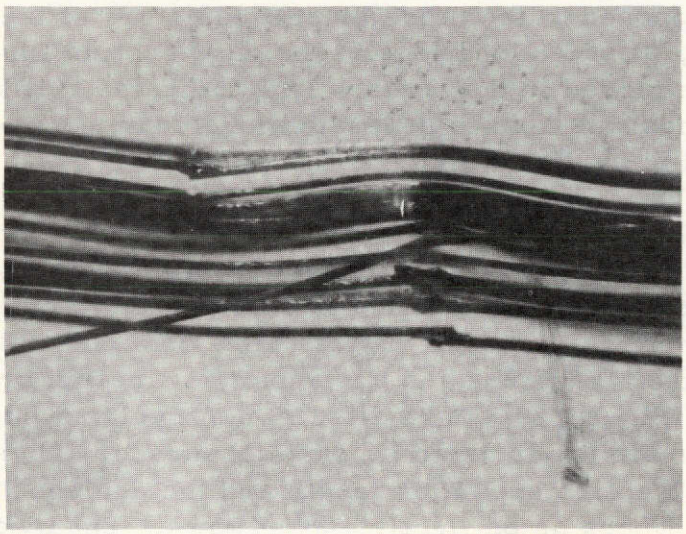

b) Local Fiber Buckling and Debonding After 15 Cycles - 150 X

Figure 26 Effect of Fast Thermal Cycling on Model Specimen of HTS Fibers in Modified (12% Elongation) Epon 828 Resin

Because the proximity of the fibers seems to affect the nature and extent of the damage resulting from thermal cycling, it was decided to examine a tightly packed tow under the same conditions. The results are shown in Figure 27. All three photos are of the same fracture site but they are focused on different areas to demonstrate different features of the fracture. The closely packed tow fails in compression and shows evidence of debonding adjacent to the failure region (upper photo). At higher magnification (photo b) we see resin crazing in fan-shaped patterns on or near the interface. The most interesting aspect of the tightly packed tow experiments is the large disk shaped crack shown in profile in the bottom photo (c). This is caused by the very concentrated tensile stresses generated in the matrix adjacent to the fiber because the tightly packed fibers did not buckle. Had they been able to buckle as in the previous photos of Figure 26 the tensile stresses would have been relieved in the resin and no disc shaped crack would result. Since the matrix tensile stress is induced by the fiber, once the crack is initiated it relieves the stresses which generated it and will not grow without application of additional tensile load.

Besides the effect of fiber proximity there is some indication that the ratio of resin area to fiber area in a given cross-section can be significant in generating thermal cycling damage. Figure 28 shows two locations in a specimen prepared for tensile testing with a reduced cross section in the middle portion having an area about half that of the ends. The end sections showed the damage in the upper photo while the gage section showed no evidence of damage from thermal cycling. This is probably due in part to the closer spacing of fibers in the upper photo as opposed to the more dispersed nature of the fibers in the lower photo. However, at other locations in the gage section fibers were much closer and no damage occurred in that area. This indicates that the greater bulk of resin near the ends was able to generate more compressive load on the fibers and this resulted in earlier damage in those regions.

Because of the very apparent thermally induced damage which occurred when HTS fibers were encapsulated in the 12% elongation resin, a series of tests were performed on the same resin modified to obtain a 17% elongation. Similar but much more dramatic results were obtained. Both the frequency and severity of the fiber fractures and accompanying matrix cracks were increased. This is shown in Figure 29 where after 15 fast cycles a number of fracture sites like that shown in the upper photo (a) were observed. These occurred at regular intervals over the entire specimen length and the damage was as obvious on remotely spaced fibers as on tightly packed tows. The lower photo (b) shows a higher magnification of the damage after 30 fast cycles. Note the fracture and debonding of the bottom fiber and how far it is from the other fibers in the photo. The previous observations in the 12% elongation resin had not indicated such extensive damage in remote fibers. The extent of the thermal cycling damage is shown more clearly in Figure 30 where typical fast and slow cycling damage are

a) Typical fracture after 15 fast cycles 60 X

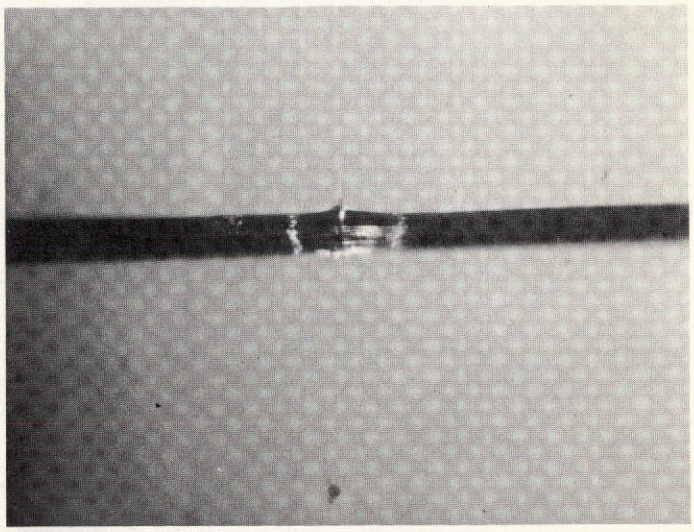

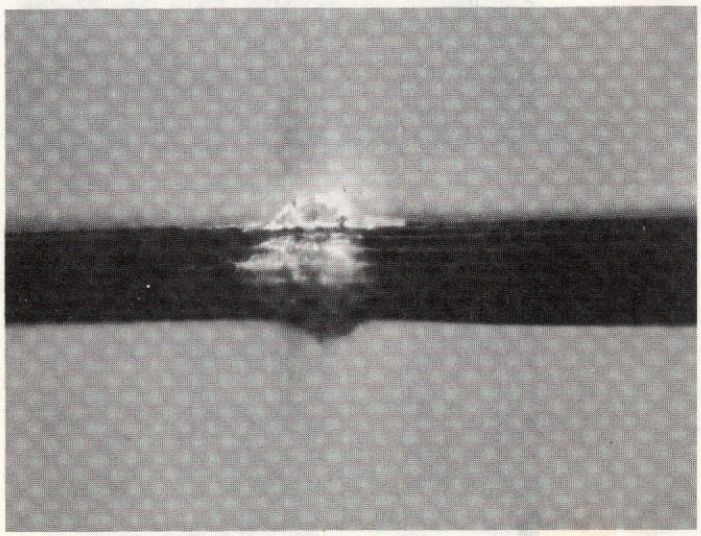

b) Same location at 150 X

c) Profile of matrix crack at some location 150 X

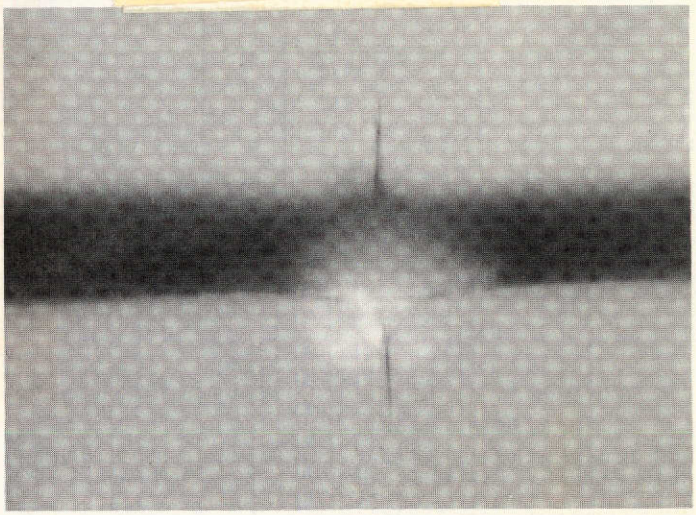

Figure 27: Tightly Packed Tow Fracture After Fast Thermal Cycling in Modified (12% Elongation) Epon 828 Resin

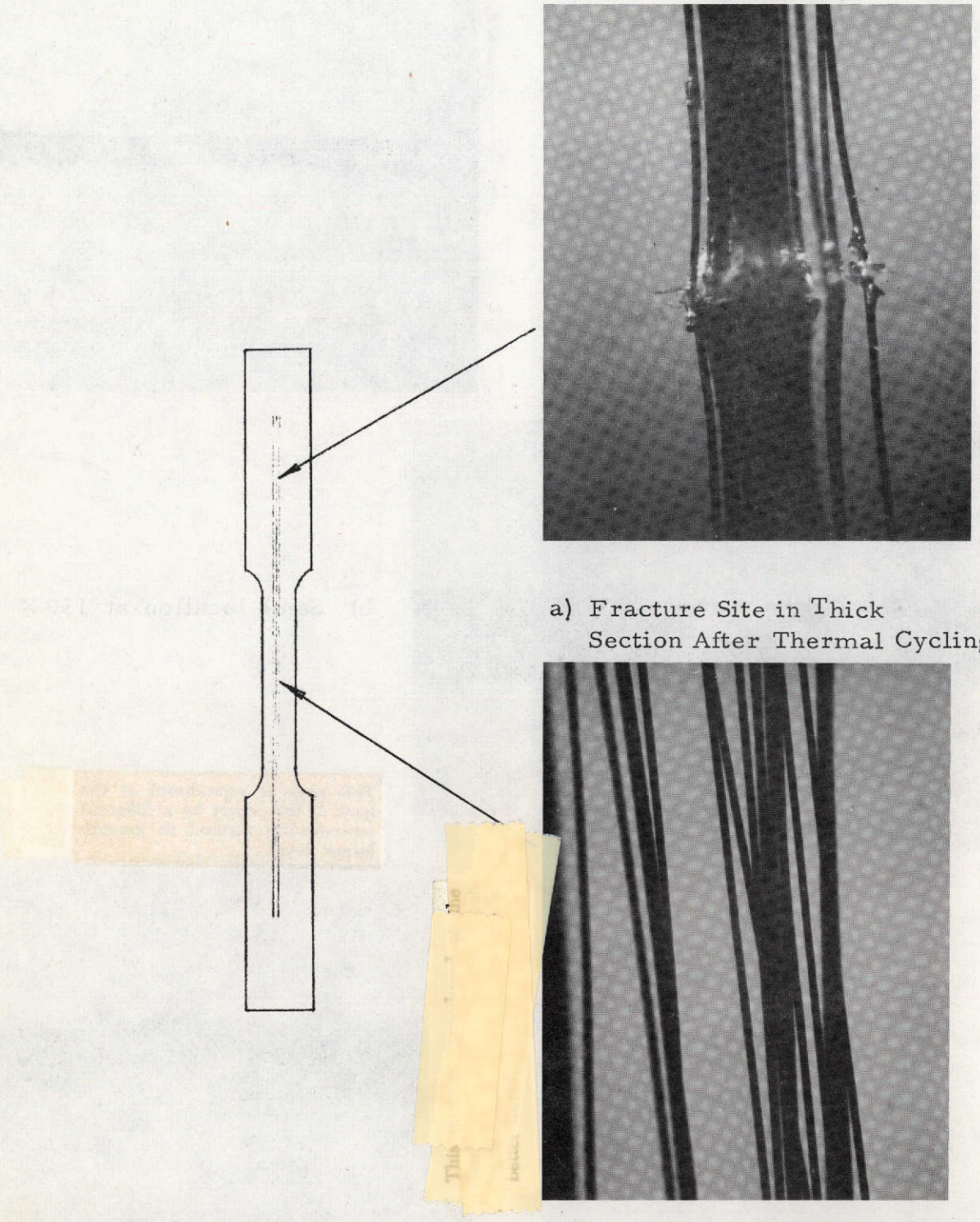

a) Fracture Site in Thick Section After Thermal Cycling 150 X

b) Typical Photo of Undamaged Fibers in Reduced Section 150 X

Figure 28 Effect of Specimen Cross-Section and Fiber Spacing on Thermal Cycling Damage for HTS Fibers in Modified (12% Elongation) Epon 828 Resin

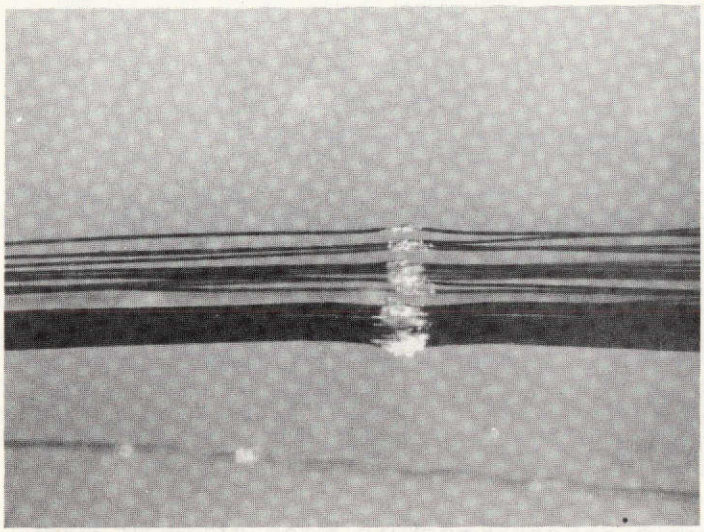

a) Typical Fractures After 15 Fast Cycles 60 X

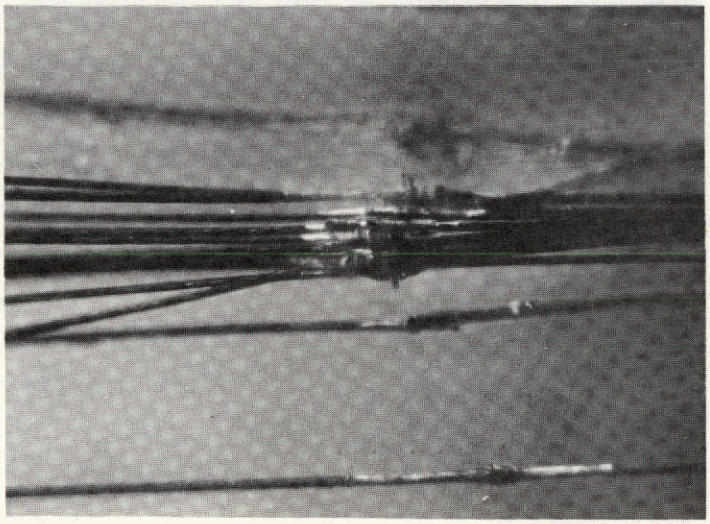

b) Typical Fractures After 30 Fast Cycles 150 X

Figure 29 Effect of Thermal Cycling on the Highly Modified (17% Elongation) Epon 828 Resin Formulations Containing HTS Fibers

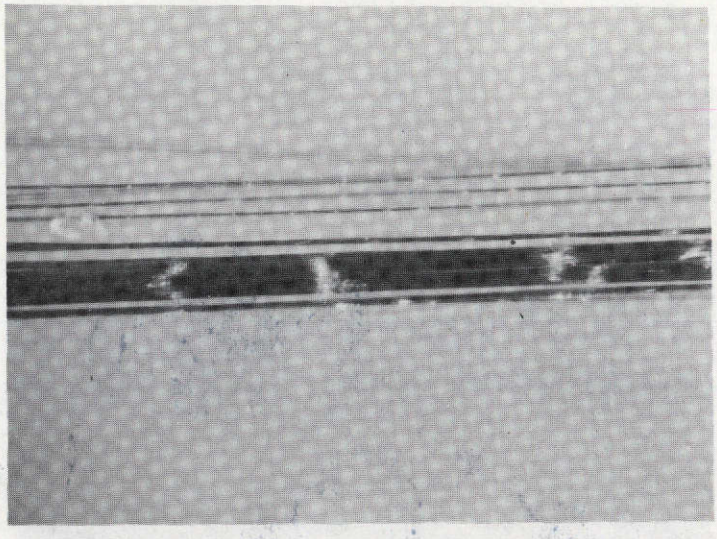

a) Uniformly Spaced Fracture Sites After 30 Fast Cycles 60 X

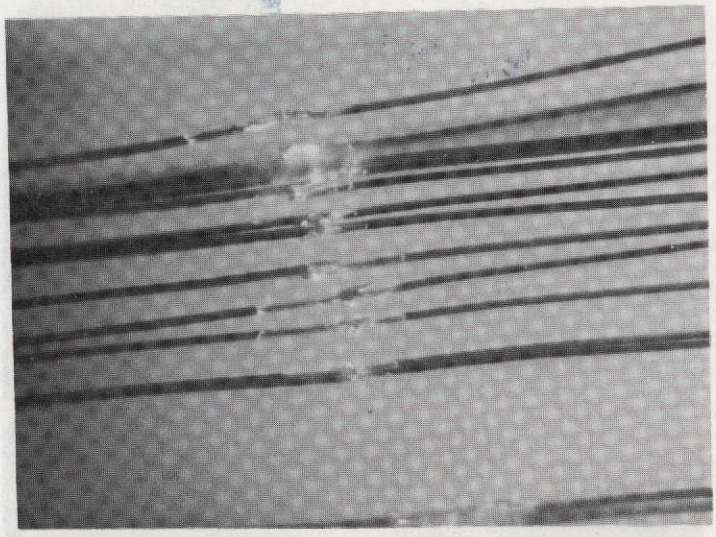

b) Typical Compression Fractures After 50 Slow Cycles 150 X

Figure 30: Comparison of Thermal Cycling Damage for Fast and Slow Cycling of Highly Modified (17% Elongation) Epon 828 Resin Containing HTS Fibers

compared for the 17% elongation resin formulation. Note in the upper photo of Figure 30 how the fracture areas are uniformly spaced on both closely spaced and remote fibers as evidenced by the bright spots. Higher magnification of similar damage sites generated by slow cycling are shown in the lower photo. In general there was no difference in the type of fracture mechanism induced by slow versus fast cycling. However, there does appear to be some evidence of earlier damage in the fast cycling mode than in the slow cycling modes.

3.3.3 Mechanical Response After Thermal Cycling of Model Specimens

3.3.3.1 Tensile Behavior

Following the thermal cycling treatment either utilizing the slow or fast apparatus, the model specimens were tested in tension as described in Section 3.2.1. Because sufficient confidence has been generated in the past on the ability of acoustic emission techniques to detect fiber fracture, the specimens were not interrupted to detect fiber and matrix damage. Rather, each test was monitored acoustically as outlined in Section 3.2.4. A plot was obtained for each specimen showing the cumulative number of fiber breaks (with the reservations discussed in Section 3.2.4), versus time (or strain). In addition, the ultimate stress, and modulus was tabulated for each specimen*.

Examining first the effect of thermal cycling upon the ultimate stress of the model specimens, the pertinent data are shown in Table VIII and Figure 31. These data show that the ultimate tensile strength is not affected by cycling up to 56 cycles. Within the limit of the data, this is true whether the specimens are cycled slowly or rapidly. The strength of the unmodified resin and the two modified ones are in the order described in Section 2.2.2.2.

Turning now to the effect of thermal cycling on the other tensile parameters, Table IX shows the strength (repeated from Table VIII), ductility, modulus, and total fiber breaks for each of the model specimens cycled. As in the case of the ultimate strength, there is no discernible effect of cycling on any of the tabulated properties. For example, the total number of fiber breaks (i.e., acoustic events) as a function of thermal cycles for all three resin formulations is shown in Figure 32. In spite of the spread of the data, it is clear that there is no correlation between total fiber fractures and degree of thermal cycling. Two typical individual test records showing the total counts (i.e., fiber breaks) as a function of stress in the composite are shown in Figure 33. The curves are tracings of

---

* The modulus value, taken as the initial slope of the stress-strain curve, underestimates the true value because the values were obtained from the cross-head record of the test. This procedure records machine deflection as specimen deflection. The same comment applies to the strain, except this value is overestimated.

TABLE VIII

EFFECT OF THERMAL CYCLING ON THE STRENGTH OF MODEL SPECIMENS

Thermal Cycling	Formulation					
	Unmodified (2.7% Elongation		Modified (12% Elong.)		Modified (17% Elongation)	
	Strength		Strength		Strength	
	MN/m^2	KSI	MN/m^2	KSI	MN/m^2	KSI
0	50.1	7.26	38.4	5.56	26.2	3.80
	49.3	7.14	38.8	5.62	31.7	4.60
					34.8	5.04
Avg.	49.7	7.20	38.6	5.59	30.9	4.48
10-Slow	48.0	6.95				
	49.9	7.23				
Avg.	49.0	7.09				
20-Slow	51.7	7.50				
30-Slow	46.0	6.67	40.0	5.80		
	45.5	6.59	41.4	6.00		
Avg.	45.8	6.63	40.7	5.90		
30-Fast			38.7	5.61	28.5	4.13
41-Slow	51.5	7.46	39.2	5.68		
	48.9	7.08	34.2	4.95		
Avg.	50.2	7.27	36.7	5.32		
45-Fast			35.5	5.20	25.2	3.65
50-Slow	52.0	7.54			32.8	4.75
51-Slow	50.8	7.36	40.0	5.80		
	49.5	7.17	36.8	5.34		
Avg.	50.1	7.26	38.4	5.57		
56-Slow			41.3	5.98	26.5	3.84
			37.9	5.49	28.1	4.07
Avg.			39.6	5.74	27.3	3.96

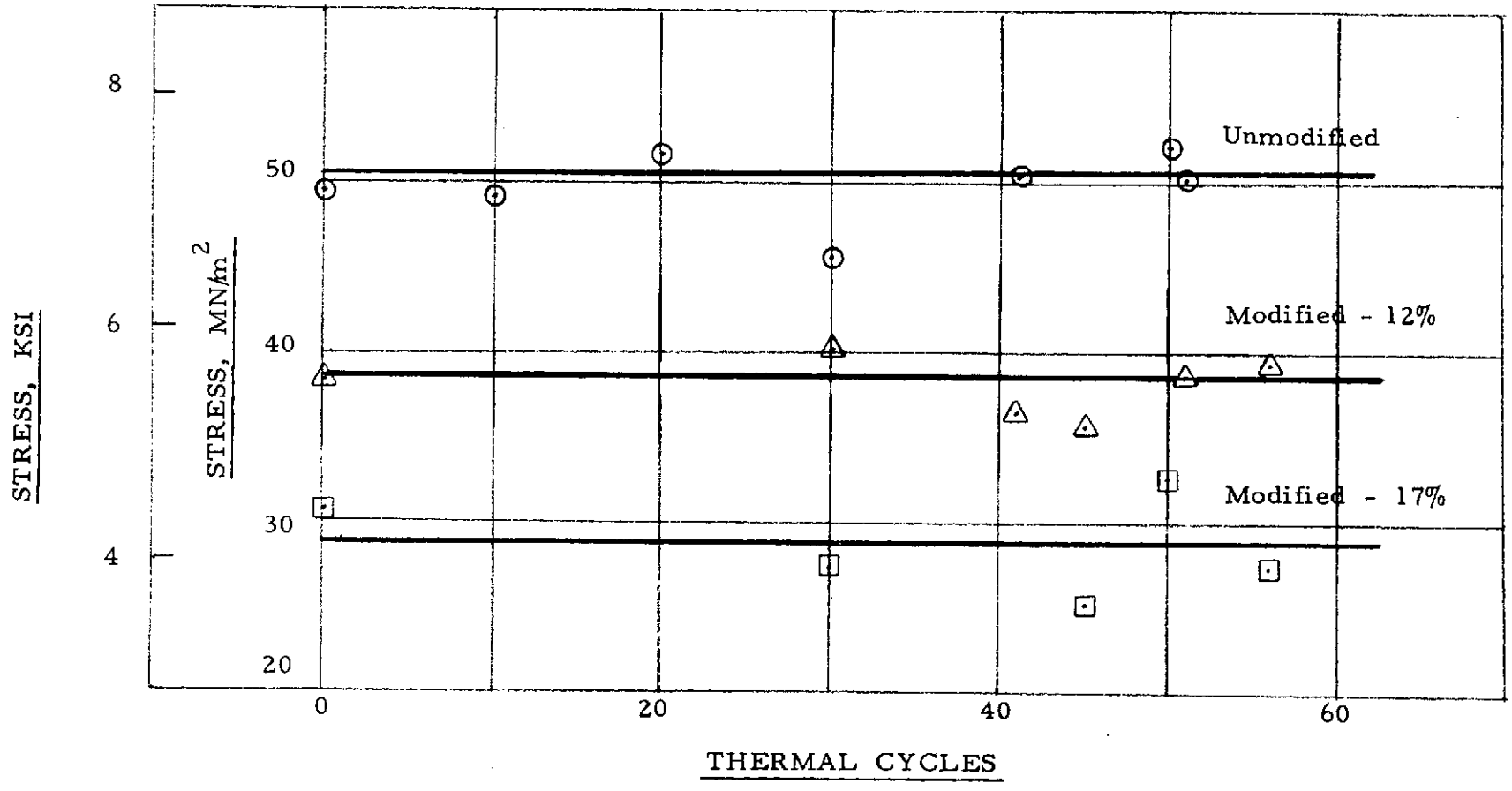

Figure 31. Strength of Model Specimen as a Function of Thermal Cycles

TABLE IX. TENSILE PROPERTIES OF MODEL SPECIMENS

Thermal Cycles	FORMULATION											
	UNMODIFIED				MODIFIED (12%)				MODIFIED (17%)			
	Strength MN/m^2	Ultimate Strain %	Modulus MN/m^2	Total Counts	Strength MN/m^2	Ultimate Strain %	Modulus MN/m^2	Total Counts	Strength MN/m^2	Ultimate Strain %	Modulus MN/m^2	Total Counts
0	50.1 49.3	2.7 3.1	1860 1587	80 115	38.4 38.8	2.6 2.6	1477 1490	70 40	26.2 31.7 34.8	3.0 6.2 9.5	876 512 366	125 680 430
10-Slow	48.0 49.9	3.17 3.73	1510 1340	140 250								
20-Slow	51.7	3.7	1400	240								
30-Slow	46.0 45.5	3.3 2.8	1410 1620	90 90	40.0 41.4	2.95 3.0	1360 1380	130 320				
30-Fast					38.7	4.6	842	100	28.5	3.9	731	55
41-Slow	51.5 48.9	3.7 3.3	1390 1480	110 60	39.2 34.2	3.5 3.2	1110 1080	350 41				
45-Fast					35.9	4.4	814	60	25.2 32.8	4.0 5.7	629 575	140 670
50-Slow	52.0	3.65	1430	40								
51-Slow	50.8 49.5	3.5 3.3	1450 1500	100 130	40.0 36.8	2.9 3.5	1380 1060	140 70				
56-Slow					41.3 37.9	4.2 4.0	980 945	180 80	26.5 28.1	3.7 3.6	718 780	85 370

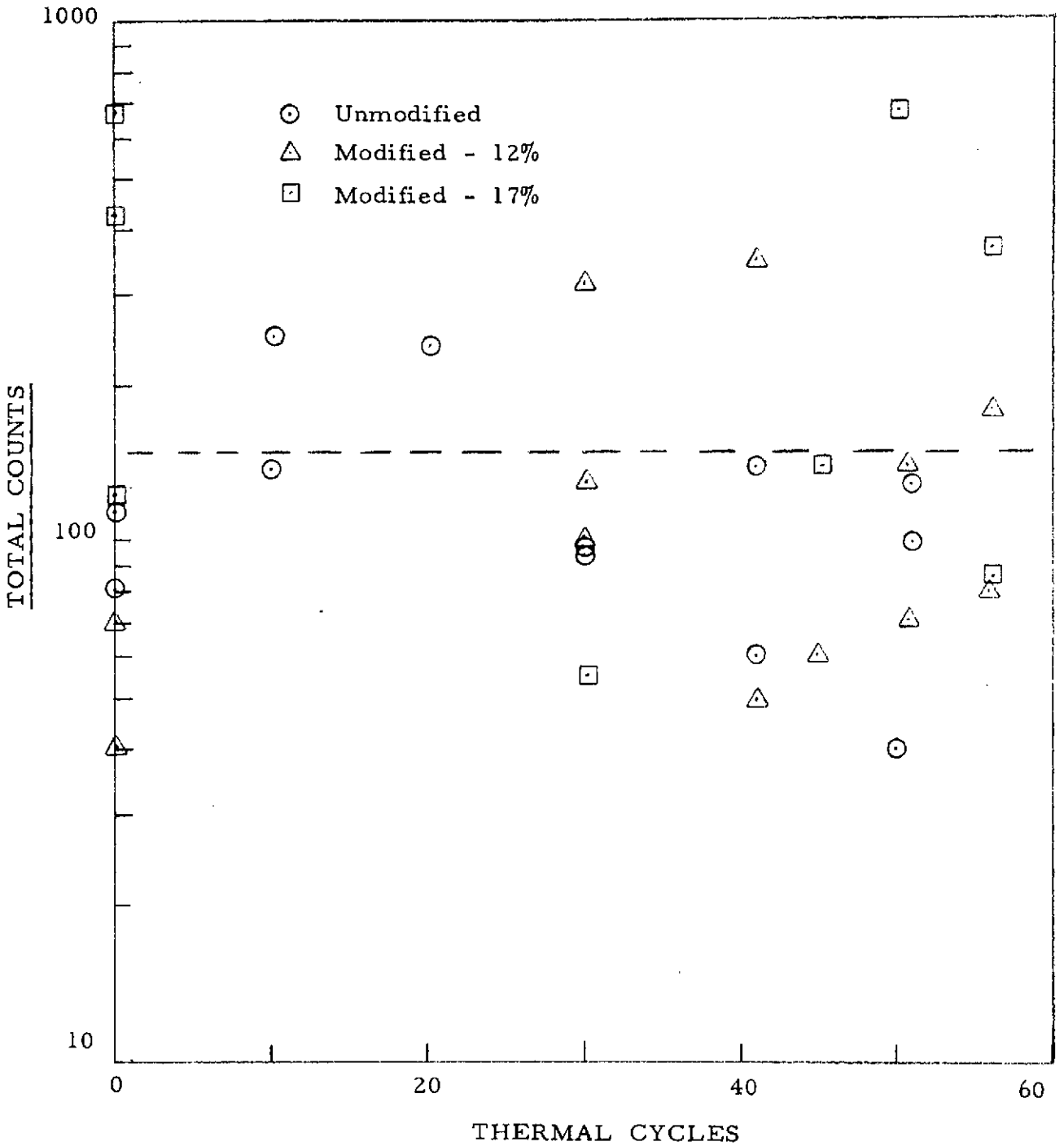

Figure 32. Acoustic Events During Tensile Testing Subsequent to Thermal Cycling of Model Specimens

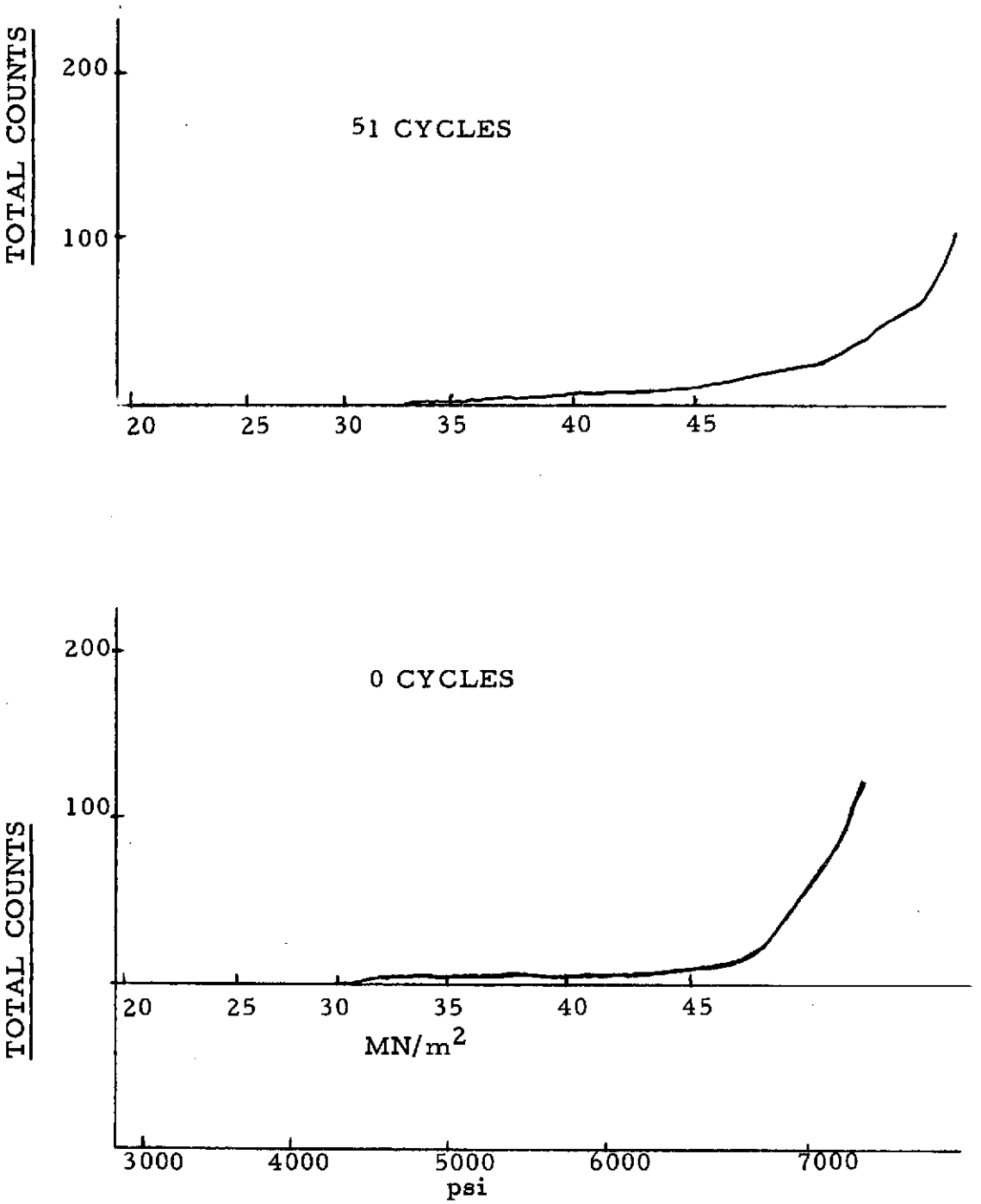

FIGURE 33. EFFECT OF THERMAL CYCLING ON ACOUSTIC EMISSION BEHAVIOR OF MODEL SPECIMENS TESTED IN TENSION AND CONSISTING OF HTS FIBERS IN AN UNMODIFIED EPON 828 RESIN

the original test data as obtained from the RCL Data Stripper and reduced on the X-Y recorder. As may be seen, fiber fracture begins between 60 to 70% of the ultimate stress, and increases rapidly at about 90% with total counts of the order of 100-200. For the case shown, no significance should be attached to the fact that the cycled specimen was somewhat stronger and showed more fractures prior to failure than the uncycled specimen. Such variations are within the scatter of the data.

The reason for the lack of any effect of thermal cycling on the tensile properties lies primarily in the nature of the thermally induced damage in the composite and perhaps the low fiber volume fraction. As shown in Section 3.3.2, when damage is caused by cycling the result is primarily fiber compression failures at only a few locations. The effect of this damage in subsequent tensile testing is equivalent to the introduction of a few broken fiber, and this appears insufficient to significantly affect the tensile strength. Of course, associated with the net fiber compression force is a localized net matrix tensile stress, but because the fiber volume fraction is so low the bulk of the matrix is unaffected and again no significant effect on the strength is noted.

Although it seems that thermal cycling has no effect on the tensile behavior of model specimens, the same is not true of the resin formulation. Resin modification has a strong effect on the strength of these specimens, as can be seen in Figure 31. In the following discussion, the tensile properties of the model specimens will be considered ignoring any possible effect of thermal cycling on these properties.

For the model specimens, the practical effect on the matrix of introducing a few fibers in the specimen center and then loading in tension is to test a resin matrix specimen with incipient internal cracks. As a fiber breaks, it causes disk-shaped cracks to be thrown out into the matrix. The effect on the matrix as testing continues is to deform it in the presence of a series of internal notches which grow in length, and at some point the critical crack size for a particular notch is reached and the composite fails.

The size of disk shaped matrix cracks generated by fiber breaks depends on the interface strength and the matrix properties. Given a constant interface strength (the likely case for the present data), the more rigid resin seems to exhibit a smaller crack than the modified resin. This can be seen in the photographs in Figure 34, where fiber breaks and the associated matrix crack are shown for the two extremes of resin toughness. As may be seen, increasing matrix ductility and decreasing strength leads to larger matrix cracks.

Although this may seem counter to what one might expect, we must remember that a ductile matrix can tolerate a larger critical sized crack (i.e., the crack length at which final specimen fracture will occur) than the more brittle one. Thus, the more highly modified resin generates more damage locally at

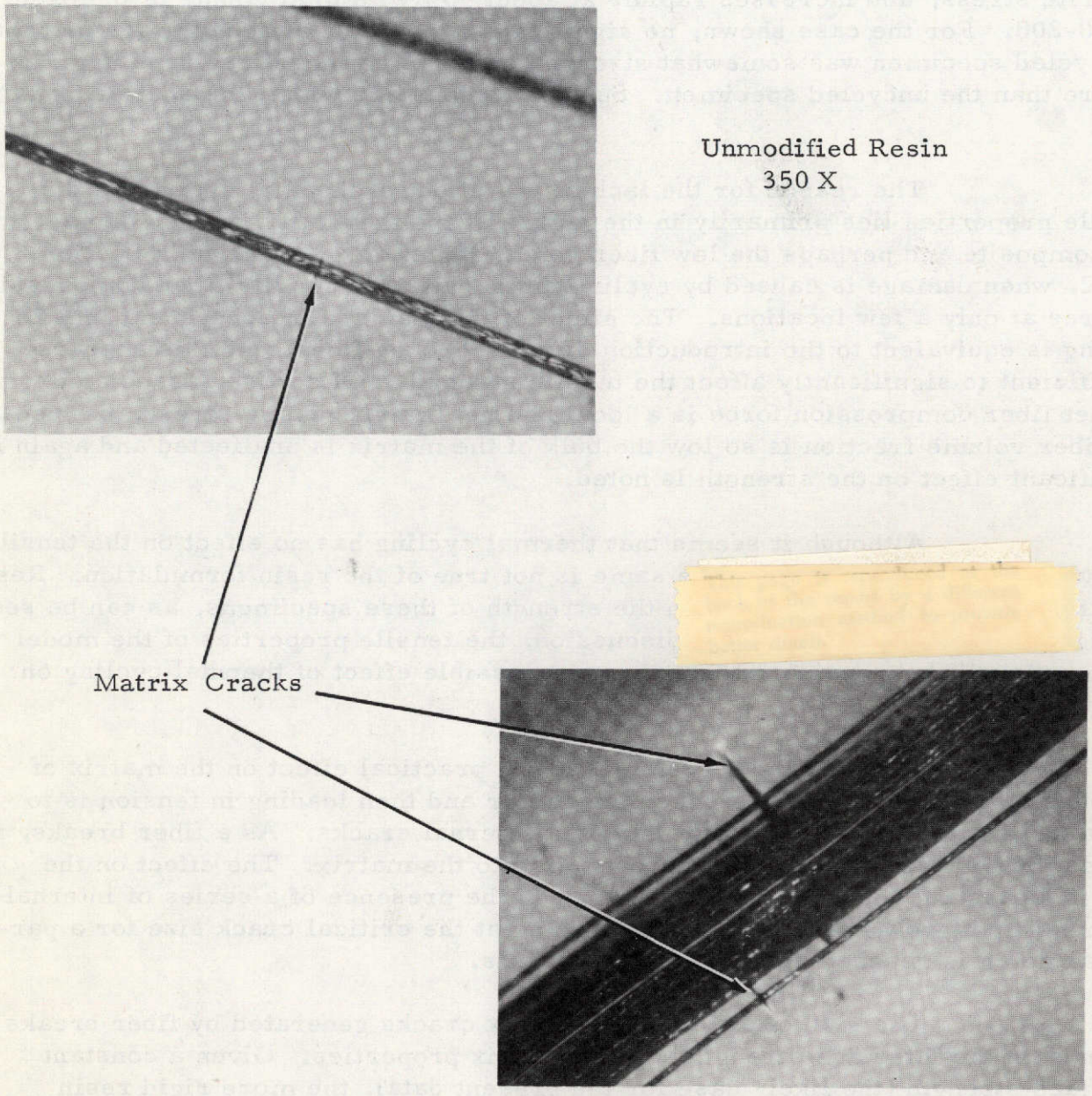

Figure 34. Photographs Illustrating the Increase in Matrix Crack Length with Increasing Resin Modification in Model Specimen Tested in Tension

fiber fracture but is less sensitive to this damage under subsequent tensile testing. The stronger unmodified resin has a lower value of K_{IC} and so it can tolerate a smaller crack as shown in the expression*

$$\sigma = \frac{K_{IC}}{\sqrt{\pi a}}$$

where a is the crack length. It may be seen that a lower K_{IC} (more rigid specimens) leads to lower fracture stresses for a given crack dimension a.

The strength of a model specimen, then, will depend on the initial matrix crack formed and the critical crack length after the crack has grown. As the matrix becomes more ductile, both values increase. The interaction between these two effects can be seen in Table X where the resin strength, model specimen strength, and their ratio are given. For the case of the unmodified and modified (12% elongation) resin, the interaction between initial crack size and critical crack size leads to about the same strength ratio, about 0.7. However, for the 17% modified resin, even though a larger crack is present initially, the resin can tolerate a much larger critical crack, as evidenced by the notch strength ratio of about 0.9.

These observations are somewhat substantiated by the acoustic emission data. Shown in Figure 35 is a plot (data taken from Table IX) of total counts (i.e., fiber breaks) for the 17% modified resin as a function of specimen strain. As the strain increases beyond 4%, the number of fiber breaks increase sharply. The specimen underwent a large uniform strain, and the fiber tow was broken up into segments of approximately equal length. This behavior is illustrated in Figure 36 , where one of these segments is shown.

The significant point here is that only the 17% modification displayed such a capacity for elongation, and even here it was evident in only three instances out of eight. Apparently, a small change in resin properties can influence the ability of the 17% modification to deform in the presence of a crack. In most cases, the ability to contain cracks was about the same as for the other two formulations. This can be best seen in Figure 37, where the number of fiber breaks for all formulations are plotted as a function of failure strain. Except for the three aforementioned specimens, all the others clustered between 2.6% and 4.6% strain, with the number of fiber breaks ranging between 40 and 370, irrespective of resin formulation. The spread in the number of fiber breaks is attributed to differing fiber contents and orientations.

A point that is still not clear is why, for resin formulations

*This expression is for a crack in an infinite sheet, but the form would not change for a crack in a bar.

TABLE X

COMPARISON OF RESIN STRENGTH AND MODEL SPECIMEN STRENGTH

Formulation	Resin Strength MN/m^2	KSI	Specimen Strength MN/m^2	KSI	Ratio: $\frac{\text{Specimen Strength}}{\text{Resin Strength}}$
Unmodified	70.9	10.25	50.0	7.25	0.76
Modified (12%)	56.5	8.2	38.6	5.6	0.684
Modified (17%)	32.4	4.7	29.0	4.2	0.895

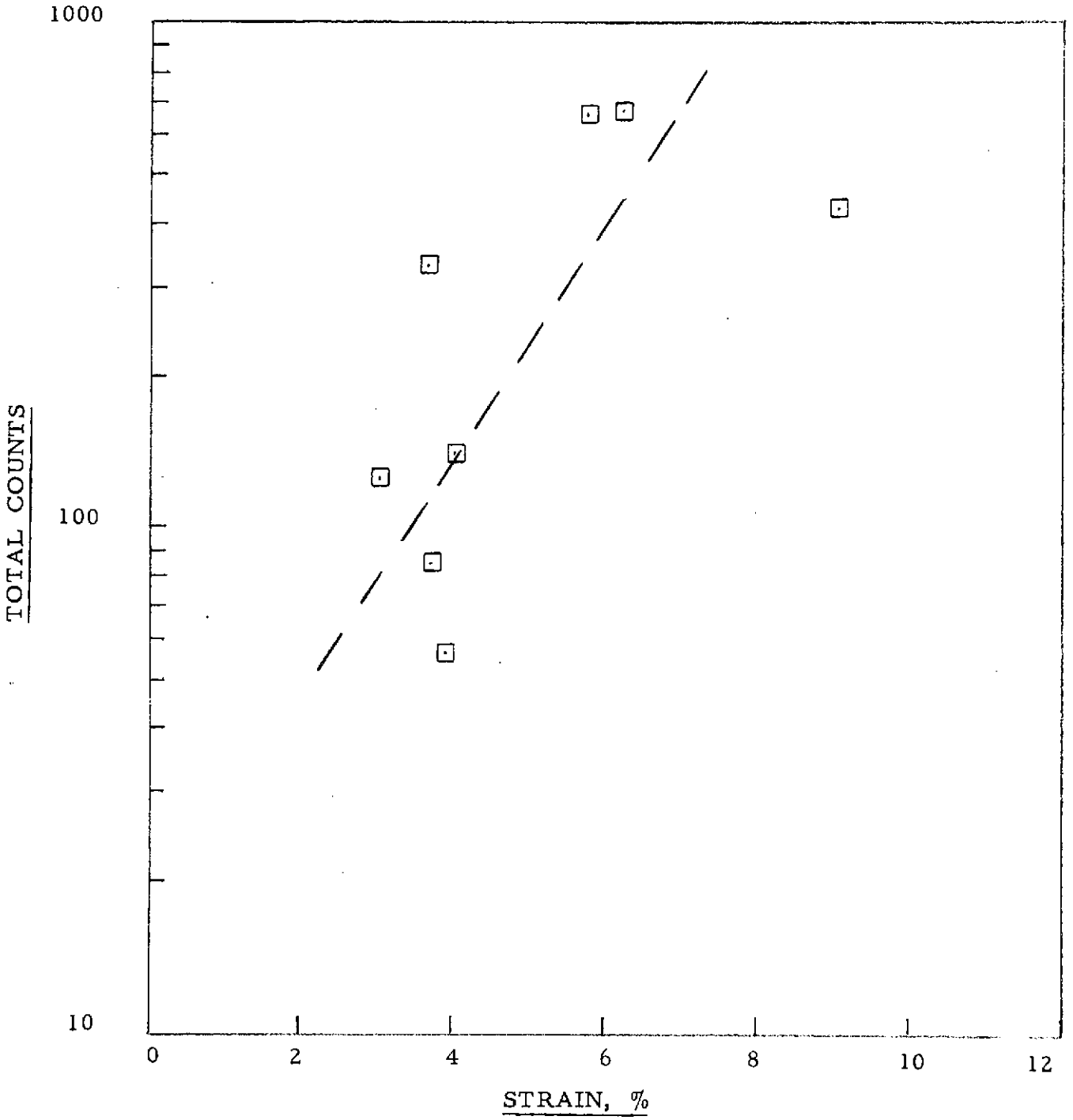

Figure 35. Total Acoustic Counts of Model Specimens with Modified (17%) Resin vs. Strain During Tensile Testing

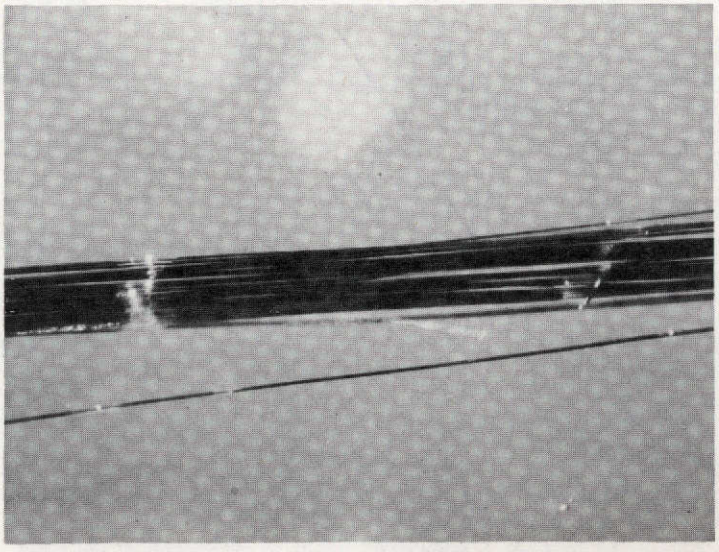

60 X

Figure 36. Photograph Illustrating the Behavior of a Model Specimen with a Modified - 17% Resin After a Tensile Strain of 6.2%

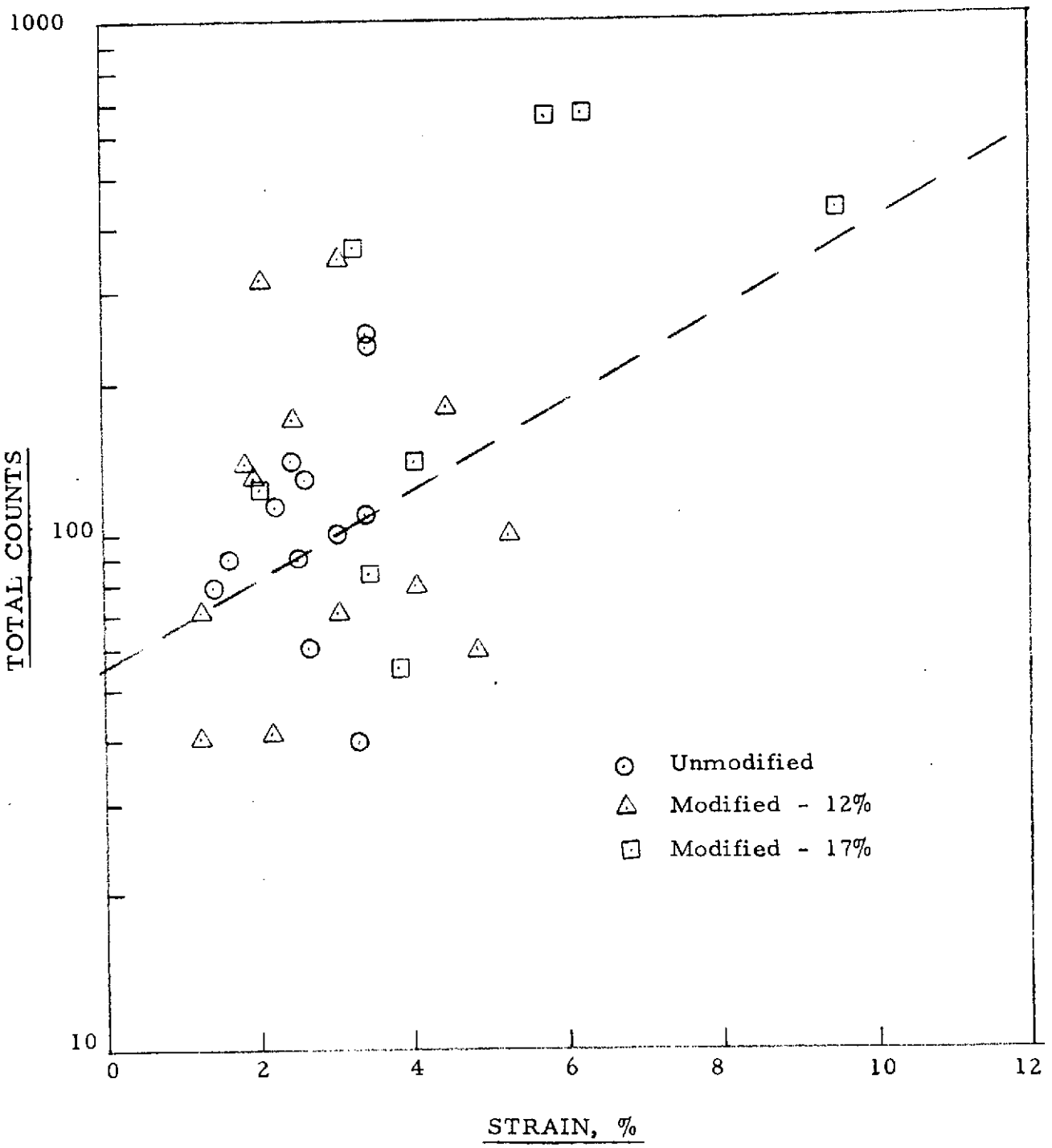

Figure 37. Total Acoustic Counts of Model Specimens vs. Strain During Tensile Testing

having failure strains varying from 3 to 17%, all the model specimens except three had failure strains in the 2.6% - 4.6% range. It is clear that the presence of the fibers and the resulting matrix response upon straining lead to failure strains of the same order regardless of the degree of resin modification. Only about 20-30% of the available ductility is reached for the modified resins, with the exception of the three specimens of the 17% modification. The unmodified resin on the other hand, retains considerably more of its available ductility when used in the model specimen. These findings are in agreement with the results reported in ref. 5. The authors of ref. 5 concluded that ultimate elongation of the resin did not correlate with composite properties.

3.3.3.2 Compression Behavior

A series of tests was conducted in which specimens were subjected to compressive loading after thermal cycling. It has already been pointed out that the unmodified resin formulation was virtually undamaged by thermal cycling and this was verified in subsequent compression tests of model specimens. Comparisons of the fracture modes for cycled and uncycled specimens showed very similar characteristics.

The modified resin formulation (12% Elongation) have quite different results. Thermal cycling damage was evident after 30 fast cycles as shown in the upper photos of Figure 38 . The lower photos show the same location after compression loading to the ultimate strength. Note how the regions adjacent to the original fracture site have debonded in the 150 X photo and how new compressive failures are evident in the 60 X photograph. Note also that the disk shaped crack generated by thermal cycling in the upper left has not propagated in the lower left photo since the compressive load tends to close rather than propagate such cracks. There is a great deal of fiber buckling and this kind of local failure mechanism is caused by both thermal cycling and compression loading.

Similar experiments were performed for the highly modified resin (17% Elongation) and the results are shown in Figure 39 . In the upper photo there is abvious damage after thermal cycling with very faint evidence of a disk shaped resin crack in the upper left photo. The lower photos show how subsequent compression has resulted in considerably more damage by fiber fracture and resin crazing which makes the disk-shaped crack more visible. Note the similarity in local failure modes in thermal cycling and compression. The major difference is that thermal cycling results in local compression failures of the fibers combined with tensile cracks in the resin. This combination of distinctly different failure modes can occur only when the fibers and resin are loaded against one another.

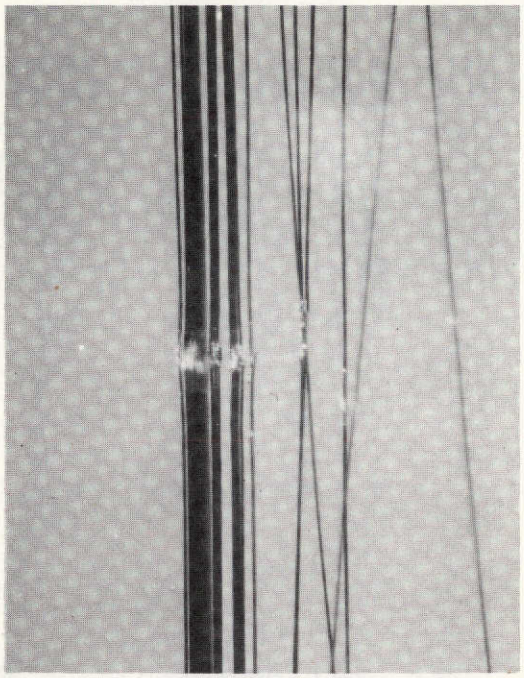

60X

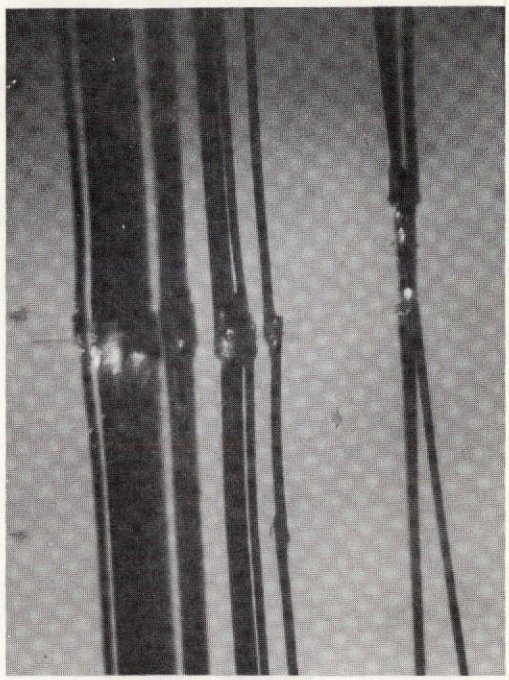

150X

a) Local Damage After 30 Fast Thermal Cycles and Before Compression

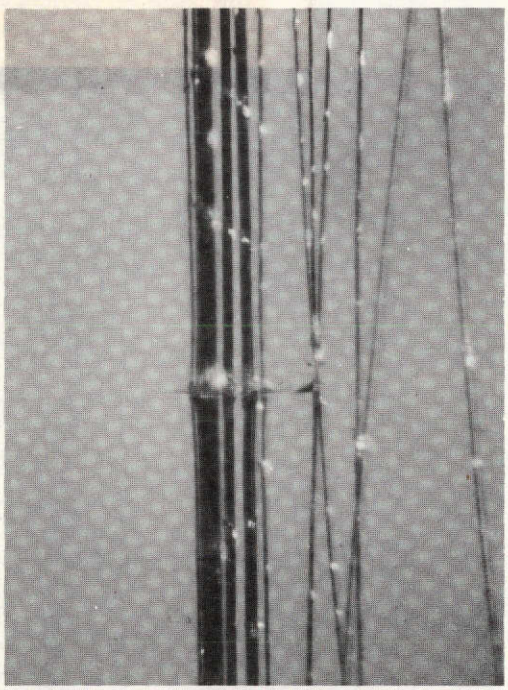

60X

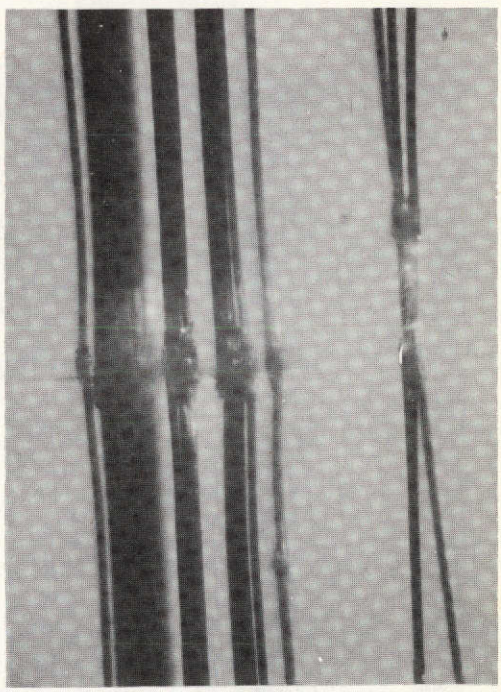

150X

b) Same Location After Compression

Figure 38 Comparison of Local Damage Before and After Compression for HTS Fibers in Modified (12% Elongation) Epon 828 Resin

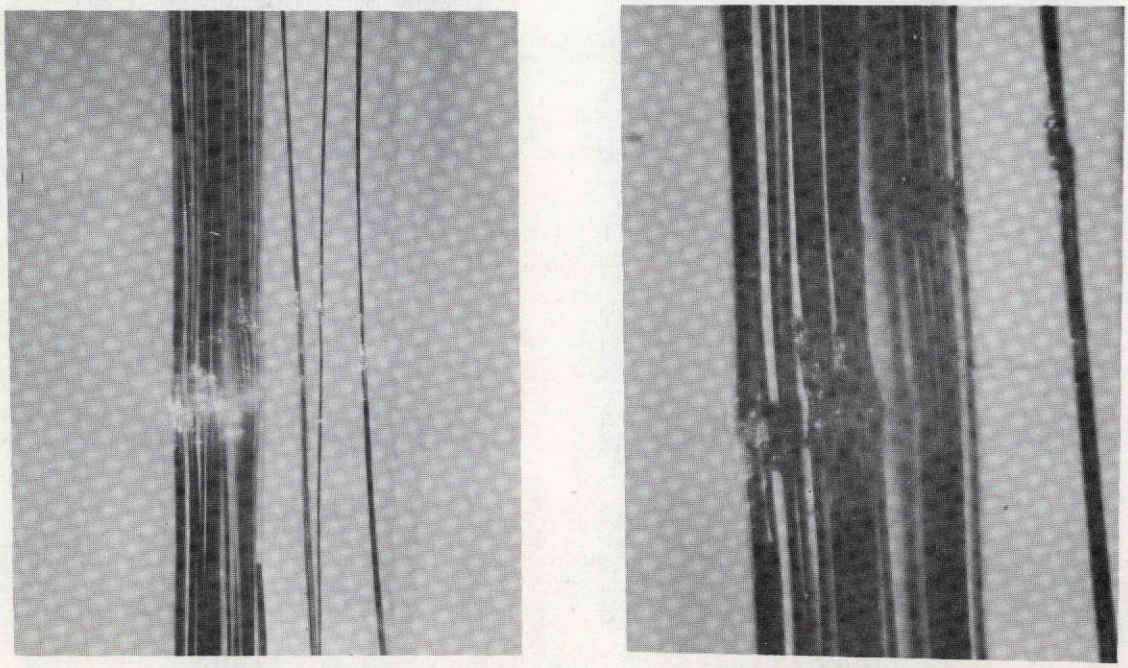

60X 150X

a) Local Damage After 30 Fast Thermal Cycles and Before Compression

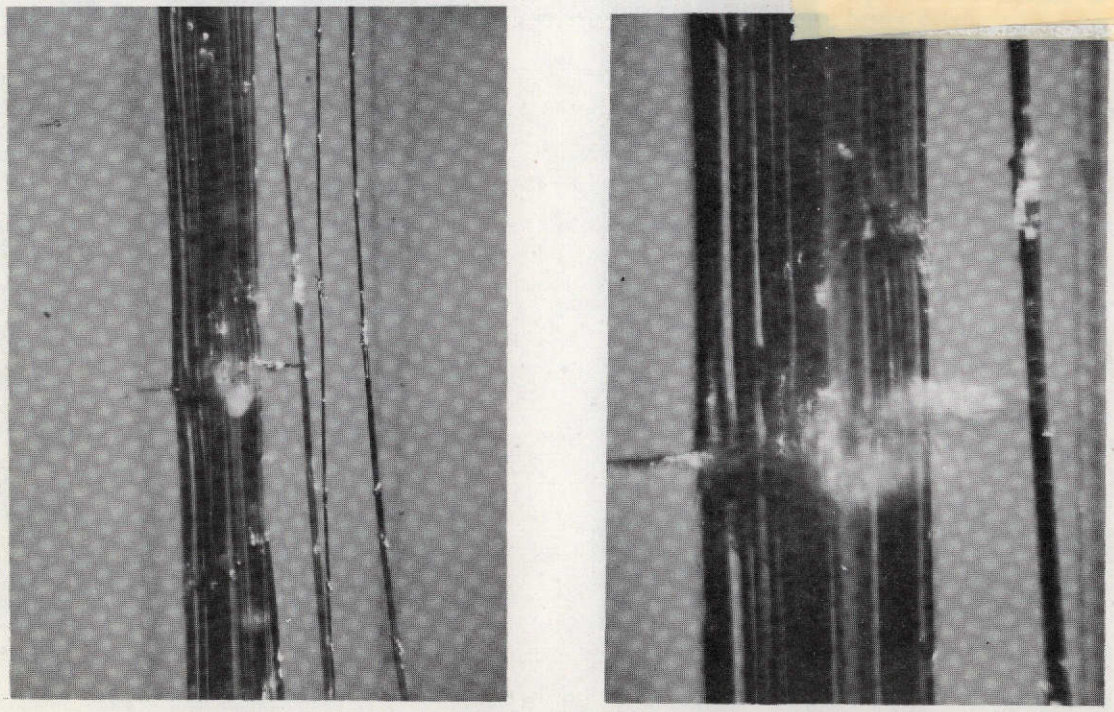

60X 150X

Figure 39 Comparison of Local Damage Before and After Compression for HTS Fibers in Highly Modified (17% Elongation) Epon 828 Resin

3.4 Mechanical Considerations of Engineering Composites

In discussing engineering composite mechanical properties reference is made to the effects of thermal cycling and volume fraction on "old" and "new" material. As was discussed in Section 2.3.3.1, "old" material refers to composites made from specialized prepreg material obtained during the early part of the program in 1972, and "new" material refers to composites made from specially prepared prepreg material obtained in early 1973. The "old" prepreg material was of such quality that it translated into poorer quality engineering composites, as compared with more improved quality "new" prepreg material which produced higher quality composites as evidenced by the data in the following sections.

Because of the large quantity of mechanical test data generated from both pre-cycle and post-thermal cycle conditions, it was decided that the data would be best presented graphically from the mean values and the range of standard deviation. A computer program was used to reduce the raw property data to a simpler form for more efficient interpretation and evaluation. The mean standard deviation, and standard deviation of the mean were calculated. The test data for 25, 40 and 55 V/O carbon fiber epoxy resin composites are presented in tabular form in Appendix A.

3.4.1 Effect of Fiber Content on Failure Mechanisms

A series of tests were performed at room temperature using the unmodified resin containing fiber volume fractions from approximately 0.25 to 0.55. The testing was performed on 5 replicates each for longitudinal tensile strength, transverse tensile strength, flexural and compressive strengths. Figure 40 shows the results for each of these properties as a function of fiber content. In this figure, the dependence of strength on volume fraction is assumed to be linear in spite of the fact that in some instances the straight line falls beyond the range of the standard deviation. The linear dependency is considered to be justified by past work, both here (4) and elsewhere. The scatter of the data is probably due to material variability, as discussed previously. It may be noted that the transverse strength values show no dependence on fiber content, which is expected behavior if this property is primarily matrix dependent. In addition, the flexural strength is essentially paralled to the values for longitudinal strength, which again is expected behavior because both fracture modes are tensile in nature.

Figure 41 shows typical fracture modes for both extremes and the middle group representing the fiber volume fractions mentioned earlier. In the upper photo (a) all specimens have distinct cleavage sites normal to the specimen axis with minimal fracture surface paralled to the fibers. This type of behavior is the same in low fiber content specimens both before and after thermal cycling. In photo (b) there is similar behavior except, at this fiber content level

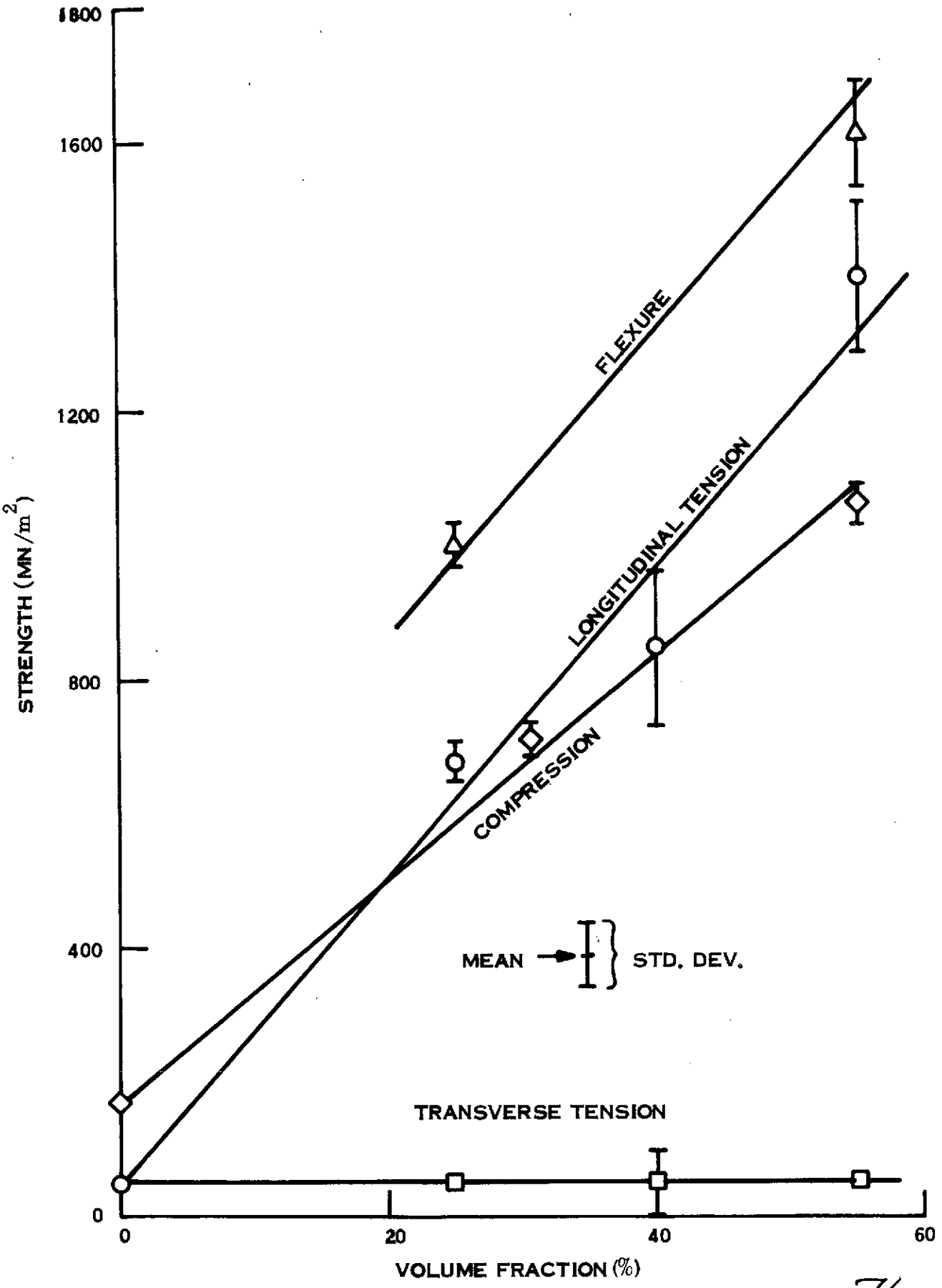

FIGURE 40. Strength of Carbon/Epoxy Composites as a Function of Fiber Content.

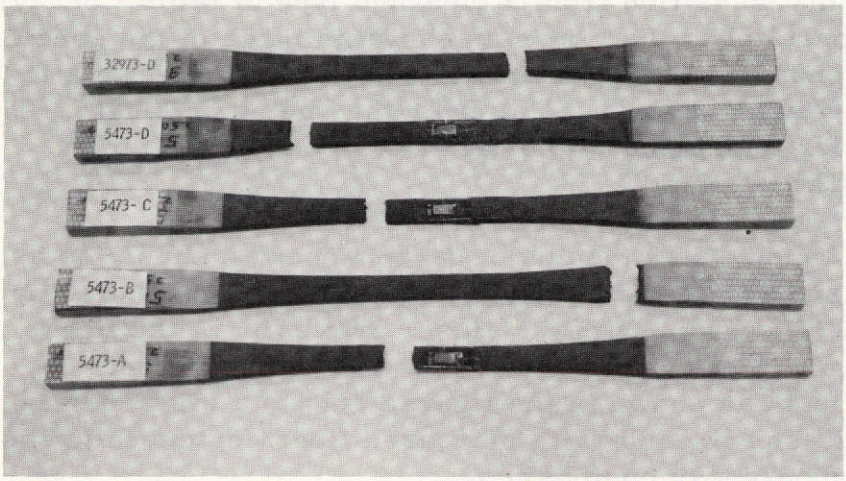

(a) V/O range (0.26-0.34)

(b) V/O range (0.38-0.46)

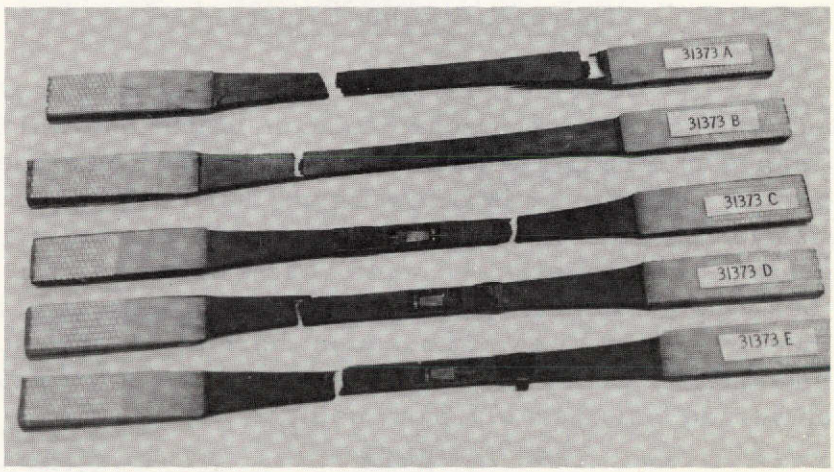

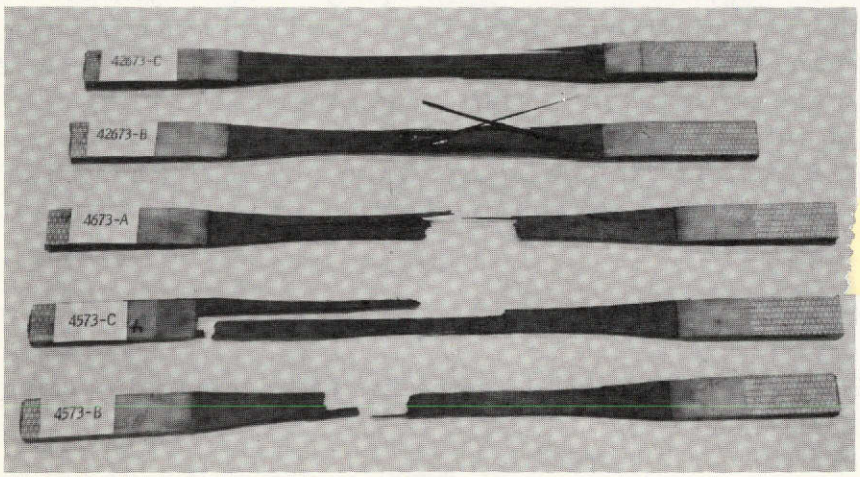

(c) V/O range (0.54-0.65)

FIGURE 41. Fracture Modes for Various Fiber Content Values for HTS Fibers in Unmodified Epon 828 Epoxy Resin.

we are beginning to witness the transition from a cleavage type of failure behavior to one of fracture surfaces parallel to the fibers as shown in three of the specimens in the photo. In the bottom photo (c) the higher fiber content shows a dramatic change in behavior to one involving several sights over the specimen length. This same type of fracture behavior took place in the high fiber content specimens before thermal cycling as after cycling.

Figure 42 shows the modulus of carbon/epoxy composites as a function of fiber volume. Here again, the transverse tensile modulus shows no dependency on fiber content. However, with the closer proximity of the fibers in the higher fiber content composites, it can be assumed that some influence is created on matrix stiffness; but, as shown in the figure, only to a slight degree. Of course, the modulus increases linearly with increased fiber content following the rule-of-mixtures for carbon/epoxy composites.

3.4.2 Thermal Cycling Effects

Besides the effect of thermal cycling on post-curing the polymer matrix there are some mechanical considerations which could account for part of the change in strength with thermal cycling. It has been observed in model specimens containing only a few fibers that residual stresses are induced by the fabrication process such that the fibers are placed in compression and the matrix in tension. In very slightly reinforced composites this often results in fiber or tow buckling (4). This same effect is present in the more heavily reinforced engineering composites but because there are many more fibers to resist resin shrinkage after cure, the result is a more complex residual stress condition which varies considerably from point to point.

The residual stress is first relieved during cycling to the original cure temperature and then the residual stress builds up again as the temperature is reduced. This exercising of the polymer gives the more highly stressed regions an opportunity to relieve themselves by breaking molecular bonds. Those locations which are most constrained are most likely to fail under thermal cycling and although this may represent only a small fraction of all the bonded and active sites in the polymer there can be sufficient damage to affect the physical strength of the composite. This behavior may account for the mechanical properties in the following ways:

3.4.2.1 Tensile Properties

In a unidirectionally reinforced composite after thermal cycling and having a fiber content of 55 V/O:

(1) The modulus in the direction of the fiber increases slightly (11%) probably due to overcoming the initial residual compression in the fibers

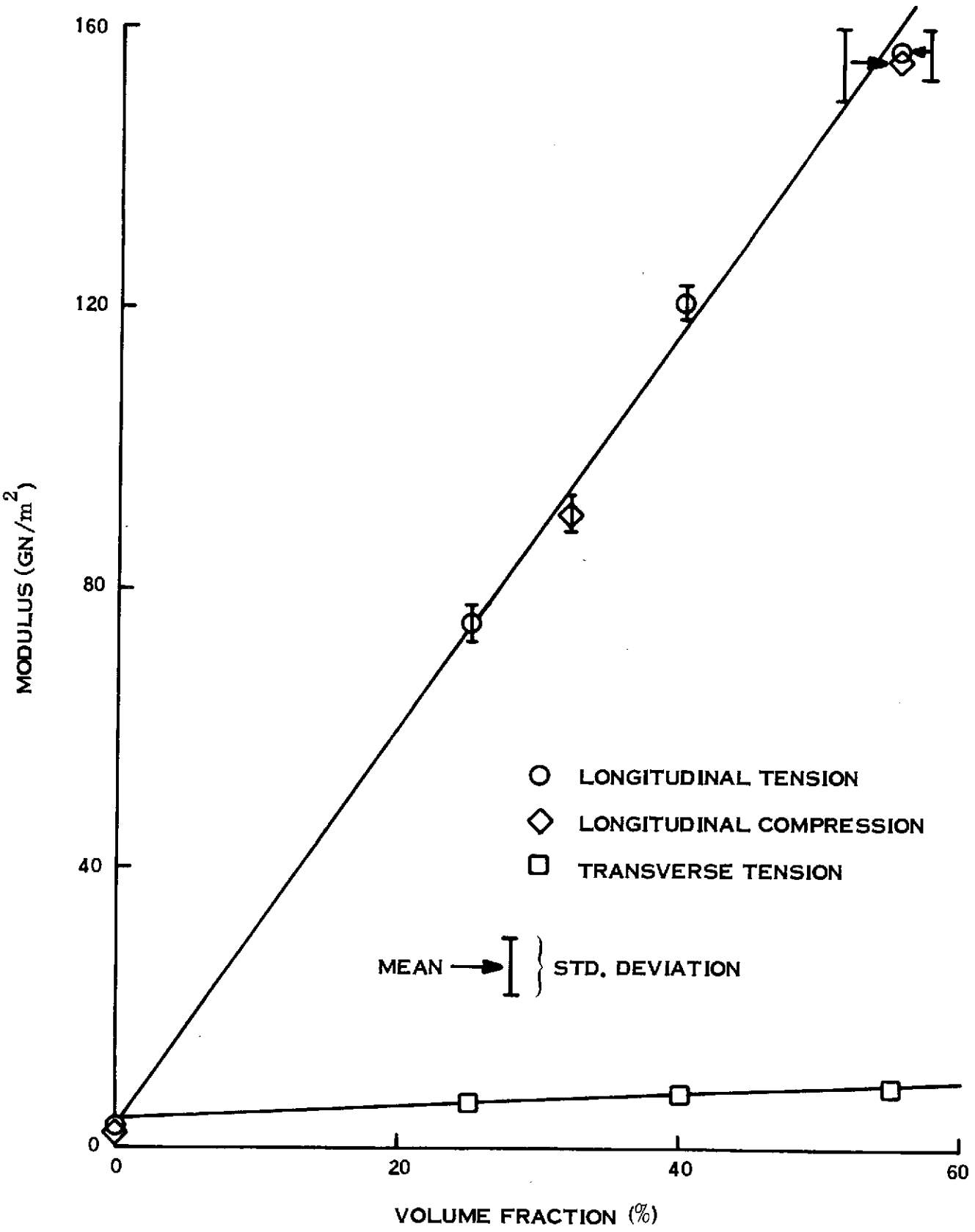

FIGURE 42. Modulus of Carbon/Epoxy Composites as a Function of Fiber Content.

which tends to misalign them and thus prevents all fibers from contributing their inherent stiffness. As thermal cycling relieves the resin induced stresses greater fiber efficiency can result and thus the slight increase in modulus.

(2) The transverse modulus is primarily that of the resin because the fibers are discontinuous in the load path. This results in loss of modulus (5%) as thermal cycling causes scission of bonds in the polymer making it less stiff.

Now consider possible strength effects on 55 V/O composites.

(1) If there is residual compression in the fibers before cycling, the tensile strength should be enhanced. As thermal cycling relieves the residual compression in the fibers, tensile strength should diminish somewhat and it appears to in Figure 43 after 200 cycles. After that point the mean strength begins to increase but with added scatter. This could represent some interfacial debonding which "toughens" the composite by suppressing the brittle cleavage failure mode which has been shown (4) to give poor tensile strengths.

(2) The transverse tensile strength should increase as cycling occurs if the residual stress relief tends to smooth out the stress field by eliminating areas of major stress concentration around fibers. However, this effect should be short lived in the thermal cycling process and this is born out in Figure 43 where the transverse tensile strength has leveled off at about 60 MN/m^2 after 200 cycles.

Now consider how a lower fiber content (25 V/O) might influence the model outlined above.

Modulus in the fiber direction should increase more rapidly since more fiber buckling would have been present initially and when relieved, a great rise in modulus should result. However, when the cycling begins to degrade the interfacial bond the modulus in the fiber direction should decrease because of poor bond between fibers and matrix (Figure 44). The transverse modulus is still dependent on the resin primarily and as scission occurs a decrease in transverse modulus should result. However, the effect should be less because we have a greater bulk of resin with which to work. This appears to be true of Figure 44.

Some strength considerations in the 25 V/O composites are: Longitudinal strength should be less with less fiber content. Once again the relieving of residual compressive stress in the fibers should result in some loss of tensile strength contribution from the fibers. However, the resin comprises 75% of the bulk material and appears to be growing stronger perhaps due to post curing effects. In Figure 44 it is this effect which is evidenced in the continuously increasing longitudinal tensile strength.

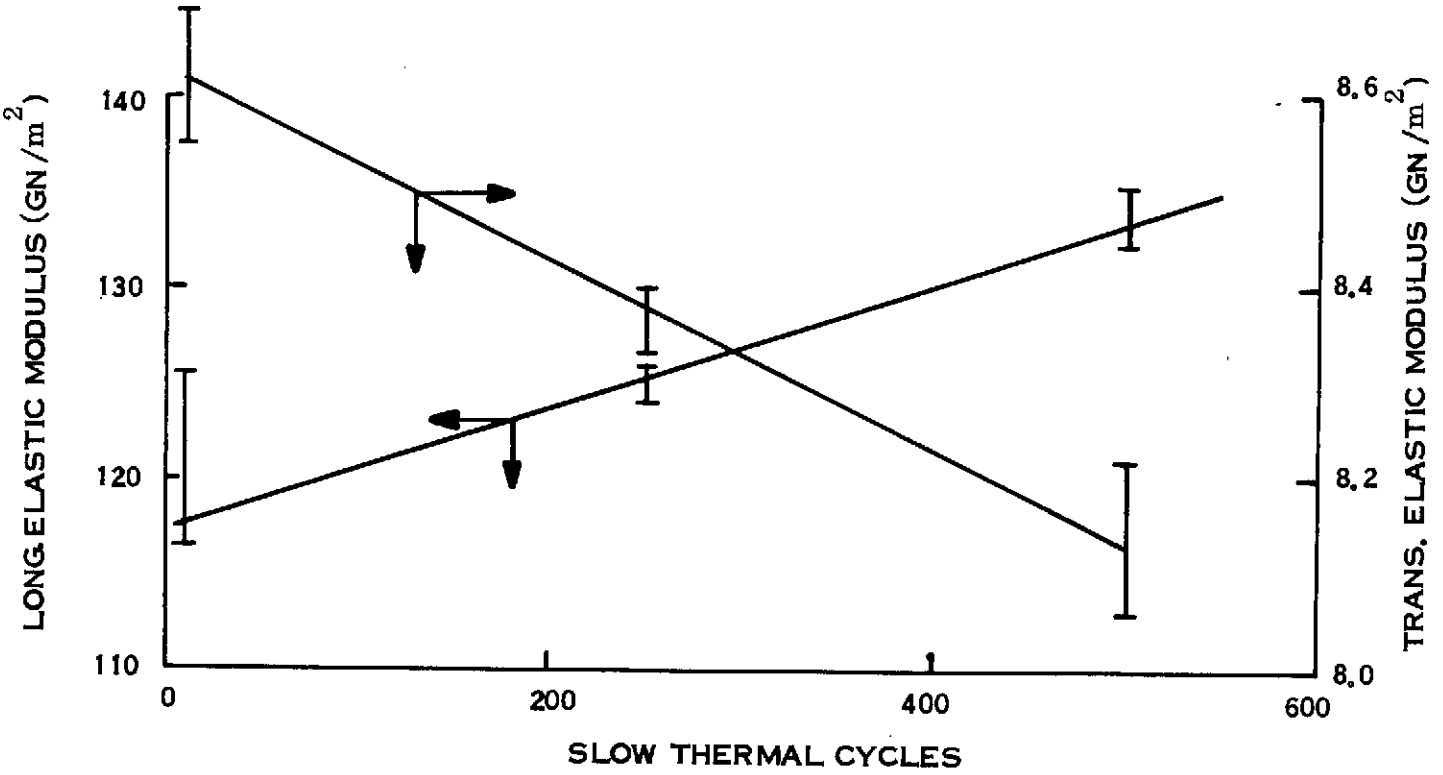

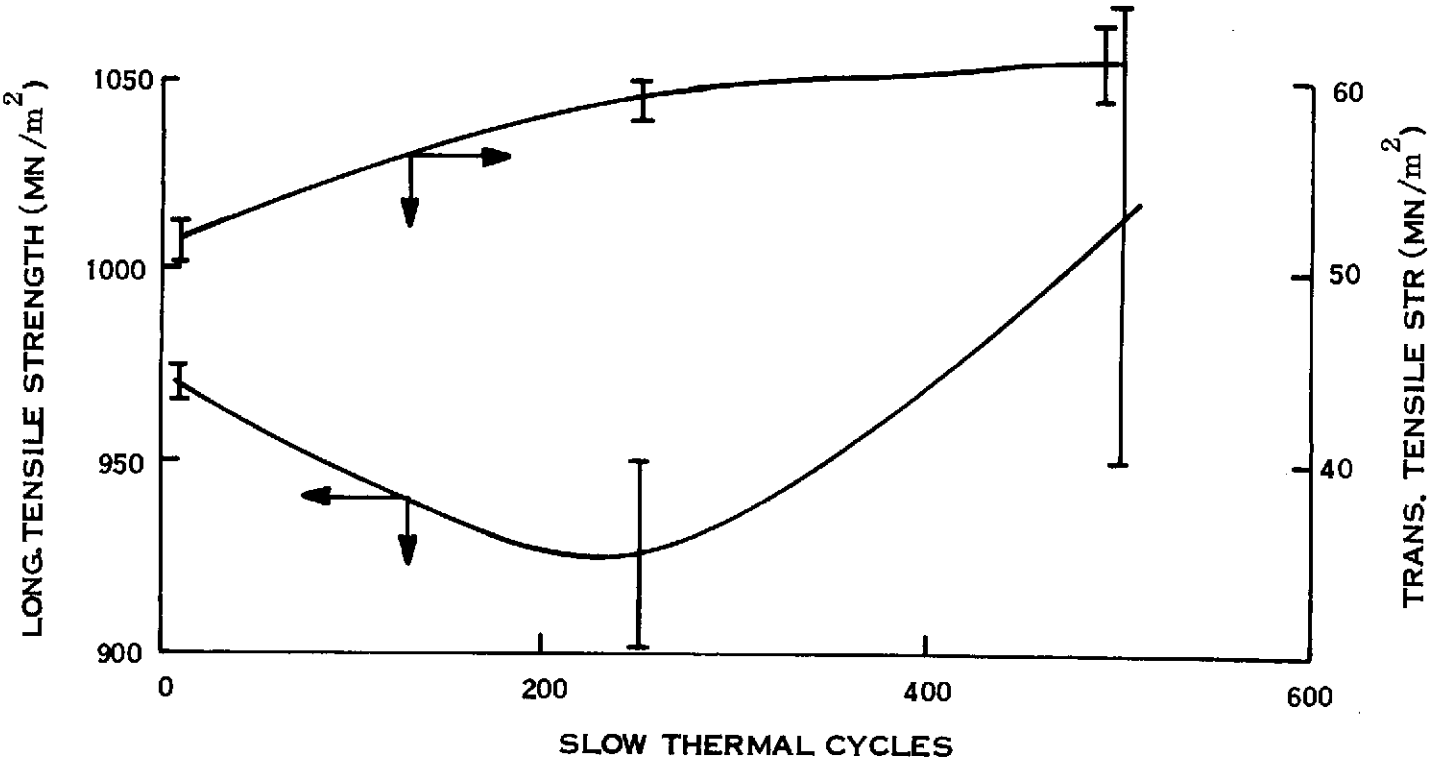

FIGURE 43. Strength and Modulus of 55 V/O Carbon/Epoxy Composites as a Function of Thermal Cycling.

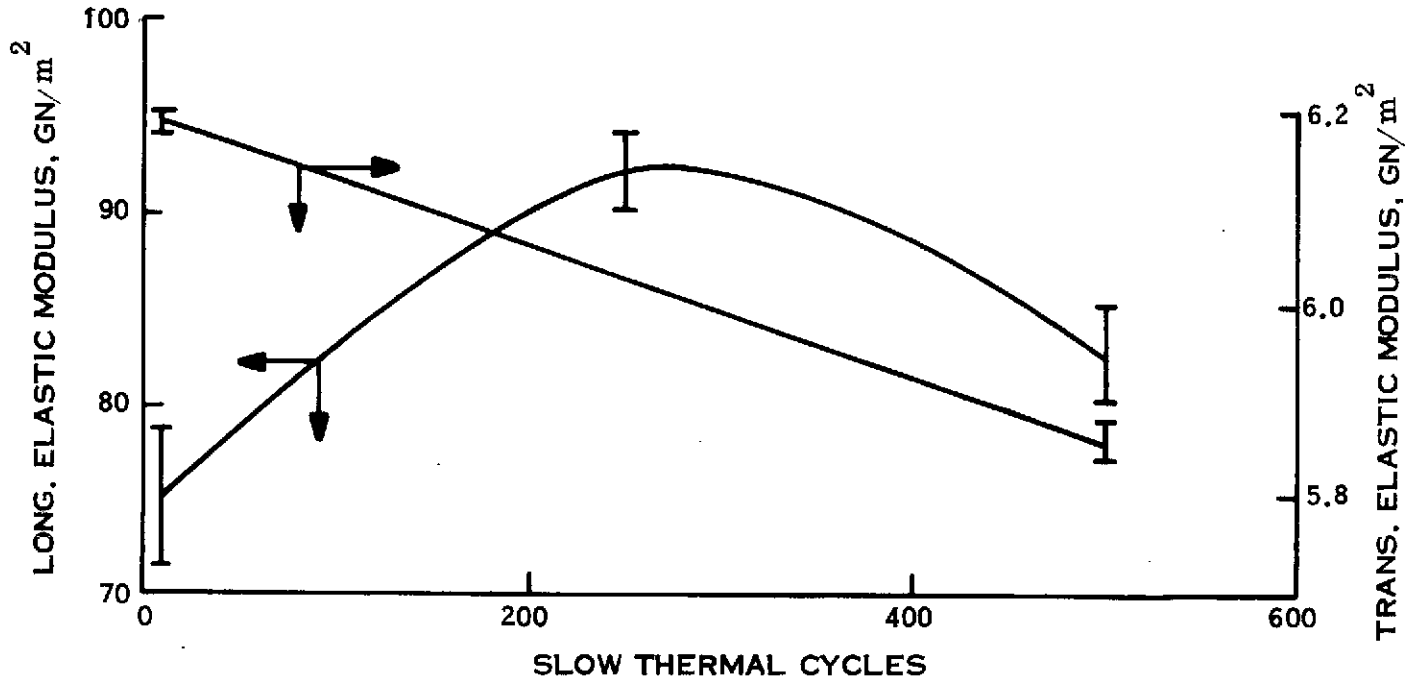

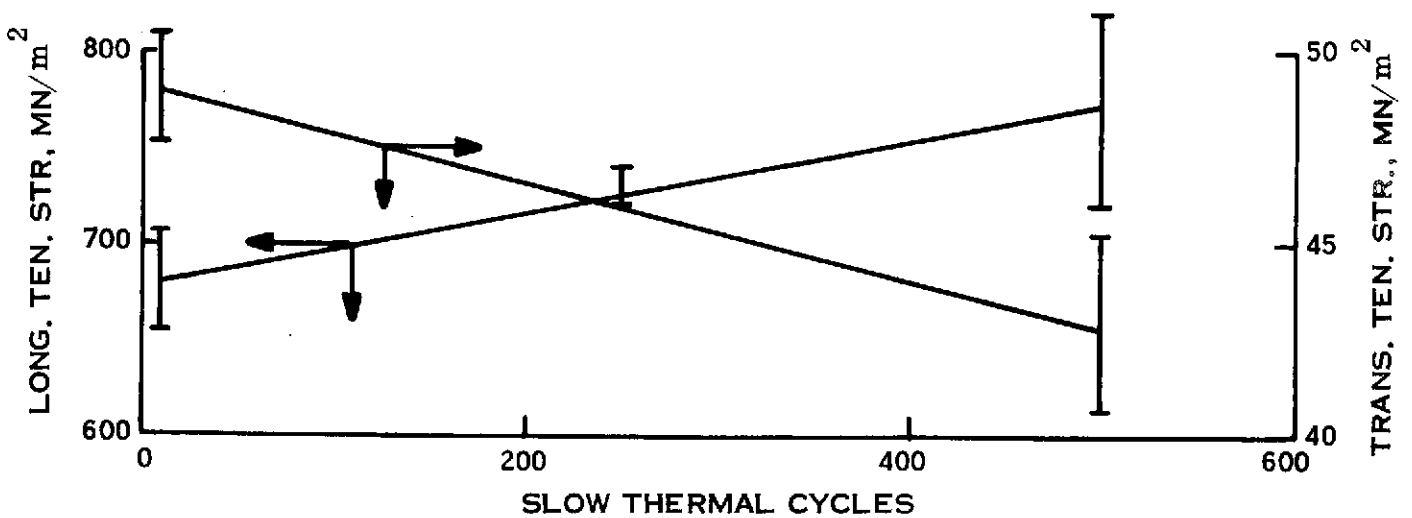

FIGURE 44. Modulus and Strength of 25 V/O Carbon/Epoxy Composites as a Function of Thermal Cycling.

The transverse tensile strength is more nearly representative of the resin itself in the lower volume fraction composite. This means that any chain scission affects the polymer primarily as the load carrier in the transverse direction. Local stress concentrations around fibers are of lesser importance at the lower fiber content so relaxation of them has no significant effect. Thus, as the polymer bonds suffer from thermal cycling so does the transverse tensile strength as shown in Figure 44.

3.4.2.2 Compression Properties

The most prominent effect of thermal cycling on compressive stress is that on compressive strength for 25 V/O and 55 V/O specimens shown in Figure 45. A significant decrease in compressive strength (in the fiber direction) results for the higher fiber content while the lower fiber content retains about the same strength after thermal cycling. This indicates considerable degradation of either fibers or interfacial bond between fiber and resin as a result of thermal cycling the higher fiber content (V/O= .55) specimens. Some evidence of interfacial failure was noted on a few specimens. The interface appears to be more susceptible to damage from thermal cycling and consequently, the compressive strength more adversely affected in the higher fiber content specimens.

3.4.2.3 Flexural Properties

Both the original prepreg (which showed brittle tensile cleavage failures in model specimens) and the new prepreg (which showed more interface limited failure modes) were evaluated. Figure 46 shows how the old material at first increases in strength and then diminishes after 200 cycles while the new material gives a continuously increasing strength.

Similar but flatter curves were obtained in the 25 V/O material. It appears that the first 200 cycles tend to increase the strength perhaps through the smoothing out of residual stresses or improved polymer strength through post curing. However, there is a drastic reduction after 200 cycles indicating a major loss of integrity probably through the accumulation of local cleavage cracks in the tensile region. The loss of interfacial bond in the compressive region would have a similar effect.

3.4.2.4 Interlaminar Shear Strength

There is considerable difference in the as-fabricated interlaminar shear strength between the original and new material (76 vs 40 MN/m^2). The new material showed little change in interlaminar shear strength with number of cycles. However, the old material showed a large gain in interlaminar shear strength over the first 100 cycles and then remained at that level through the next 100 cycles. This indicates an increase in bond strength between fibers and resin

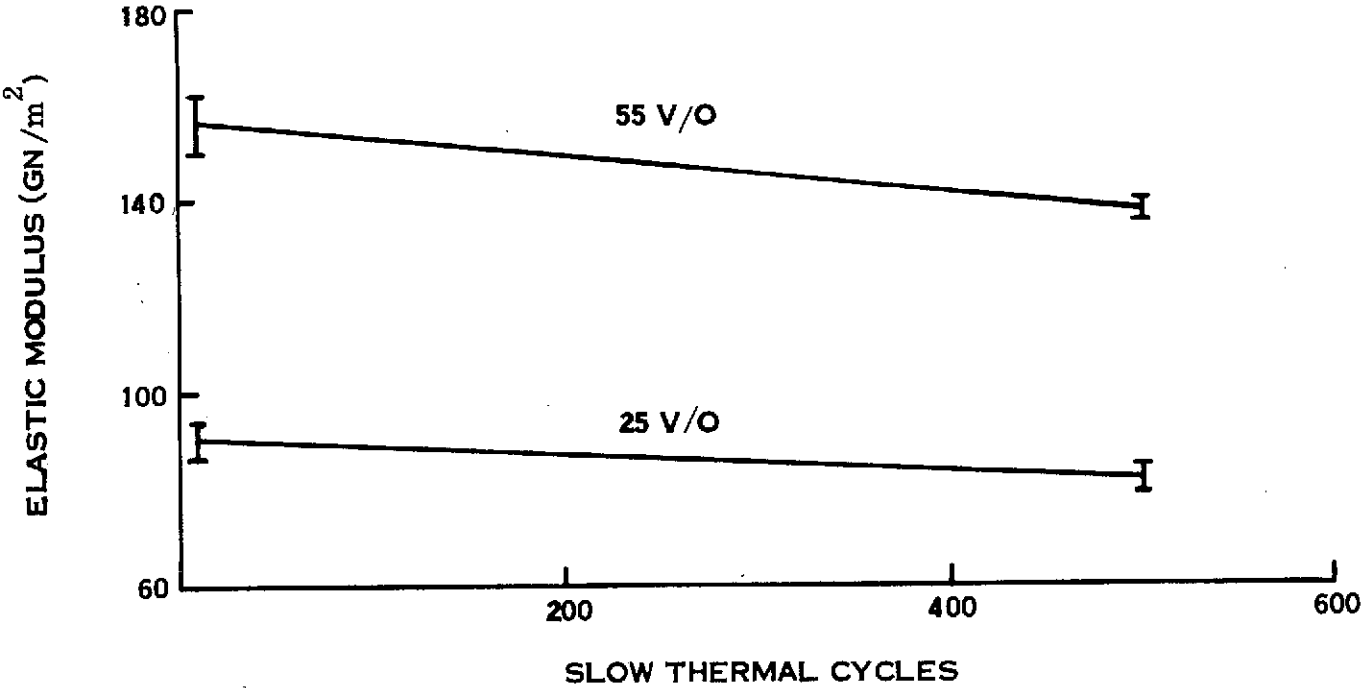

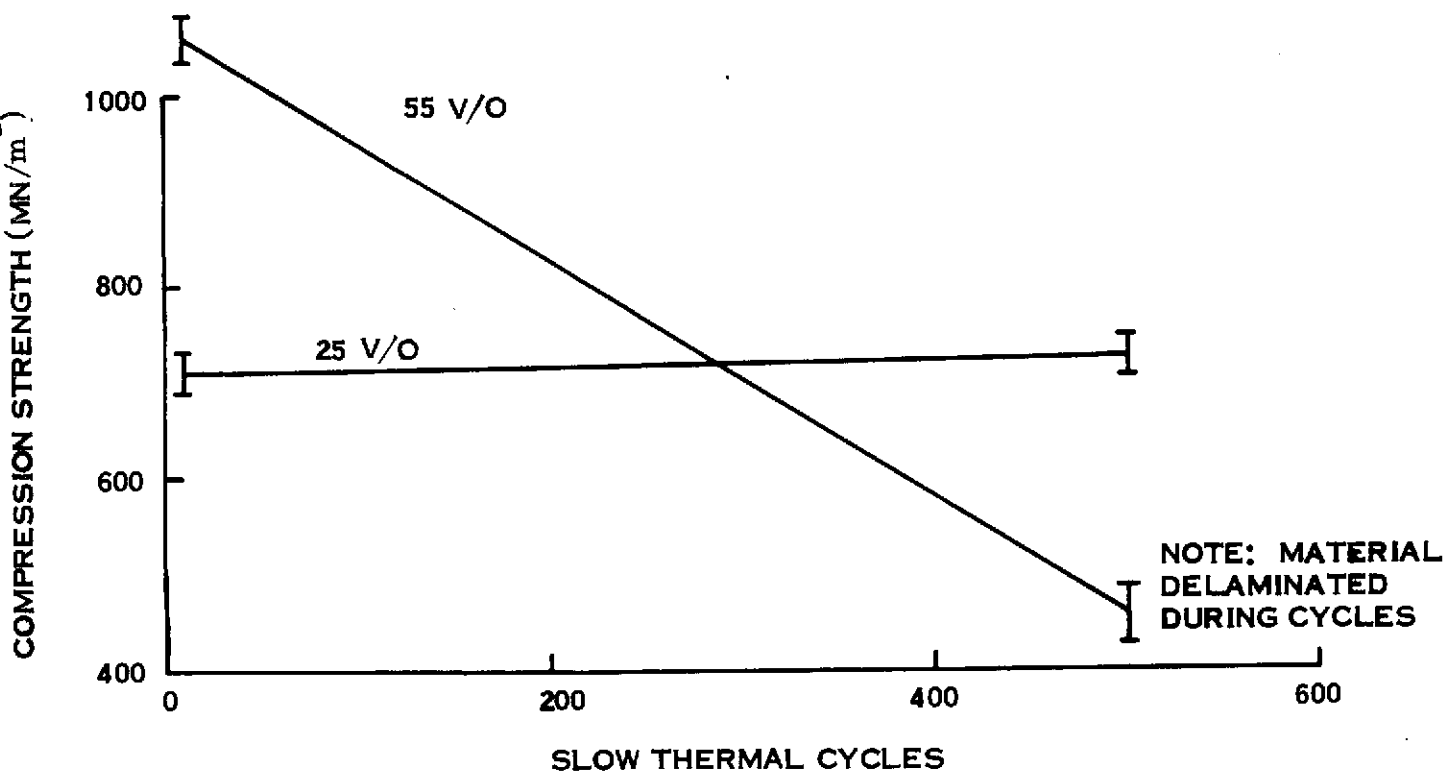

Figure 45. Compressive Properties of 55 V/O and 25 V/O Carbon/Epoxy Composites as a Function of Slow Thermal Cycling.

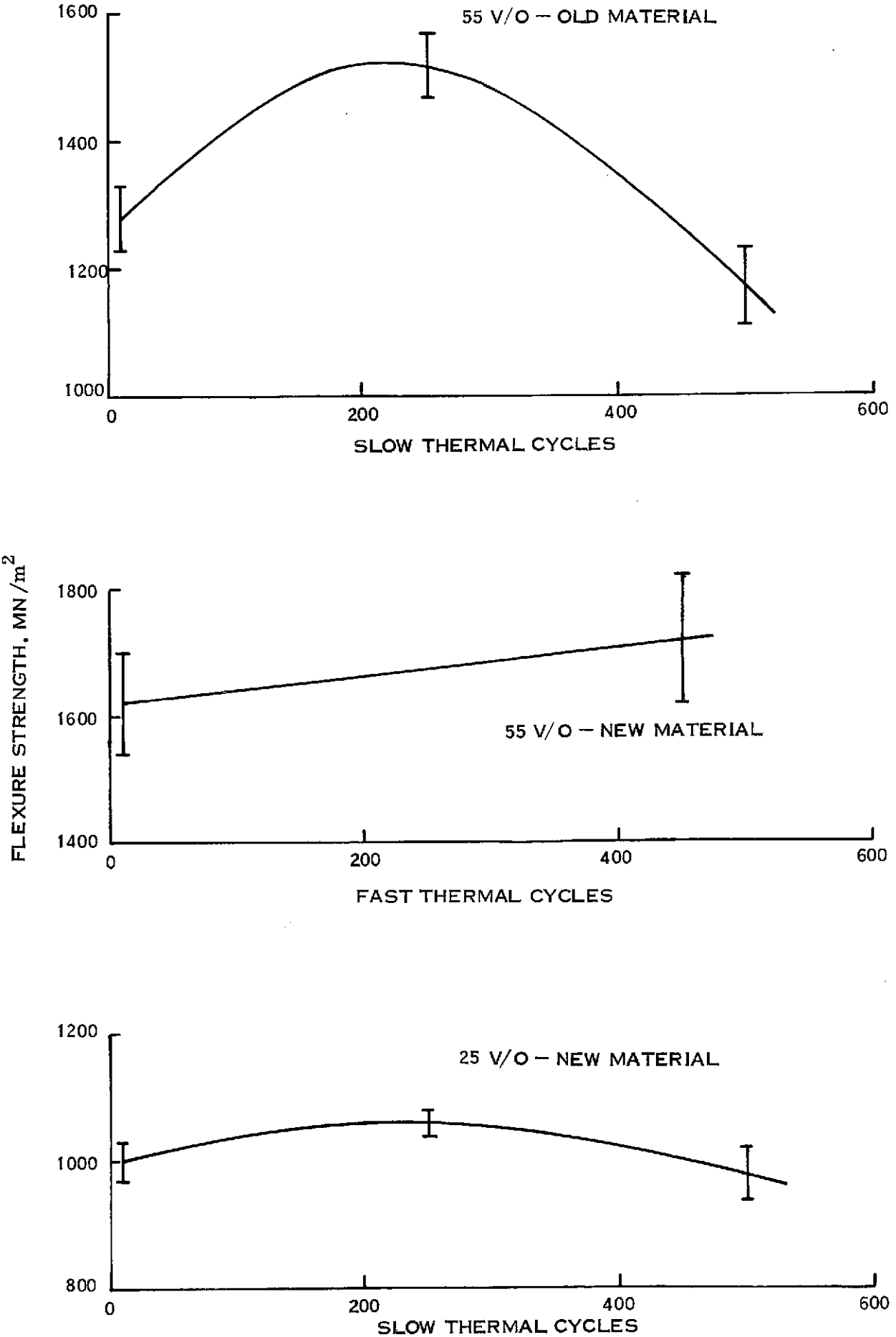

FIGURE 46. Flexural Strength of Carbon/Epoxy Composites as a Function of Thermal Cycling.

during the first 100 cycles which reaches a steady state condition thereafter, suggesting that the specimen as-fabricated had insufficient cure even though manufacturer's directions were followed. Since interlaminar shear strength is not just dependent on the adhesive interfacial bond but also on the cohesive shear strength of the resin between plies, this effect could be inherently resin dominated. If so, this could explain the earlier observations of cleavage when a fiber fractured in the original material. A weak resin strength even with a moderate bond strength would result in brittle cleavage fracture mechanisms.

Finally, in Figure 47, the behavior of the new material shows a slight decrease at 100 cycles and then an increase in interlaminar shear strength of about 15%. This follows the behavior discussed earlier where residual stresses are first relieved with some slight loss of resin integrity. After this the composite shear strength is enhanced by a combination of post curing resin strengthening and improved interfacial action.

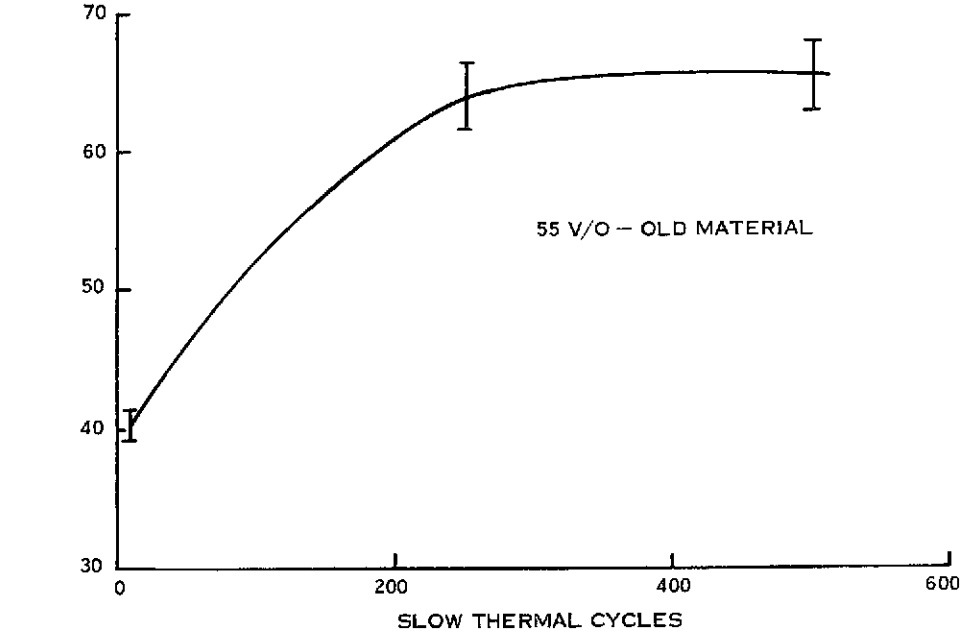

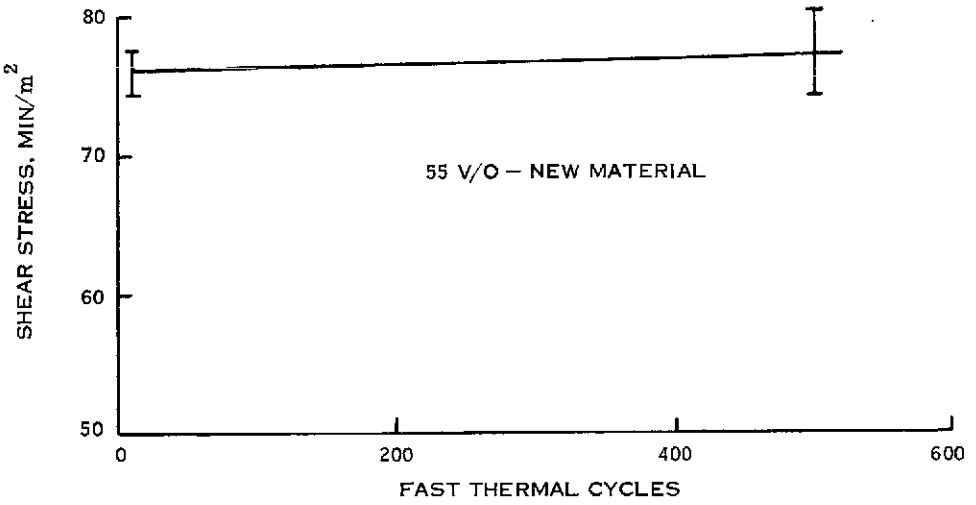

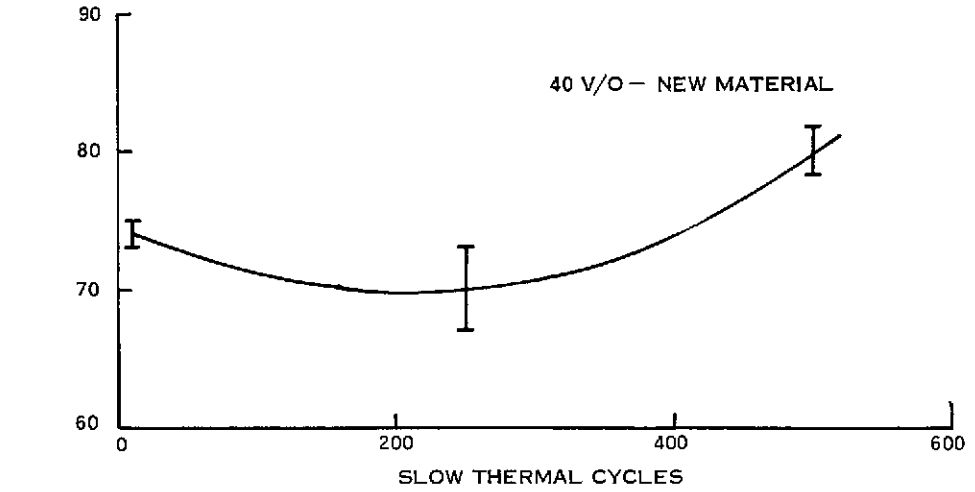

FIGURE 47. Shear Strength of Carbon/Epoxy Composites as a Function of Thermal Cycling.

4.0 CONCLUSIONS

Based on the work performed during this investigation, the following conclusions may be drawn:

1. Thermal cycling does induce damage in model specimens containing a very low fiber volume fraction. The damage consists of local fiber compression failure with accompanying debonding, and increases with increasing resin modification. In spite of this damage, the tensile properties are not affected by cycling.

2. Increasing the volume fraction of carbon fibers increases the tensile, compressive and flexural properties in a linear predictable manner.

3. There is no unambiguous change in tensile properties that is statistically valid after thermal cycling 25, 40 and 55 fiber volume fraction carbon-epoxy (unmodified) composites up to 500 cycles; nor is there an effect of cycling rate within the limits studied. Several possible trends were noted and discussed, but these postulated mechanisms are necessarily conjectural.

REFERENCES

1) Hoffman, C.A., "Effects of Thermal Loading on Composites with Constituents of Differing Thermal Expansion", NASA TND-5926, August 1970.

2) Johnson, J.B. and Owston, C.N., "The Effect of Cure Cycle on the Mechanical Properties of Carbon Fiber/Epoxide Resin", Composites, Vol. 4 No. 3, May 1973.

3) Mullin, J.F., Mazzio, V.F., Mehan, R.L., "Basic Failure Mechanisms in Advanced Composites", NASA Progress Report, October 1971, Contract NASw-2093.

4) Mullin, J.F., Mazzio, V.F., Mehan, R.L., "Basic Failure Mechanisms in Advanced Composites", NASA Final Report, CR-121000 (2420-NO3), March 1972.

5) C.C. Chamis, M.P. Hanson and T.T. Serafini, "Criteria for Selecting Resin Matrices for Improved Composite Strength," Modern Plastics, May 1973.